

2

AD-A236 359



PL-TR-91-2003

DTIC

FLECTE

JUN 03 1991



Physical Property Measurements on Samples
From an Analogue Soviet Nuclear Test Site:
Northern Maine

R.L. Biegel
C.H. Scholz

Columbia University
Lamont-Doherty Geological Observatory
Palisades, New York 10964



Accession For	
WIL GRAAI	<input checked="" type="checkbox"/>
DTIC TAB	<input type="checkbox"/>
Unannounced	<input type="checkbox"/>
Justification	
By	
Distribution/	
Availability Codes	
Avail and/or	
Dist	Special
A-1	

11 April 1991

Scientific Report No. 1

91-00837



Approved for public release; distribution unlimited




PHILLIPS LABORATORY
AIR FORCE SYSTEMS COMMAND
HANSCOM AIR FORCE BASE, MASSACHUSETTS 01731-5000

SPONSORED BY
Defense Advanced Research Projects Agency
Nuclear Monitoring Research Office
ARPA ORDER NO. 2309

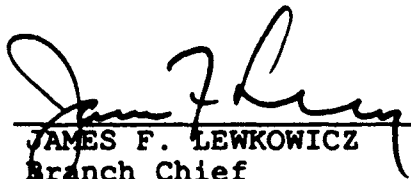
MONITORED BY
Phillips Laboratory
F19628-88-K-0039

The views and conclusions contained in this document are those of the authors and should not be interpreted as representing the official policies, either expressed or implied, of the Defense Advanced Research Projects Agency or the U.S. Government.

This technical report has been reviewed and is approved for publication.



JAMES F. LEWKOWICZ
Contract Manager
Solid Earth Geophysics Branch
Earth Sciences Division



JAMES F. LEWKOWICZ
Branch Chief
Solid Earth Geophysics Branch
Earth Sciences Division

FOR THE COMMANDER



DONALD H. ECKHARDT, Director
Earth Sciences Division

This report has been reviewed by the ESD Public Affairs Office (PA) and is releasable to the National Technical Information Service (NTIS).

Qualified requestors may obtain additional copies from the Defense Technical Information Center. All others should apply to the National Technical Information Service.

If your address has changed, or if you wish to be removed from the mailing list, or if the addressee is no longer employed by your organization, please notify PL/IMA, Hanscom AFB, MA 01731-5000. This will assist us in maintaining a current mailing list.

Do not return copies of this report unless contractual obligations or notices on a specific document requires that it be returned.

REPORT DOCUMENTATION PAGE

Form Approved
OMB No. 0704-0188

Public reporting burden for this collection of information is estimated to average 1 hour per response, including the time for reviewing instructions, searching existing data sources, gathering and maintaining the data needed, and completing and reviewing the collection of information. Send comments regarding this burden estimate or any other aspect of this collection of information, including suggestions for reducing this burden, to Washington Headquarters Services, Directorate for Information Operations and Reports, 1215 Jefferson Davis Highway, Suite 1204, Arlington, VA 22202-4302, and to the Office of Management and Budget, Paperwork Reduction Project (0704-0188), Washington, DC 20503

1. AGENCY USE ONLY (Leave blank)		2. REPORT DATE 11 April 1991	3. REPORT TYPE AND DATES COVERED Scientific Report No. 1	
4. TITLE AND SUBTITLE Physical Property Measurement on Samples From an Analogue Soviet Nuclear Test Site: Northern Maine			5. FUNDING NUMBERS PE: 62714E PR 8A10 TA DA WU AR Contract F19628-88-K-0039	
6. AUTHOR(S) R. L. Biegel C. H. Scholz				
7. PERFORMING ORGANIZATION NAME(S) AND ADDRESS(ES) <u>PRIME CONTRACTOR</u> Columbia University Lamont Doherty Geological Observatory Palisades, NY 10964			8. PERFORMING ORGANIZATION REPORT NUMBER University of California, San Diego, Scripps Inst of Oceanography, UCSD A-025, La Jolla, CA 92093	
9. SPONSORING / MONITORING AGENCY NAME(S) AND ADDRESS(ES) Phillips Laboratory Hanscom AFB, MA 01731-5000 Contract Manager: James Lewkowicz/LWH			10. SPONSORING / MONITORING AGENCY REPORT NUMBER PL-TR-91-2003	
11. SUPPLEMENTARY NOTES				
12a. DISTRIBUTION / AVAILABILITY STATEMENT APPROVED FOR PUBLIC RELEASE; DISTRIBUTION UNLIMITED			12b. DISTRIBUTION CODE	
13. ABSTRACT (Maximum 200 words) The Joint Verification Experiments (JVE) between the US and USSR were designed to improve yield estimates and verification methods for underground nuclear tests. Members of US team retrieved cores of underground rock samples from Semipalatinsk test site. The mechanical properties of these rocks are being measured in a number of US laboratories. DARPA has begun geological and geophysical characterization of a potential analogue test site here in the U.S. It was decided to first measure a number of mechanical properties of end member samples retrieved from the analogue site to compare with similar lithologies from USSR. A team of scientists from USGS, LDGO, and Smithsonian Institute traveled to No. Maine and studied the geology of Mt Katahdin region. Samples of rocks were selected and shipped to Lamont, Standard Research Institute and New England Research for testing. The Lamont test compared strengths of end member samples under different confining pressures, strain rates, saturation conditions and pore pressures. The two selected end members were Katahdin "granite" and a tuffaceous sandstone. The same tests were conducted on Sierra White granite for comparison with a standard.				
14. SUBJECT TERMS Rock mechanics JVE			15. NUMBER OF PAGES 140	
Source medium properties			16. PRICE CODE	
17. SECURITY CLASSIFICATION OF REPORT Unclassified	18. SECURITY CLASSIFICATION OF THIS PAGE Unclassified	19. SECURITY CLASSIFICATION OF ABSTRACT Unclassified	20. LIMITATION OF ABSTRACT SAR	

TABLE OF CONTENTS

I. Introduction.....	1
II. Description of Rocks Tested.....	1
III. Experimental Procedure.....	2
IV. Experimental Results	
Hydrostatic Test.....	4
Fracture Test.....	5
V. Discussion	
Katahdin and Sierra White granite experiments.....	6
Tuffaceous Sandstone.....	8
VI. References.....	10
Table 1.....	11
Table 2.....	13
Table 3.....	13
List of Figures.....	15
Appendix I.....	61
Appendix II.....	66
Appendix III.....	70

1. Introduction

The Joint Verification Experiments (JVE) between the US and the USSR were designed to improve yield estimates and verification methods for underground nuclear test conducted in the US and the Soviet Union. As part of this agreement, members of a US team retrieved cores of underground rock samples from the Semipalatinsk test site, USSR. The mechanical properties of these rocks are now being measured in a number of laboratories in the US. In support of this project, the Defense Advanced Research Project Agency (DARPA) has begun geological and geophysical characterization of a potential analogue test site here in the US. As a first step, it was decided to measure a number of mechanical properties of end member samples retrieved from the analogue site for comparison with similar lithologies from the Soviet Union. A team of scientist and engineers from the US Geological Survey, the Lamont-Doherty Geological Observatory (Lamont), and the Smithsonian Institute traveled to Northern Maine and studied the geology of the Mt. Katahdin region. Samples of rock were selected and shipped to Lamont, Stanford Research Institute (SRI), and New England Research, Inc. for testing.

The test conducted at Lamont compared strengths of end member samples under different confining pressures, strain rates, saturation conditions and pore pressures. The two selected end members were Katahdin "granite" and a tuffaceous sandstone. The same test were conducted on Sierra White granite for comparison with a standard. This paper reports the results of these test as obligated under DARPA Contract No. UCS10-G-98021-3218.

2. Description of Rocks Tested

The analogue Soviet test site, selected in the late 1970's by members of the U.S Geological Survey, is located in the Shin Pond quadrangle of northern Maine shown on the map in Appendix 1. The region has a total of 11 different rock types listed in Appendix 2. In August, 1989, a team of researchers spent more than 2 weeks in the field inspecting the rock types and concluded that the end member rock strengths were best represented by a Katahdin "granite" and either a tuffaceous sandstone or a fossiliferous limestone. Samples of all

three were collected and delivered to LDGO for testing along with a granite from Nickerson Lake, Maine.

At a workshop held at Lamont on September 15 and 16, 1989, Katahdin granite was chosen for testing as representing the strongest member of the 11 possible rock types while the tuffaceous sandstone was chosen for testing as the weakest end-member. Katahdin granite is really a quartz monzonite, a medium-gray to light-gray, medium-grained massive plutonic rock characterizing the Katahdin batholith (Station 8, Appendix I). It is mostly massive and structureless, composed of 45% microcline, 34% quartz, 9% albite, 10% biotite and 2% opaque (Neuman, 1967). Although the rock shows evidence of possessing a slight crack population, there has been little trouble obtaining intact cores from the block. Nickerson Lake granite, a rock type similar to Katahdin, but with smaller grain size, was retrieved from a quarry (Appendix I, Station 11a). The weakest member of the suite is a tuffaceous sandstone from the Shin Brook formation (Station 6, Appendix I). This rock shows moderate evidence of tectonic shearing and jointing which has made core recovery for testing extremely difficult.

In addition to the two types discussed above, two blocks of Sierra White granite were shipped from SRI to Lamont for testing. This rock has been used in shock test at Alex Florence's lab at SRI and it was considered important to see how the results from fracture test on Sierra White compared with results from the SRI test.

3.) Experimental Procedure

In this study 32 experiments were conducted, 11 each for Katahdin granite and Tuffaceous sandstone, 8 for Sierra White and 2 for Nickerson Lake granite. Samples were cored from the blocks in two different sizes. Katahdin, Nickerson Lake and Sierra White granite cores were approximately 9 cm in length and 3.5 cm in diameter. The Tuffaceous sandstone was highly fractured and sheared, so it was nearly impossible to core intact samples of comparable size. Consequently, we chose to reduce the size of the cores to 2.54 cm in diameter and 4 cm in length to improve our chances of intact recovery.

We conducted hydrostatic compression test on samples cored in three perpendicular orientations to assure detection of any strain anisotropy in the specimens. As described in Scholz and Koczyński (1979), the KG 10 sample was oriented perpendicular to the the plane of greatest crack density which also corresponds to the plane of variably developed biotite foliation. The KG 13 sample was oriented with reference to the secondary preferred orientation of cracks, whereas KG 14 was cored relative to the plane of low preferred crack orientation. All Katahdin granite samples used in fracture experiments were cored similarly to KG 10.

In like manner, three specimens of tuffaceous sandstones for the hydrostatic test were cored with reference to the bedding plane. TS 6 was oriented perpendicular to the bedding plane, while TS 11 was oriented perpendicular to the plane of maximum jointing.

All ends were ground parallel to within .002 mm / mm and cleaned *in vacuo* with acetone. The samples were jacketed in copper and three strain gages, two radial and one axial were mounted on each sample. The samples used in hydrostatic test were mounted with two axial and two radial strain gages.

All experiments were conducted at room temperature, in a programmable, servo-controlled, triaxial apparatus. Table 1 list the experiments and the conditions for the experiments performed. Kerosene was used as a confining medium and pressure was controlled to within 0.01MPa. Compressibility measurements were made by increasing the confining pressure at a rate of 0.2 MPa S-1 from room pressure to 200 MPa. In the fracture test, a hydraulic ram applied the axial load with a piston that was displacement-controlled to within 0.1 microns. Pore pressure was servo-controlled to within 0.01 MPa. Data was recorded using a Digital Equipment Corporation, PDP 1103 computer. The data was then transferred to a Sun microsystem computer for processing and analysis. Both saturated and dry (laboratory humidity) samples were used for fracture test. Strain rates were varied between 10-3 and 10-6 sec-1. Three confining pressures of 0.35, 6.9 and 13.8 MPa were used to match the conditions of experiments performed by A. Florence.

4.) Experimental Results

Hydrostatic Test

Three hydrostatic test were done on each specimen type, results from one test will be discussed. Representative plots of linear strains recorded during a hydrostatic compression test on Katahdin granite are shown in Figure 1. Each curve is a plot of strain from the KG 10 sample measured in one of three perpendicular orientations. The non-linearity observed in the stress-strain curves at the lower pressures represents closing of flat cracks (Brace, 1965; Walsh, 1965). At higher pressure, about 100 MPa, the graphs are nearly linear suggesting the cracks have been closed. Even so, at 200 MPa, there remains a difference in the slopes of these three curves which represents a slight mineral anisotropy in the sample. Linear compressibility as a function of confining pressure is plotted in Figure 2. Only slight differences are observed for the three orientations over the range of the pressures of the experiment, suggesting an absence of any preferred crack orientation in the sample. In Figure 3 confining pressure is plotted against the volumetric strain. From the slopes of this curve we obtain the bulk modulus as a function of pressure, as well as an estimate of the porosity of the sample. The hysteresis in the unloading curves results from friction along internal cracks.

Figure 4 gives the linear strains in three orientations for the tuffaceous sandstone sample, T 6, plotted against confining pressure. In contrast to the plots from the Katahdin granite in Figure 1 above, the curves in Figure 4 are more linear even at the lower pressures. At first glance, this suggest that this rock has fewer cracks to close, but the presence of visible joints in the rock suggest otherwise. We will return to this problem in the discussion below. The compressibility curves in Figure 5 are nearly constant above 50 MPa, whereas below 20 MPa the presence of a small number of highly oriented cracks is shown by the different slopes in compressibility for one of the orientations. As for the Katahdin granite examined above, the graphs show that at 200 MPa there remains a small difference in the compressibility curves depending upon orientation suggesting a mineral anisotropy. Volumetric strain, the sum of the three linear strains, is plotted against the confining pressure in Figure 6. Note

the absence of the hysteresis portion of the curve at low pressures, in contrast to KG 10 in Figure 3.

The bulk moduli as a function of pressure are given in Table 2 and plotted in Figure 7 for both rock types. Values for Sierra White granite from Martin and Koyner (1987) are included for comparison. The incompressibility of Katahdin granite is slightly less than Sierra White at lower pressures possibly due to a difference in crack density. The convergence of the two parameters at 200 MPa supports this interpretation. The incompressibility of the tuffaceous sandstone is also plotted in the figure. Although this rock type contains a number of joints, the bulk moduli is significantly higher than the values measured from any of the other rock types. Again, the reasons for this difference will be discussed later.

Fracture Test

Table 3 list the Young's Modulus from the stress-strain curves taken at 50% of fracture. The Katahdin granite and Sierra White granite both have nearly identical values, while the tuffaceous sandstone are more compliant probably due to the nature of the crack population.

Figure 8 gives the fracture strengths for the rocks tested over the range of confining pressures tested at 10^{-4} s⁻¹ strain rate. It shows that there is very little difference in strength between Sierra White and Katahdin granite for either dry or saturated samples. The Nickerson Lake granite, a smaller grain rock than the Katahdin or Sierra granite, is stronger than either of these two rock types, and its strength increases with pressure at the same rate as the other two granites. The tuffaceous sandstones are similar in strength to the granites at low pressures. The dry samples show almost no confining pressure dependence, but the saturated sample are slightly dependent.

Figures 9-11 show the fracture stress as a function of confining pressure for each of the four rock types along with the results of test with controlled pore pressure. These experiments were performed at strain rates of 10^{-4} s⁻¹. For the three rock types tested, almost no difference is detected between

samples with effective pressures of 6.7 MPa and saturated, drained samples having effective pressures of 13.8 MPa. Also note that the experiments done with pore pressure do not obey the effective stress law. Rather, they exhibit fracture strengths comparable to the saturated, drained samples. We will discuss below how this is probably due to dilatancy hardening of the sample.

The effects of strain rate on the fracture strength are shown in Figure 12. Sierra White granite exhibits a strain rate dependence of about 4.6% increase for a 10-fold increase in strain rate. This is comparable to values of 4% to 5% for Westerly granite (Brace and Martin, 1968). Tuffaceous sandstone, however, shows a 10% increase between 10^{-6} S-1 and 10^{-4} s-1, but no difference from 10^{-4} S-1 to 10^{-3} s-1. Katahdin granite has an 8% increase in strength over all strain rates tested.

Figures 16 to 22 are the complete stress strain curves for the fracture test conducted on Katahdin granite. In each plot, the axial and two circumferential strains are shown with solid lines, while the volumetric strains are shown with dotted lines. Figures 23 to 30 are stress-strain plots for Tuffaceous sandstone, and Figures 31 to 38 are the stress-strain plots for Sierra White granite. Figures 39 and 40 are the stress-strain plots for Nickerson Lake granite.

5.) Discussion

We will discuss the Katahdin and Sierra White granites together since they both have similar strengths and both are low-porosity brittle rocks. The tuffaceous sandstone is discussed separately since this specimen contains macroscopic fractures and joints which appear to strongly control the strength properties .

a.) *Katahdin and Sierra White granite experiments*

The most significant observation from these experiments is the similarity of the fracture strength and elastic moduli for the Katahdin and Sierra White granites over the range of strain rates, confining pressures and saturation conditions examined. This is not unexpected since the incompressibility curves

for both specimens are similar, suggesting that any difference in crack density is not significant enough to change the macroscopic fracture or elastic properties of the sample. From these results, it appears that Sierra White can substitute for Katahdin granite in future test, which may be helpful since the mechanical properties of Sierra White granite are already well known.

The results of the controlled pore pressure experiments at strain rates of 10^{-4} s⁻¹ and confining pressures of 13.8 MPa show that pore pressures of 6.9 MPa were insufficient to change the fracture strength. In the cases of Katahdin and Sierra White granite, this is explained by dilatancy hardening of the sample (Brace and Martin, 1968). Figure 13 shows a plot of the radial strain, pore pressure, and axial load plotted in real time for Katahdin granite. Figure 14 shows the same for Sierra White granite. Note the increase in radial strain with application of the pore pressure, which occurs over a characteristic time dependent on the permeability of the rock and the properties of the pore fluid. This characteristic time is longer than the time scale of the fracture experiment as shown by the time span of the axial loading. During a fracture experiment, axial loading of the sample opens microcracks parallel to maximum compression, a phenomenon called dilatancy (Brace, Paulding, and Scholz, 1966). Dilatancy reduces the pore fluid pressure within the sample, thus increasing the effective stress. When this happens faster than the characteristic time for sample saturation, the pore fluid cannot continue to equalize the confining pressure. Consequently, the effective stress on the sample approaches that of the confining pressure, which increases the strength of the rock to a magnitude equal to that found in the saturated and dry sample experiments. Therefore, it is improbable that pore fluid pressure will affect the effective stress of low porosity brittle rocks at low confining pressures, and strain rates higher than 10^4 s⁻¹. More testing is recommended to better define these results at different strain rates, confining and pore pressures.

Figure 15 is a plot of the data from an experiment with Tuffaceous sandstone, similar to Figures 13 and 14 above. Note, however, that application of the pore fluid pressure does not produce an expected volumetric expansion; rather, the volume stays constant. This result supports the observation from the incompressibility test that the *solid matrix* of this rock type is very impermeable (see below). This property enhances dilatancy hardening in the

sample and explains why the fracture strengths for the sandstones were the same for test done in dry, saturated, and controlled pore fluid environments.

Tuffaceous Sandstone

Visual inspection of the tuffaceous sandstone confirms this is a highly sheared and jointed rock. Any one of these cracks will propagate when the stresses at the tips exceeds a critical value. The stress intensity factor for a crack in a solid medium scales as the inverse root of the crack length (Scholz, 1982, 1990). So it is not unexpected that the large size of the joints in the sandstone significantly lower the strength of the sample, since compressive failure of rock is usually accomplished by the propagation and coalescence of microcracks into a fault (Scholz, 1968a,b; Peng and Johnson, 1972). Moreover, the Young' s modulus for the sandstone is lower than the modulus for the Katahdin granite and the Sierra White, as shown in Table 3, another characteristic of jointed rock (Jaeger, 1979).

However, the incompressibility values measured for the tuffaceous sandstone were markedly higher than the bulk moduli of both Katahdin and Sierra White granite. The usual interpretation of this is the sandstones contain a crack population *less* than the granites, a result which may lead lead one to casually predict that the sandstones will be stronger. It appears then that the presence of the large joints were undetected by the hydrostatic test.

This is because the total volume change of the sample is equal to the solid matrix deformation plus closure of the joint (Walsh and Grosenbaugh, 1979). During a compressibility test, the strain gages measure only the strain of the solid matrix material: joints accommodate compressive stresses by closure which is not detected unless the gage happens to be in close proximity, or across, the joint. The potential for damage to a strain gage during an experiment made us avoid the area of obvious joints when mounting the gages. Therefore, compressibility measurements of tuffaceous sandstone underestimates the volumetric strain, since a portion of the closure which should be included in the calculation is of necessity missing. These experiments suggest that results from hydrostatic test must be interpreted with care and analyzed in conjunction with results from other test to accurately characterize

the mechanical properties of a sample.

Acknowledgements: The authors would like to thank G.N.Boitnott and F. Chester for many helpful and insightful discussions throughout this experimental program, and T. Koczynski for invaluable technical assistance. This research was supported by Defense Advanced Research Project Agency contract number UCS IO-G-980221-3218.

References

- Brace, W. F., Some new measurements of linear compressibility of rocks, J. Geophys. Res., **70**, 391-398, 1965.
- Brace, W. F., B. W. Paulding, Jr., and C. Scholz, Dilatancy in the fracture of crystalline rocks, J. Geophys. Res., **71**, 3939-3953, 1966.
- Brace, W. F., and R. Martin, A test of the law of effective stress for crystalline rocks of low porosity, Int. J. Rock Mech. Min. Sci., **5**, 415-426, 1968.
- Martin, R. J., and R. W. Haupt, Physical property measurements on analog granites related to the joint verification experiment, New England Research, Inc., White River Junction, Vermont, 1990.
- Martin, R. J., and K. B. Koyner, Physical properties of Sierra White Granite for intact and crack-enhanced specimens, New England Research, Inc., Norwich, Vermont, 1987.
- Neuman, R. B., Bedrock geology of the Shin Pond and Stacyville Quadrangles, Penobscot County, Maine, Geological Survey Professional Papers **524-I**, U. S. Government Printing Office, Washington D. C., 1967.
- Scholz, C. H., Rock strength under confined shock conditions, Air Force Office of Scientific Research, Bolling Air Force Base, Washington, D. C., 1982.
- Scholz, C. H., The Mechanics of Earthquakes and Faulting, Cambridge University Press, 1990.
- Scholz, C. H., and T. A. Koczyński, Dilatancy Anisotropy and the Response of Rock to Large Cyclic Loads, J. Geophys. Res., **84**, 5525-5534, 1979.
- Walsh, J. B., The effects of cracks on the compressibility of rocks, J. Geophys. Res., **70**, 381-389, 1965.
- Walsh, J. B., and M. A. Grosenbaugh, A new model for analyzing the effect of fractures on compressibility, J. Geophys. Res., **84**, 3532-3536, 1979.

Table 1

Hydrostatic Compression Experiments

Katahdin Granite

<u>Experiment</u>	<u>Confining Pressure, MPa</u>
KG 10	0 to 200
KG 13	0 to 200
KG 14	0 to 200

Tuffaceous Sandstone

<u>Experiment</u>	<u>Confining Pressure, MPa</u>
TS 6	0 to 200
TS 11	0 to 200
TS 12	0 to 200

Fracture Experiments

Katahdin Granite

<u>Experiment</u>	<u>Confining Pressure, MPa</u>	<u>Saturation</u>	<u>Strain Rate</u>
KG 5	13.8	Saturated, drained	10^{-3} s^{-1}
KG 15	13.8	Saturated, drained	10^{-4} s^{-1}
KG 6	13.8	Saturated, drained	10^{-6} s^{-1}
KG 17	6.7	Saturated, drained	10^{-4} s^{-1}
KG 18	13.8	Pp = 6.7 MPa	10^{-4} s^{-1}
KG 19	0.34	Saturated, drained	10^{-4} s^{-1}
KG 20	0.34	Dry	10^{-4} s^{-1}
KG 4	13.8	Dry	10^{-4} s^{-1}

Tuffaceous Sandstone

<u>Experiment</u>	<u>Confining Pressure,MPa</u>	<u>Saturation</u>	<u>Strain Rate</u>
TS 7	13.8	Saturated, drained	10^{-3} s^{-1}
TS 1B	13.8	Saturated, drained	10^{-4} s^{-1}
TS 9	13.8	Saturated, drained	10^{-6} s^{-1}
TS 8	6.7		10^{-4} s^{-1}
TS 10	13.8	Pp = 6.7 MPa	10^{-4} s^{-1}
TS 2	0.34	Saturated, drained	10^{-4} s^{-1}
TS 4	0.34	Dry	10^{-4} s^{-1}
TS 6C	13.8	Dry	10^{-4} s^{-1}

Sierra White Granite

<u>Experiment</u>	<u>Confining Pressure,MPa</u>	<u>Saturation</u>	<u>Strain Rate</u>
SW 1	13.8	Saturated, drained	10^{-3} s^{-1}
SW 3	13.8	Saturated, drained	10^{-4} s^{-1}
SW 8	13.8	Saturated, drained	10^{-6} s^{-1}
SW 2	6.7		10^{-4} s^{-1}
SW 6	13.8	Pp = 6.7 MPa	10^{-4} s^{-1}
SW 5	0.34	Saturated, drained	10^{-4} s^{-1}
SW 7	0.34	Dry	10^{-4} s^{-1}
SW 4	13.8	Dry	10^{-4} s^{-1}

Nickerson Lake Granite

<u>Experiment</u>	<u>Confining Pressure,MPa</u>	<u>Saturation</u>	<u>Strain Rate</u>
NL 1	13.8	Saturated, drained	10^{-4} s^{-1}
NL 2	0.34	Saturated, drained	10^{-4} s^{-1}

Table 2

Bulk Modulus from Hydrostatic Compression Test, GPa

<u>Experiment</u>	<u>5 MPa</u>	<u>25MPa</u>	<u>50 MPa</u>	<u>100 MPa</u>	<u>200 MPa</u>
KG 10	8.3	21	32	41	48
KG 13					46
KG 14					49
SW	14.2	28	35	43	51
TS 6B	31.4	40	46	51	60
TS 11					57
TS 12					59

Table 3

Young's Modulus from Fracture Test, GPa

Katahdin Granite

Experiment

KG 5	56.5
KG 15	57.7
KG 6	56.5
KG 17	57.4
KG 18	56.6
KG 19	46.1
KG 20	NA
KG 4	62.6

Tuffaceous Sandstone

Experiment

TS 7	42.7
TS 1B	45.5
TS 9	42.5
TS 8	34.9
TS 10	37.4
TS 2	NA
TS 4	44.4
TS 6C	50.6

Sierra White Granite

Experiment

SW 1	55.4
SW 3	55.0
SW 8	56.3
SW 2	58.8
SW 6	47.2
SW 5	53.5
SW 7	51.9
SW 4	56.3

Nickerson Lake Granite

Experiment

NL 1	56.1
NL 2	NA

List of Figures

Figure 1	Plot of hydrostatic pressure vs. linear strains for a Katahdin granite sample KG 10.....	20
Figure 2	Linear compressibility vs. confining pressure from three orthogonal orientations measured for sample KG 10.....	21
Figure 3	Plot of hydrostatic pressure vs. volumetric strain for a Katahdin granite sample KG 10.....	22
Figure 4	Plot of hydrostatic pressure vs. linear strains for a Tuffaceous sandstone sample TS 6	23
Figure 5	Linear compressibility vs. confining pressure from three orthogonal orientations measured for sample TS 6.....	24
Figure 6	Plot of hydrostatic pressure vs. volumetric strain for a Tuffaceous sandstone sample TS 6	25
Figure 7	Bulk modulus for Katahdin and Sierra White granites and tuffaceous sandstone plotted as a function of confining pressure.....	26
Figure 8	Plot of fracture stress at different confining pressures for all rock specimens tested, in dry and saturated states	27
Figure 9	Plot of fracture stress at different confining pressures for Katahdin granite.....	28
Figure 10	Plot of fracture stress at different confining pressures for Tuffaceous sandstone	39
Figure 11	Plot of fracture stress at different confining pressures for Sierra White granite.....	30
Figure 12	Plot of fracture stress at different strain rates for Katahdin and Sierra White granites and tuffaceous sandstone	31

Figure 13	Data from pore pressure experiment illustrating radial strain, pore pressure and axial load for Katahdin granite plotted in real time.....	32
Figure 14	Data from pore pressure experiment illustrating radial strain, pore pressure and axial load for Tuffaceous sandstone plotted in real time.....	33
Figure 15	Data from pore pressure experiment illustrating radial strain, pore pressure and axial load for Sierra White granite plotted in real time.....	34
Figure 16	Graph of axial, radial, and volumetric strains plotted as a function of differential stress for specimen KG 5. The two left-most solid lines are the radial strains, the dotted line is the volumetric strain, the right-most solid line is the axial strain	35
Figure 17	Graph of axial, radial, and volumetric strains plotted as a function of differential stress for specimen KG 15. The two left-most solid lines are the radial strains, the dotted line is the volumetric strain, the right-most solid line is the axial strain..	36
Figure 18	Graph of axial, radial, and volumetric strains plotted as a function of differential stress for specimen KG 15. The two left-most solid lines are the radial strains, the dotted line is the volumetric strain, the right-most solid line is the axial strain K6.....	37
Figure 19	Graph of axial, radial, and volumetric strains plotted as a function of differential stress for specimen KG 17. The two left-most solid lines are the radial strains, the dotted line is the volumetric strain, the right-most solid line is the axial strain	38
Figure 20	Graph of axial, radial, and volumetric strains plotted as a function of differential stress for specimen KG 18. The two left-most solid lines are the radial strains, the dotted line is the volumetric strain, the right-most solid line is the axial strain	39

Figure 21	Graph of axial, radial, and volumetric strains plotted as a function of differential stress for specimen KG 19. The two left-most solid lines are the radial strains, the dotted line is the volumetric strain, the right-most solid line is the axial strain	40
Figure 22	Graph of axial, radial, and volumetric strains plotted as a function of differential stress for specimen KG 20. The two left-most solid lines are the radial strains, the dotted line is the volumetric strain, the right-most solid line is the axial strain	41
Figure 23	Graph of axial, radial, and volumetric strains plotted as a function of differential stress for specimen KG 4. The two left-most solid lines are the radial strains, the dotted line is the volumetric strain, the right-most solid line is the axial strain	42
Figure 24	Graph of axial, radial, and volumetric strains plotted as a function of differential stress for specimen TS 7. The two left-most solid lines are the radial strains, the dotted line is the volumetric strain, the right-most solid line is the axial strain	43
Figure 25	Graph of axial, radial, and volumetric strains plotted as a function of differential stress for specimen TS 1B. The two left-most solid lines are the radial strains, the dotted line is the volumetric strain, the right-most solid line is the axial strain	44
Figure 26	Graph of axial, radial, and volumetric strains plotted as a function of differential stress for specimen TS 9. The two left-most solid lines are the radial strains, the dotted line is the volumetric strain, the right-most solid line is the axial strain	45
Figure 27	Graph of axial, radial, and volumetric strains plotted as a function of differential stress for specimen TS 8. The two left-most solid lines are the radial strains, the dotted line is the volumetric strain, the right-most solid line is the axial strain	46

Figure 28 Graph of axial, radial, and volumetric strains plotted as a function of differential stress for specimen TS 10. The two left-most solid lines are the radial strains, the dotted line is the volumetric strain, the right-most solid line is the axial strain47

Figure 29 Graph of axial, radial, and volumetric strains plotted as a function of differential stress for specimen TS 2. The two left-most solid lines are the radial strains, the dotted line is the volumetric strain, the right-most solid line is the axial strain48

Figure 30 Graph of axial, radial, and volumetric strains plotted as a function of differential stress for specimen TS 4. The two left-most solid lines are the radial strains, the dotted line is the volumetric strain, the right-most solid line is the axial strain49

Figure 31 Graph of axial, radial, and volumetric strains plotted as a function of differential stress for specimen TS 6. The two left-most solid lines are the radial strains, the dotted line is the volumetric strain, the right-most solid line is the axial strain50

Figure 32 Graph of axial, radial, and volumetric strains plotted as a function of differential stress for specimen SW 1. The two left-most solid lines are the radial strains, the dotted line is the volumetric strain, the right-most solid line is the axial strain51

Figure 33 Graph of axial, radial, and volumetric strains plotted as a function of differential stress for specimen SW 3. The two left-most solid lines are the radial strains, the dotted line is the volumetric strain, the right-most solid line is the axial strain52

Figure 34 Graph of axial, radial, and volumetric strains plotted as a function of differential stress for specimen SW 8. The two left-most solid lines are the radial strains, the dotted line is the volumetric strain, the right-most solid line is the axial strain53

Figure 35	Graph of axial, radial, and volumetric strains plotted as a function of differential stress for specimen SW 6. The two left-most solid lines are the radial strains, the dotted line is the volumetric strain, the right-most solid line is the axial strain	54
Figure 36	Graph of axial, radial, and volumetric strains plotted as a function of differential stress for specimen SW 2. The two left-most solid lines are the radial strains, the dotted line is the volumetric strain, the right-most solid line is the axial strain	55
Figure 37	Graph of axial, radial, and volumetric strains plotted as a function of differential stress for specimen SW 5. The two left-most solid lines are the radial strains, the dotted line is the volumetric strain, the right-most solid line is the axial strain	56
Figure 38	Graph of axial, radial, and volumetric strains plotted as a function of differential stress for specimen SW 7. The two left-most solid lines are the radial strains, the dotted line is the volumetric strain, the right-most solid line is the axial strain	57
Figure 39	Graph of axial, radial, and volumetric strains plotted as a function of differential stress for specimen SW 4. The two left-most solid lines are the radial strains, the dotted line is the volumetric strain, the right-most solid line is the axial strain	58
Figure 40	Graph of axial, radial, and volumetric strains plotted as a function of differential stress for specimen NL 1. The two left-most solid lines are the radial strains, the dotted line is the volumetric strain, the right-most solid line is the axial strain	59
Figure 41	Graph of axial, radial, and volumetric strains plotted as a function of differential stress for specimen NL 2. The two left-most solid lines are the radial strains, the dotted line is the volumetric strain, the right-most solid line is the axial strain	60

KG 10

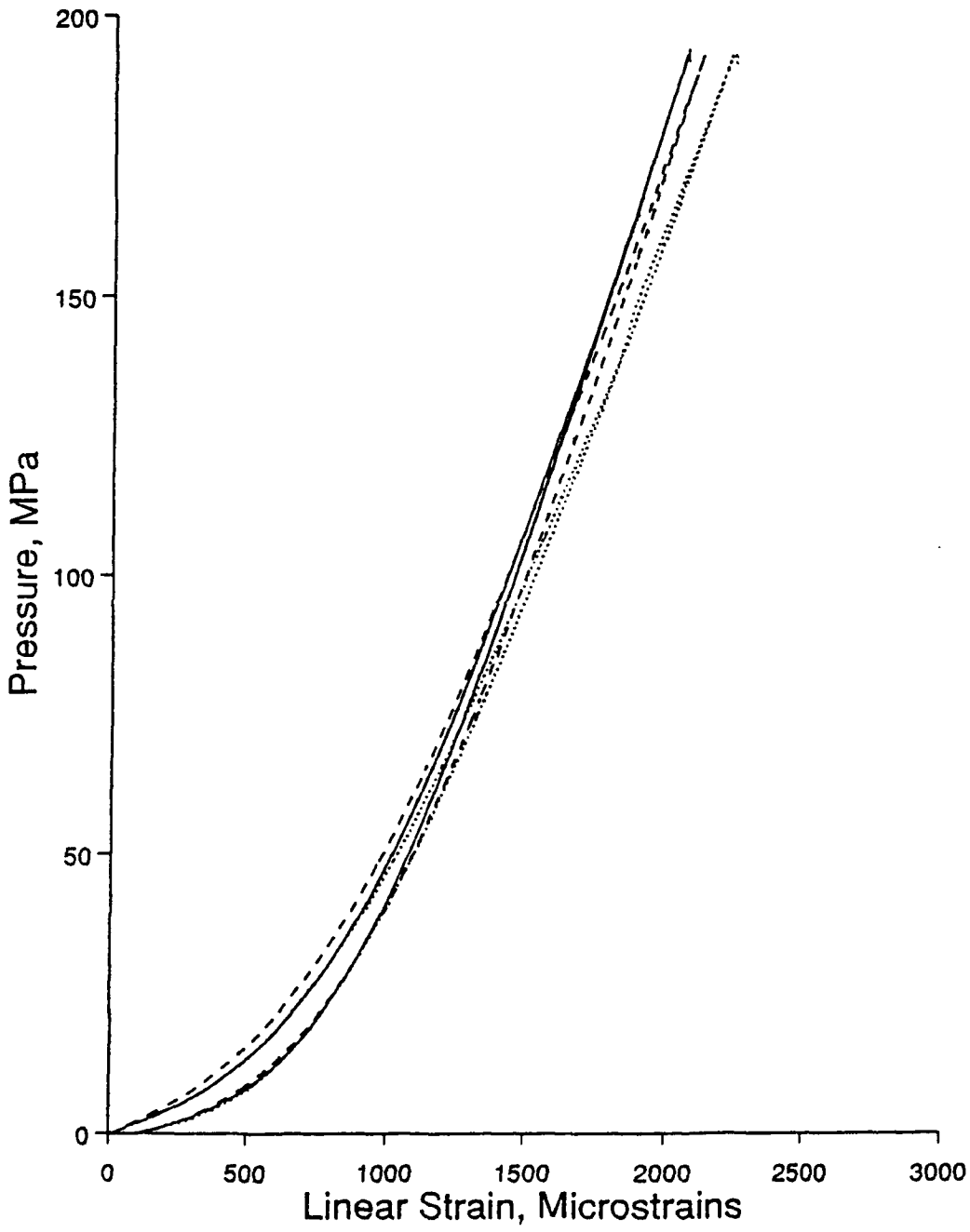


Figure 1

KATAHDIN GRANITE LINEAR COMPRESSIBILITY

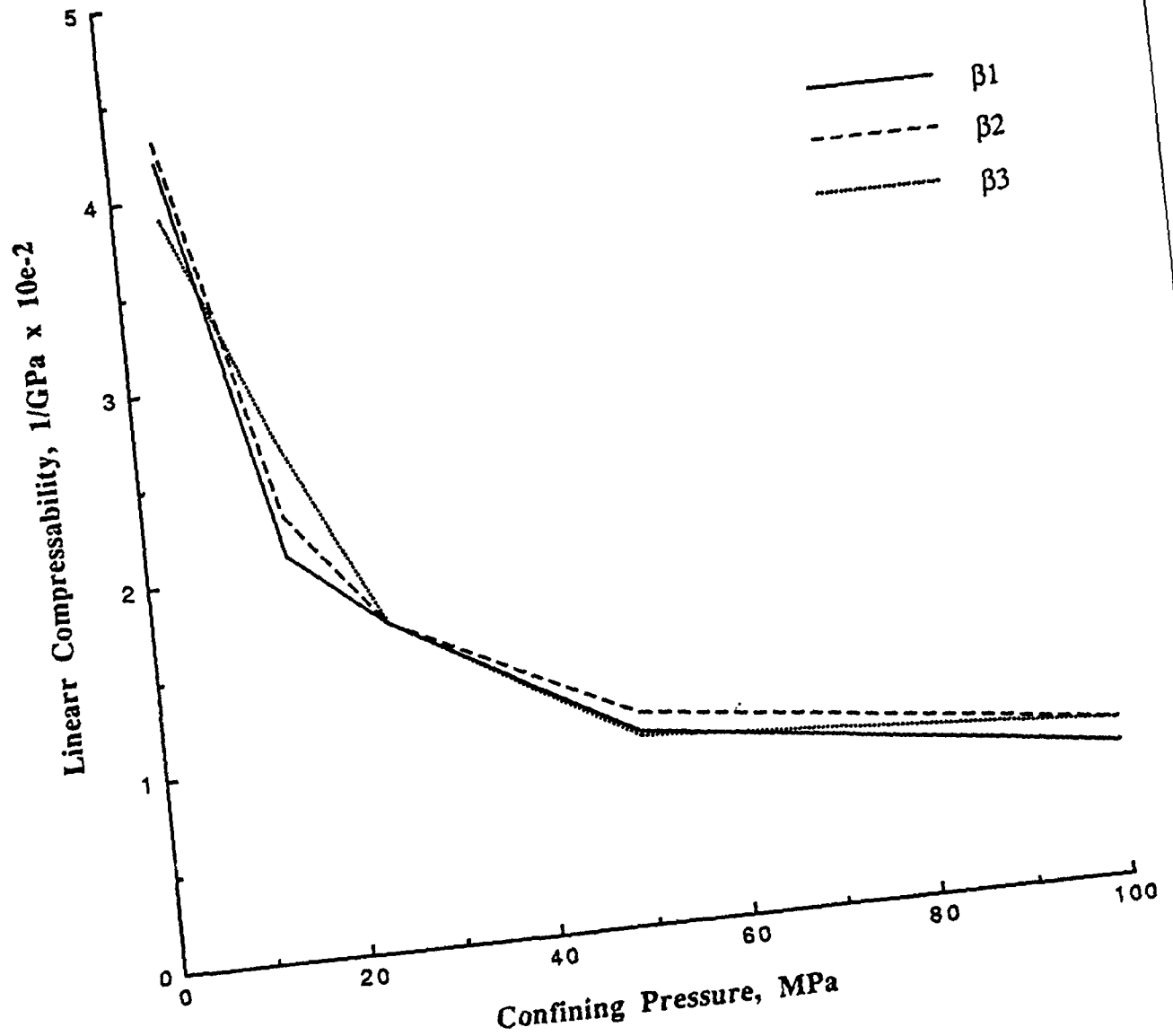


Figure 2

KG 10

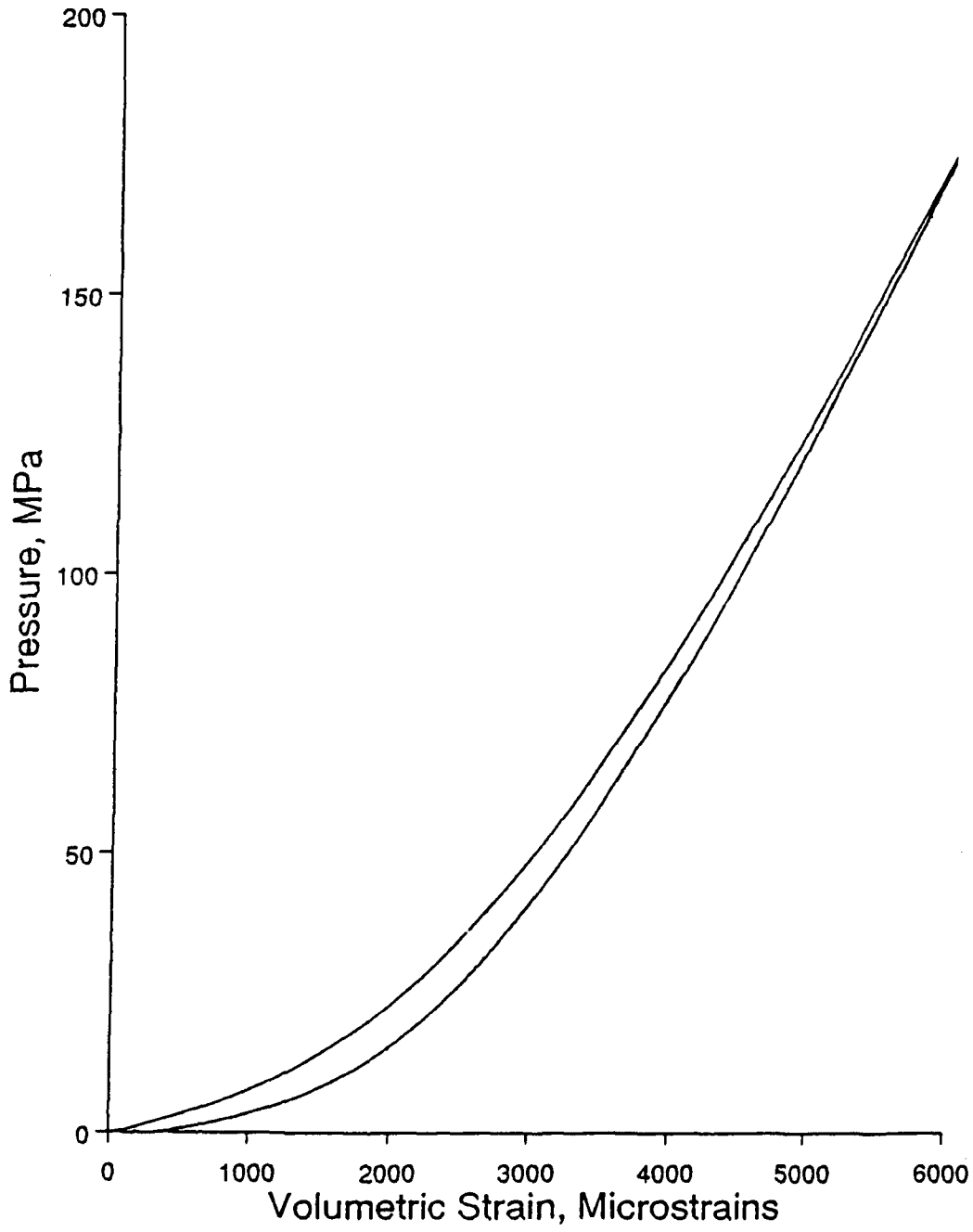


Figure 3

TS 6

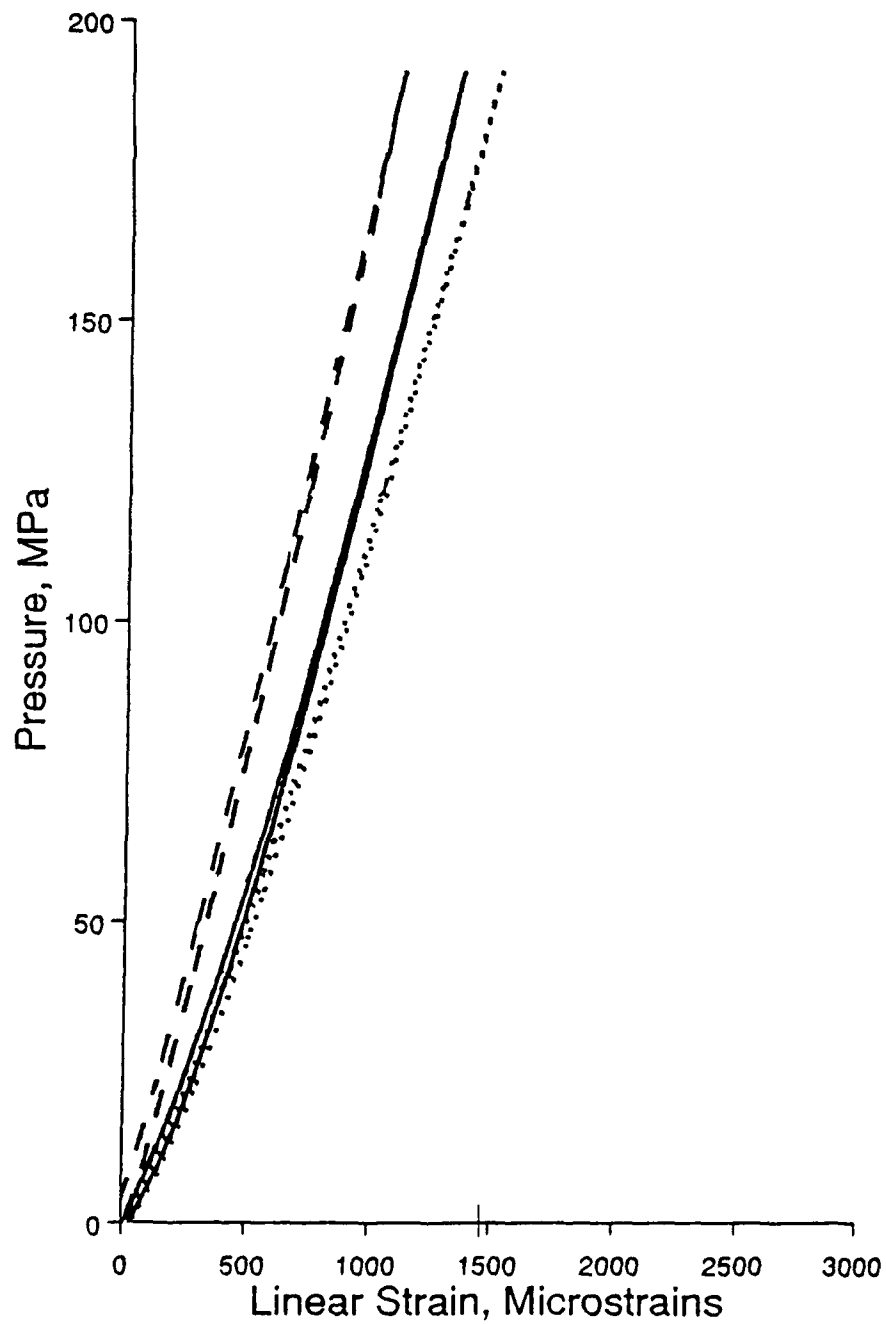


Figure 4

TUFFACEOUS SANDSTONE
LINEAR COMPRESSIBILITY

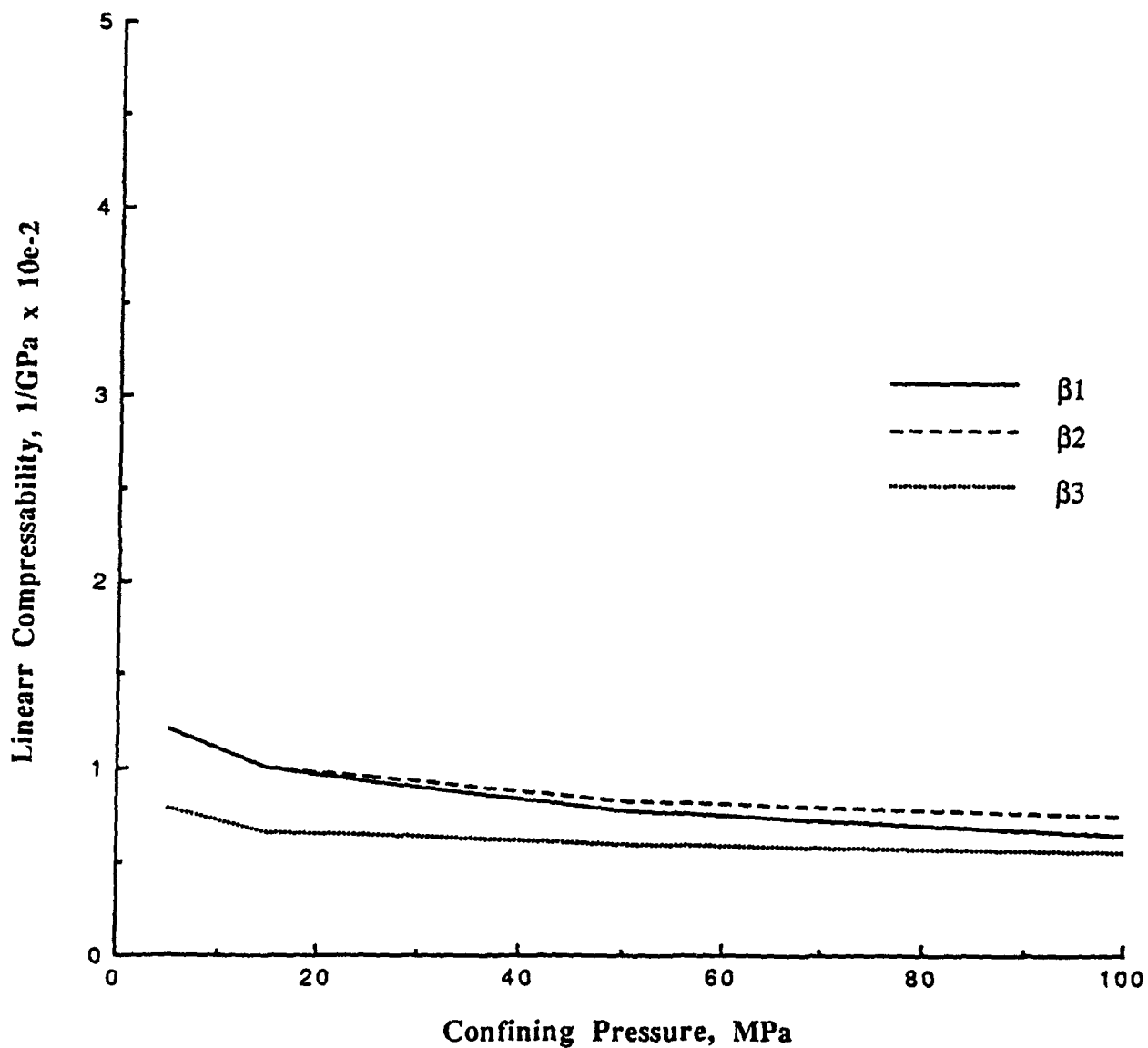


Figure 5

TS 6

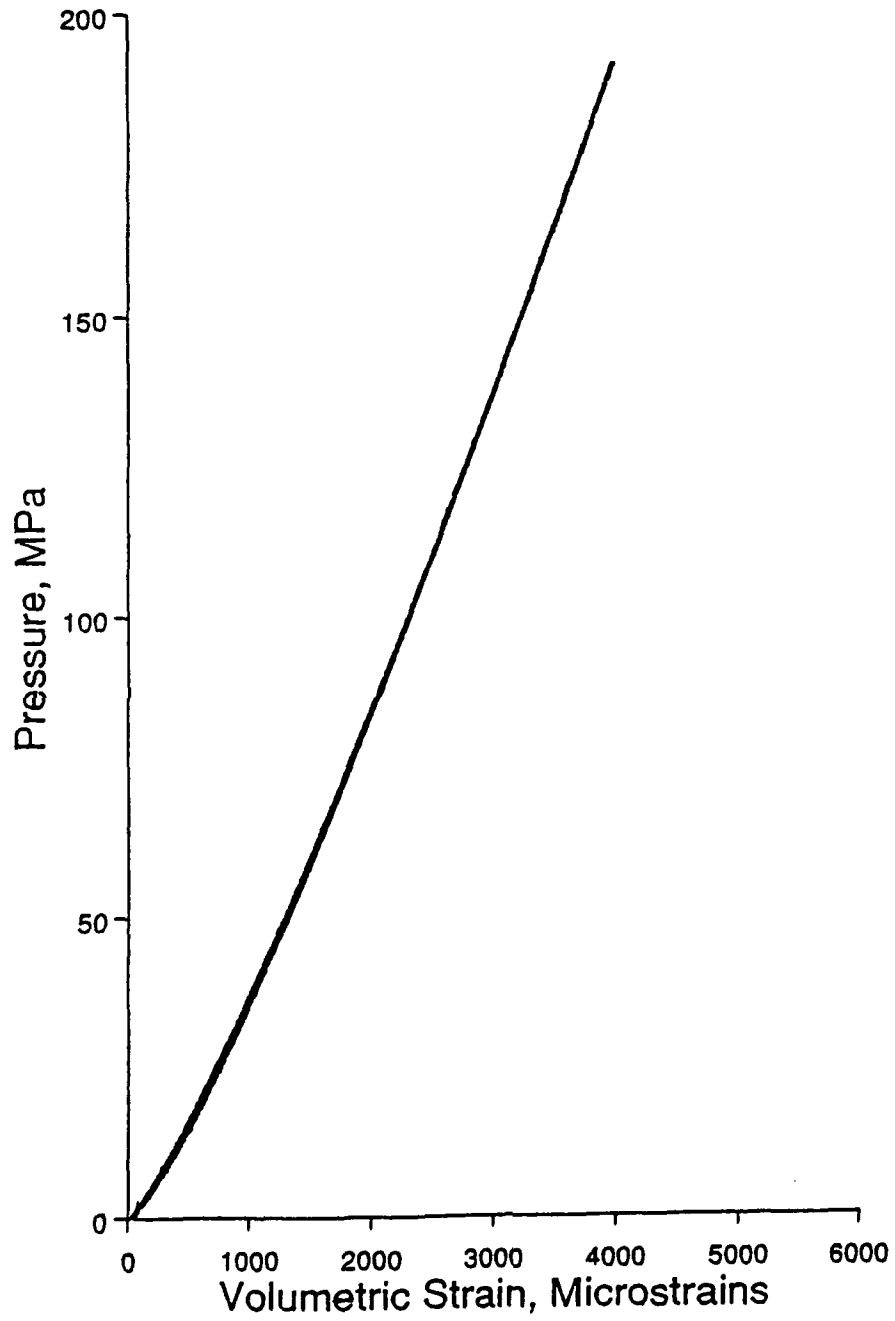


Figure 6

**BULK MODULUS
KATAHDIN AND SIERRA WHITE GRANITE
AND TUFFACEOUS SANDSTONE**

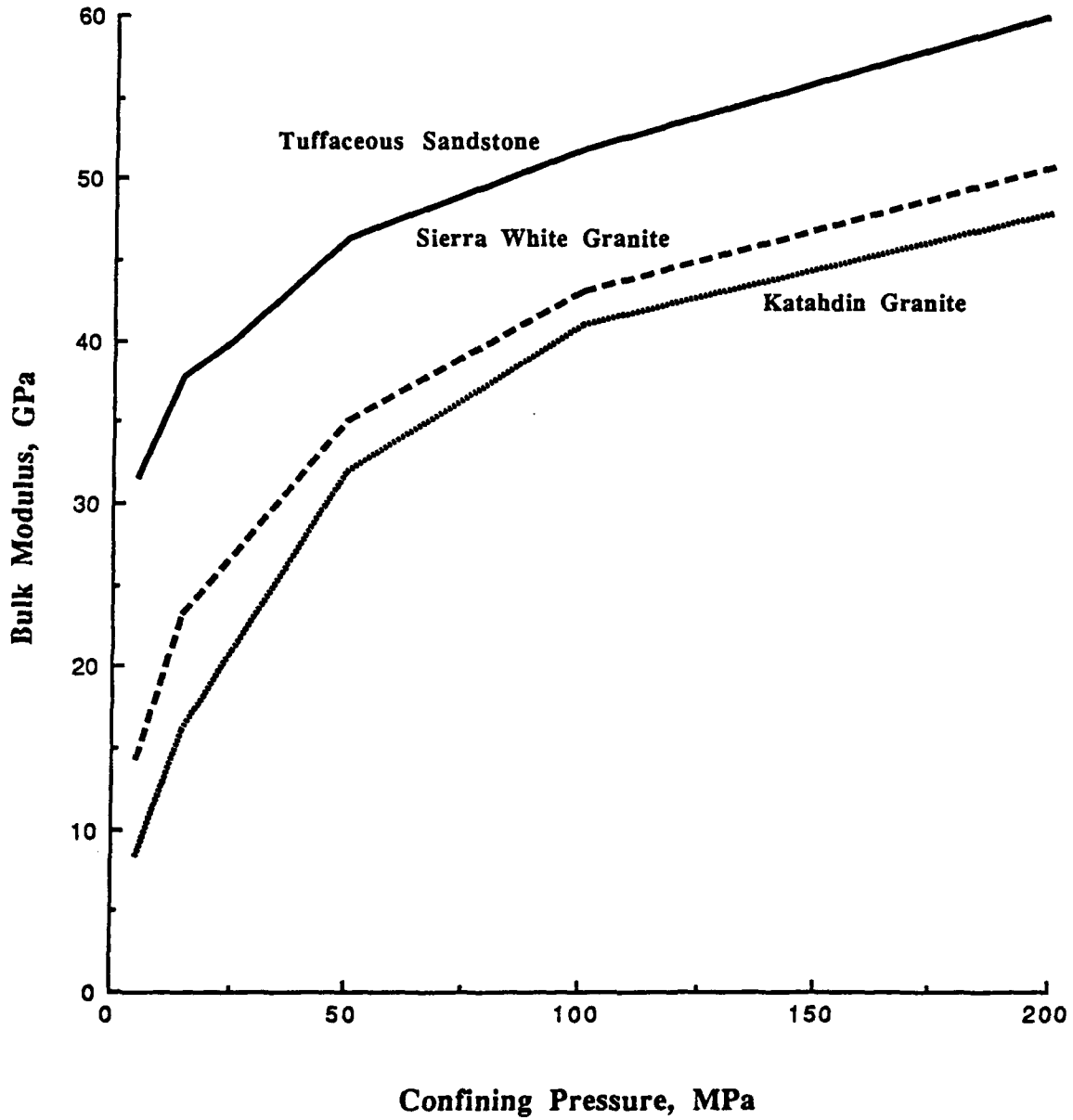


Figure 7

Failure Stress vs. Confining Pressure

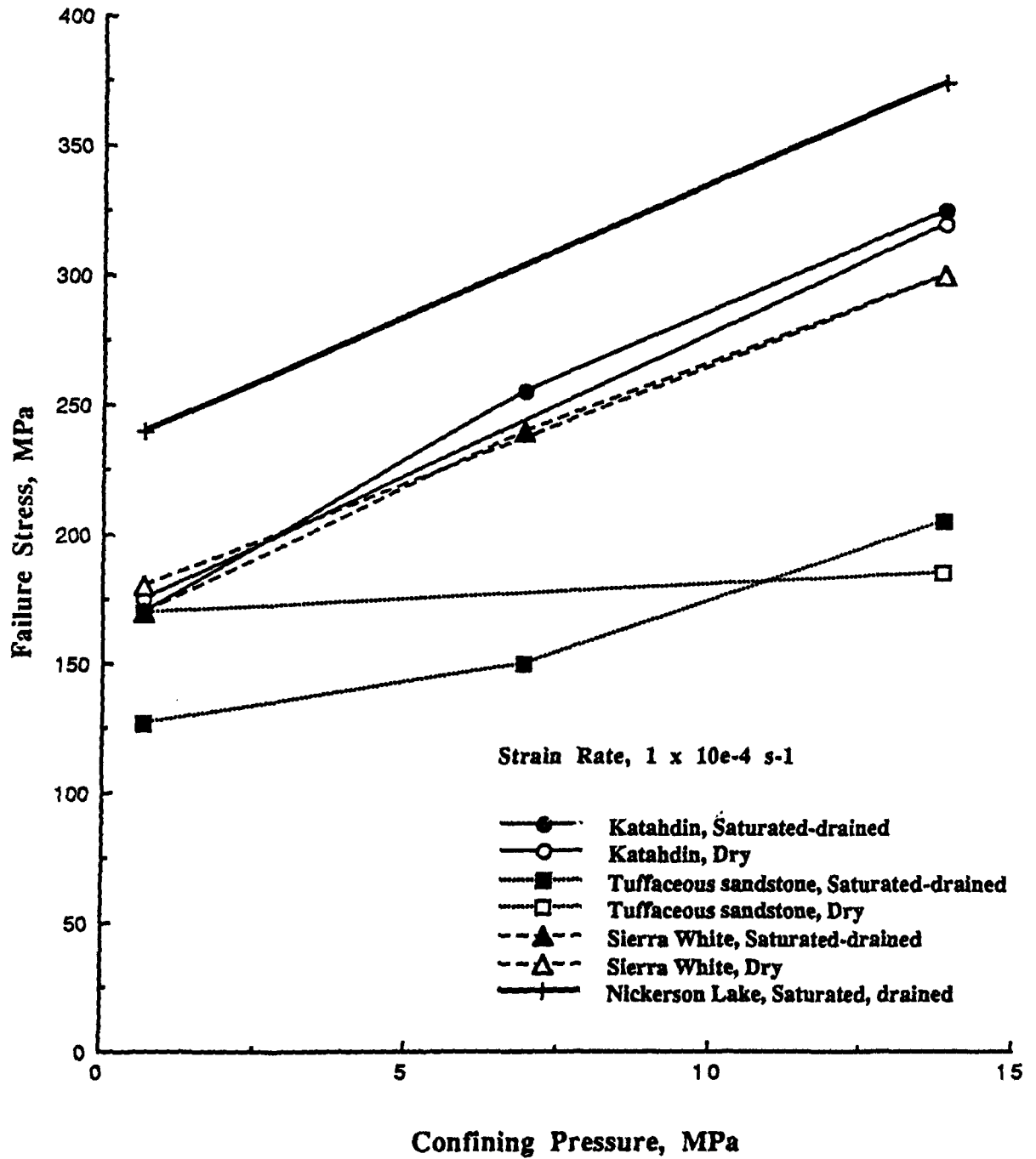


Figure 8

Failure Stress vs. Confining Pressure

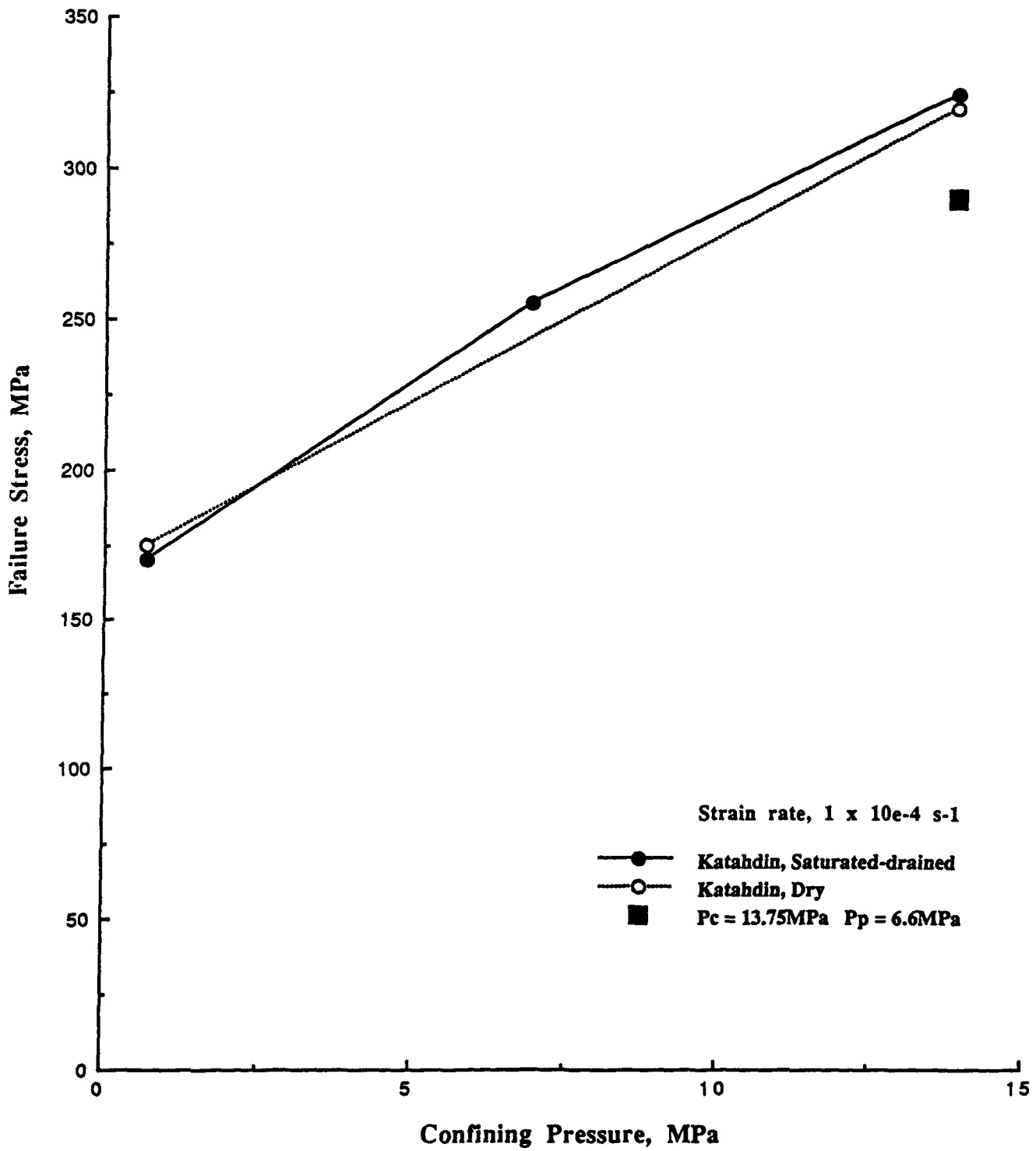


Figure 9

Failure Stress vs. Confining Pressure

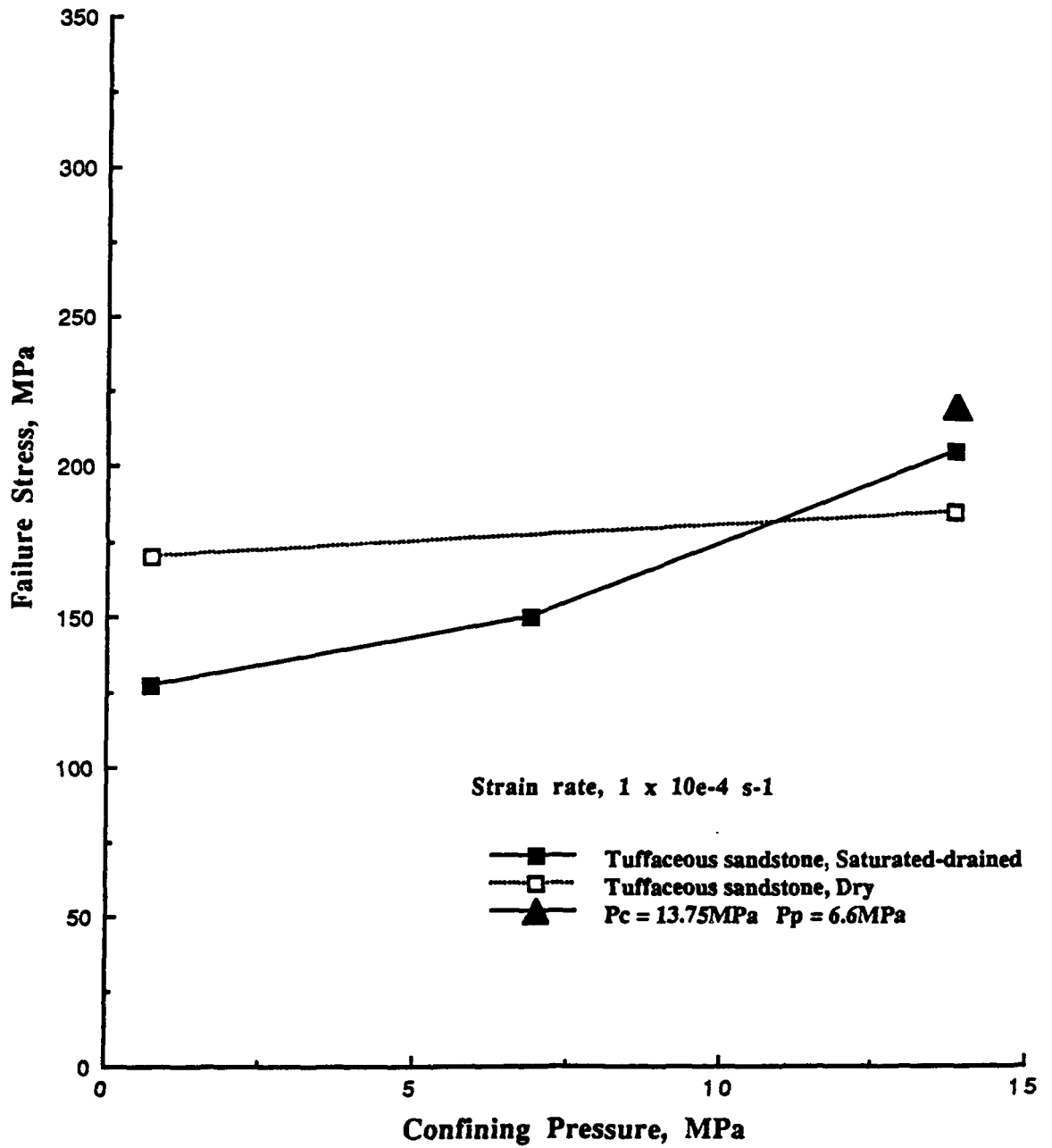


Figure 10

Failure Stress vs. Confining Pressure

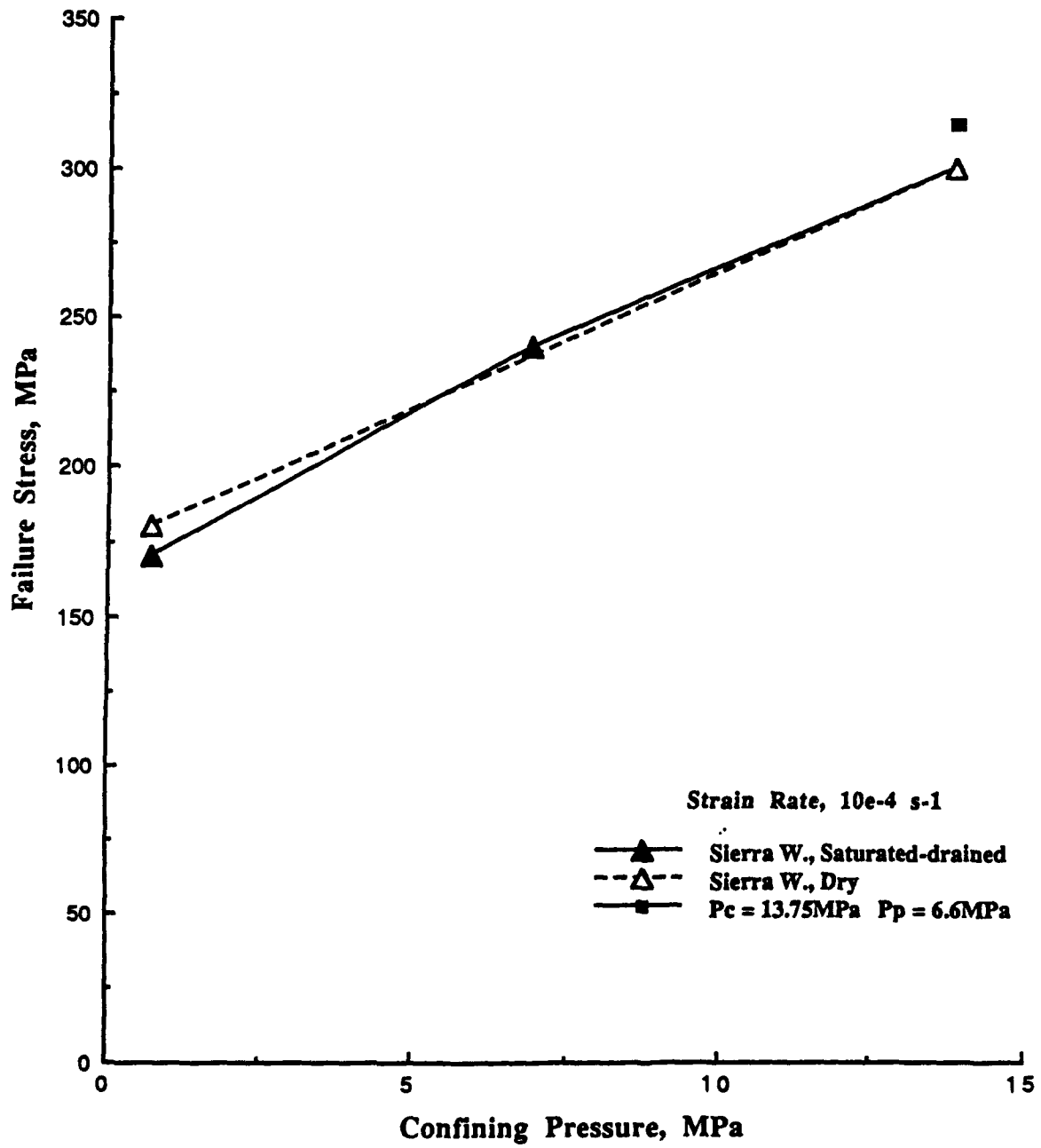


Figure 11

FAILURE STRESS VS. STRAIN RATE

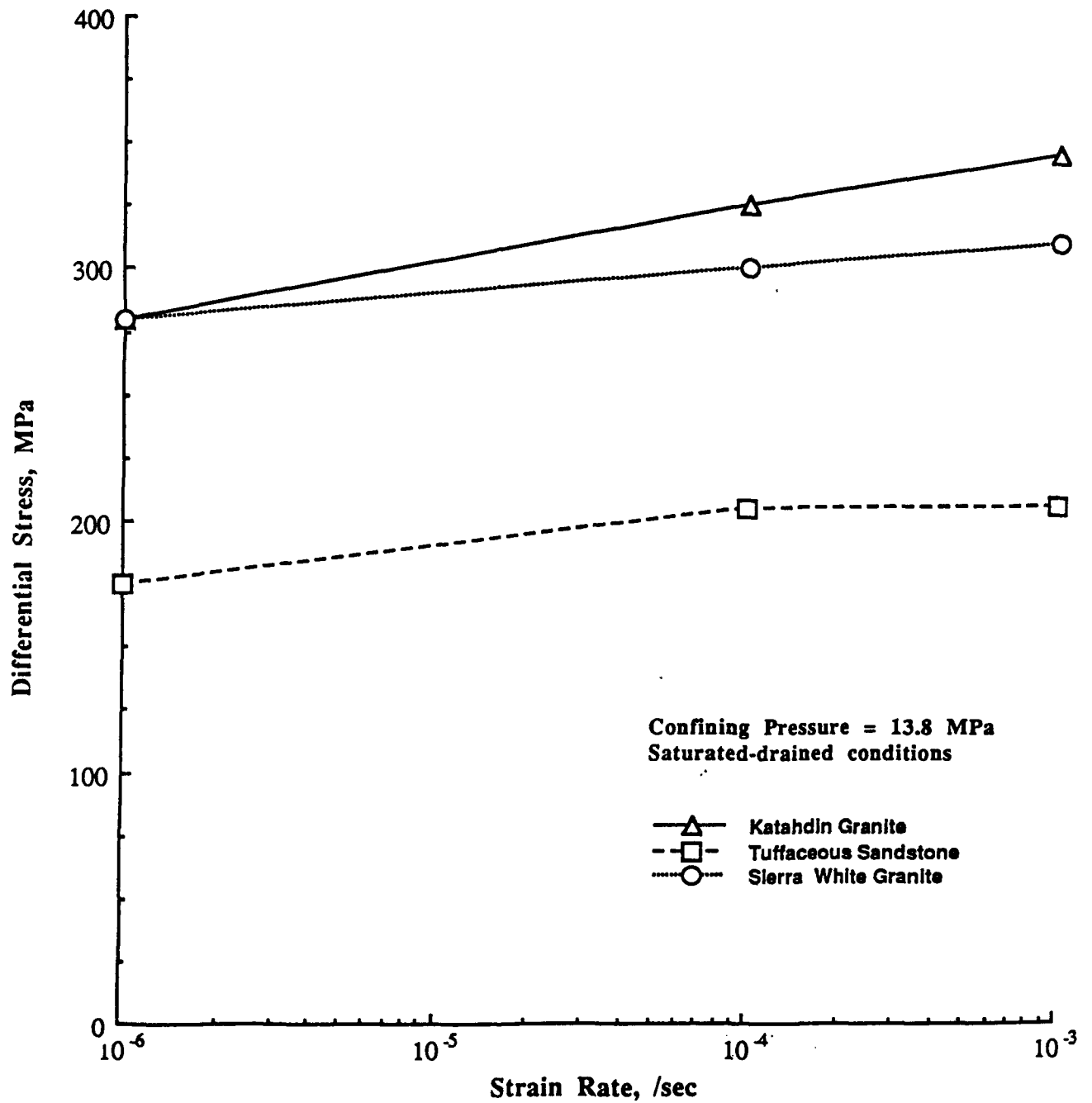


Figure 12

1 ——— KG18
 2 - - - - KG18
 3 - - - - KG18

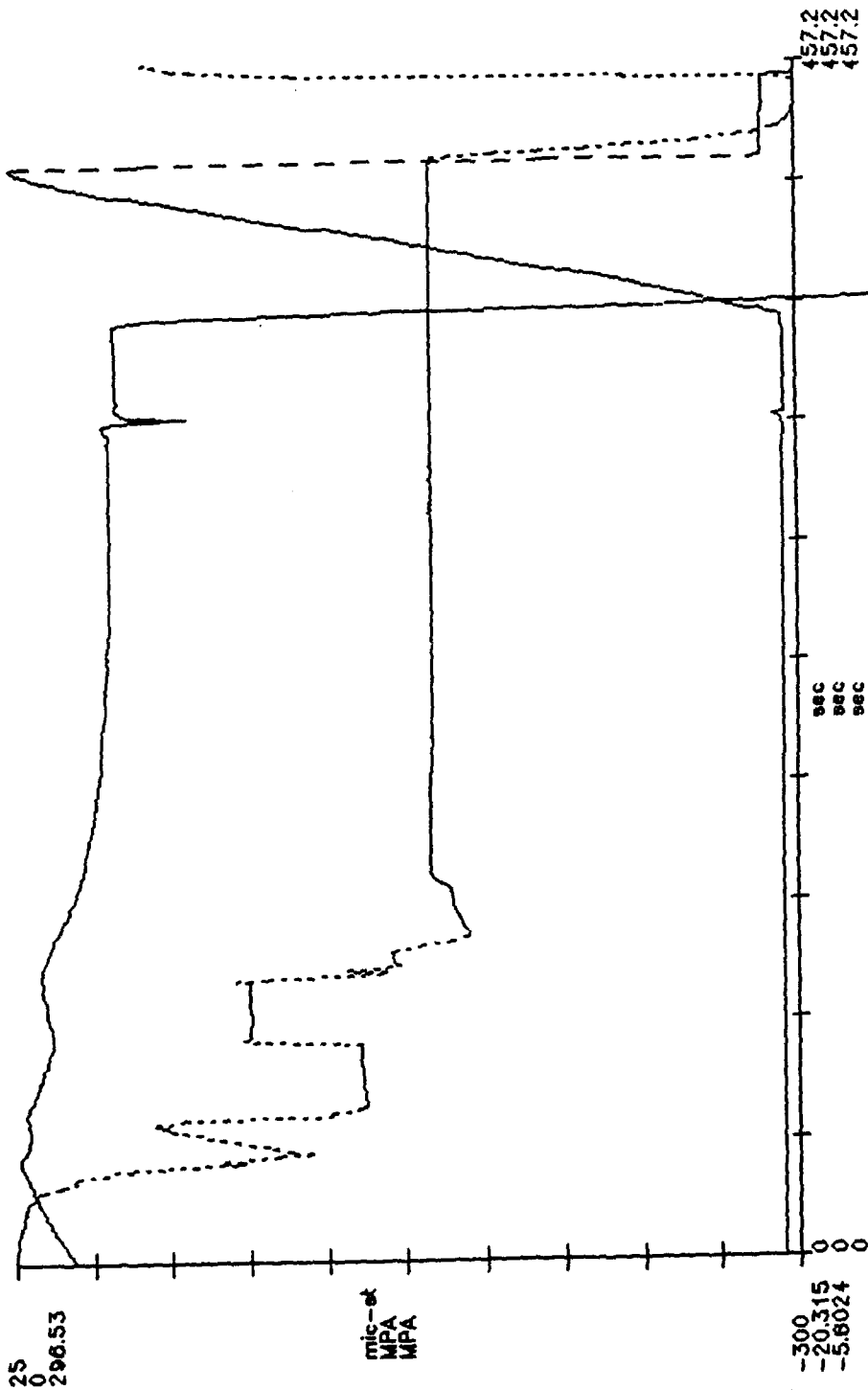


Figure 13

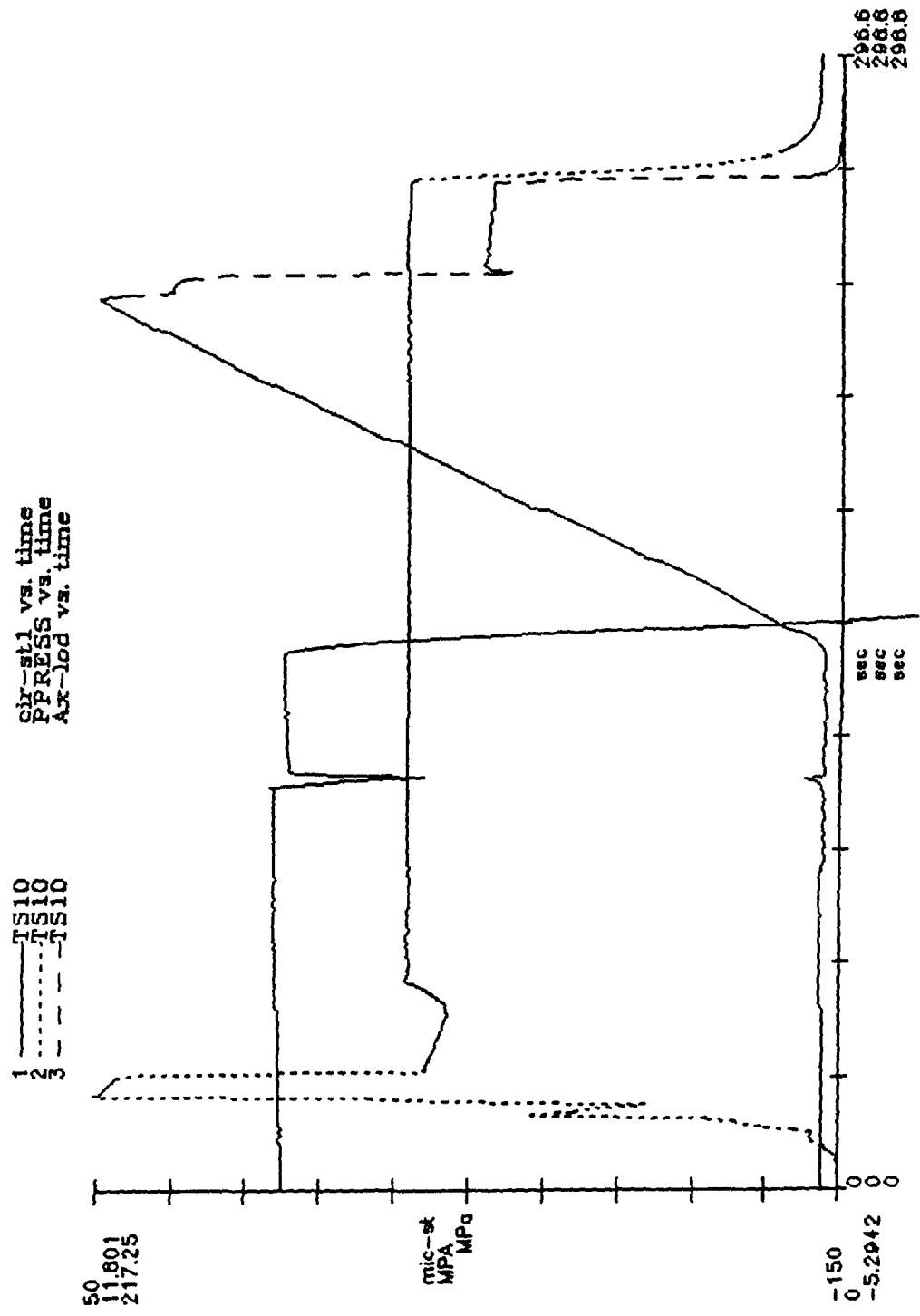


Figure 14

1 cr-st1 vs. time
 2 PRESS vs. time
 3 AX-LOD vs. time

1 SW6
 2 SW6
 3 SW6

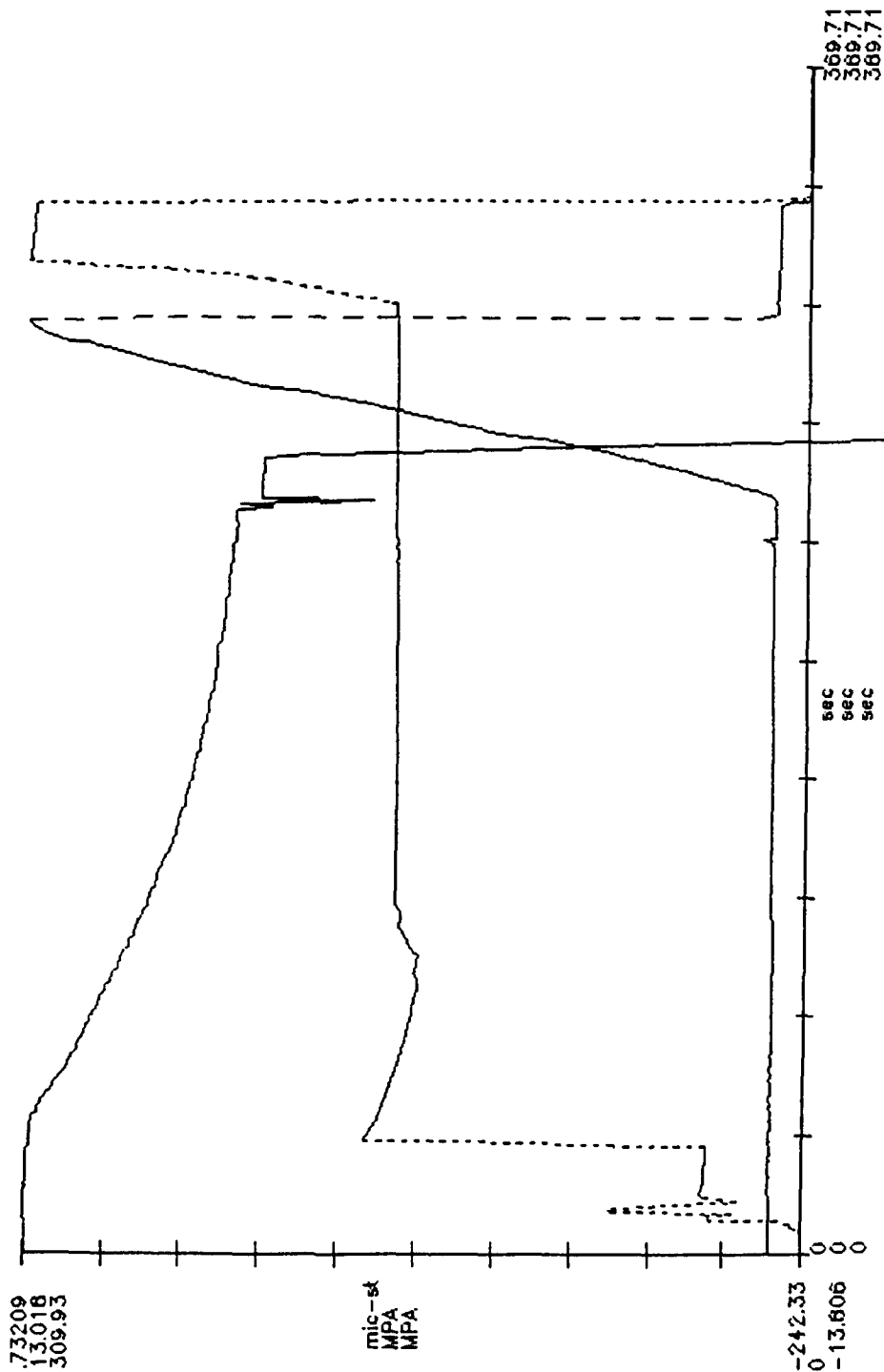


Figure 15

KG 5

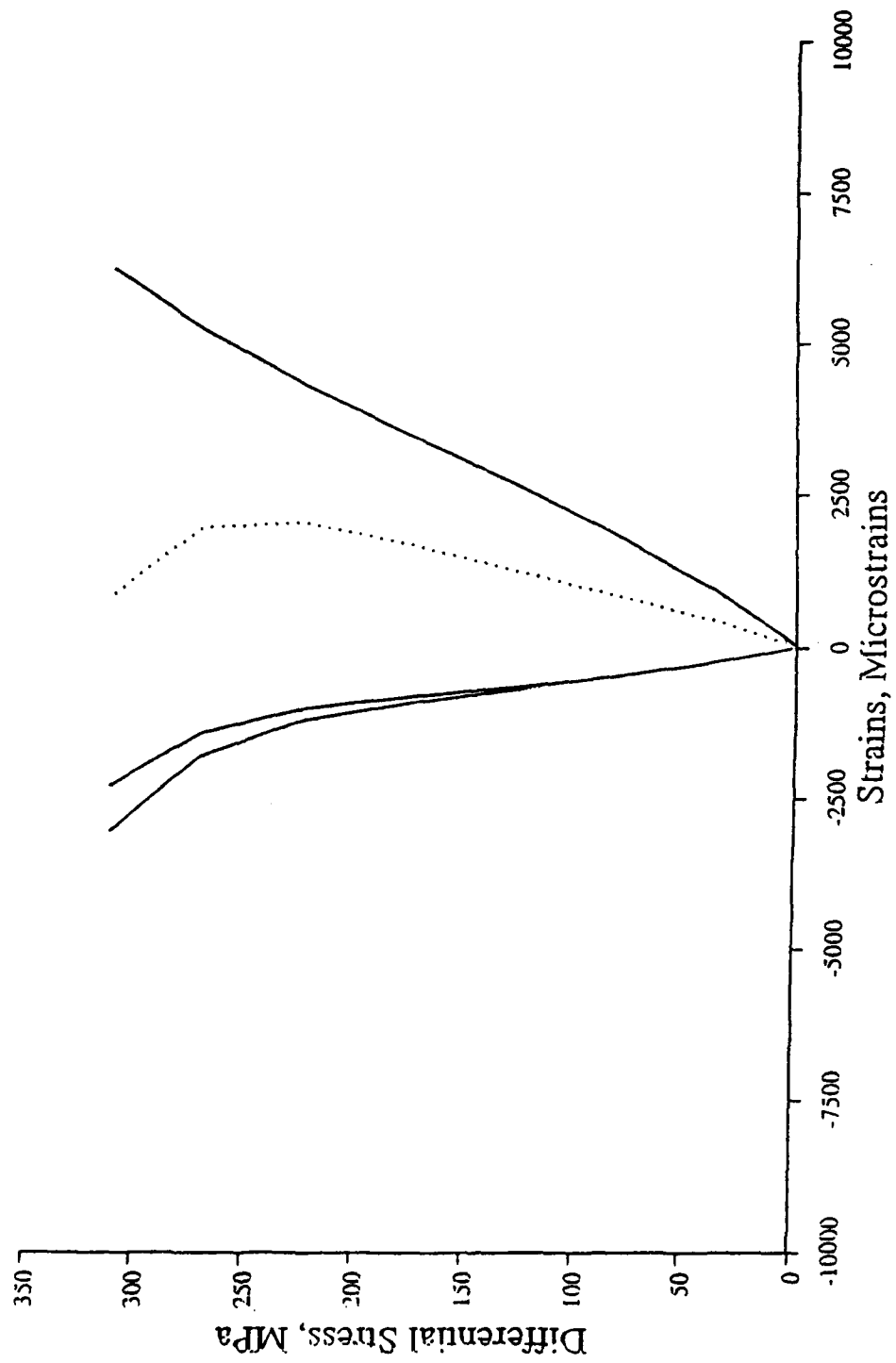


Figure 16

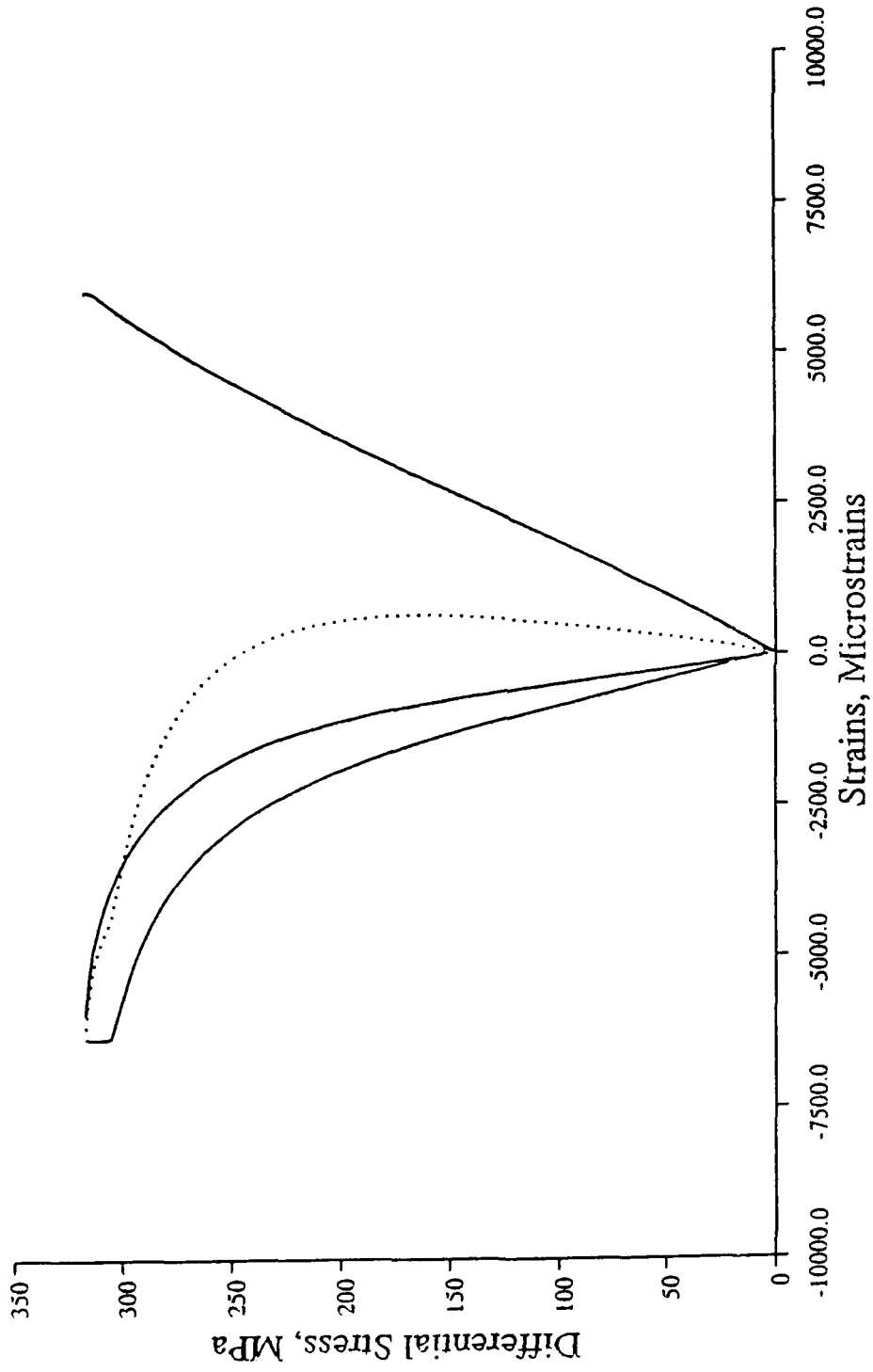


Figure 17

KG 6

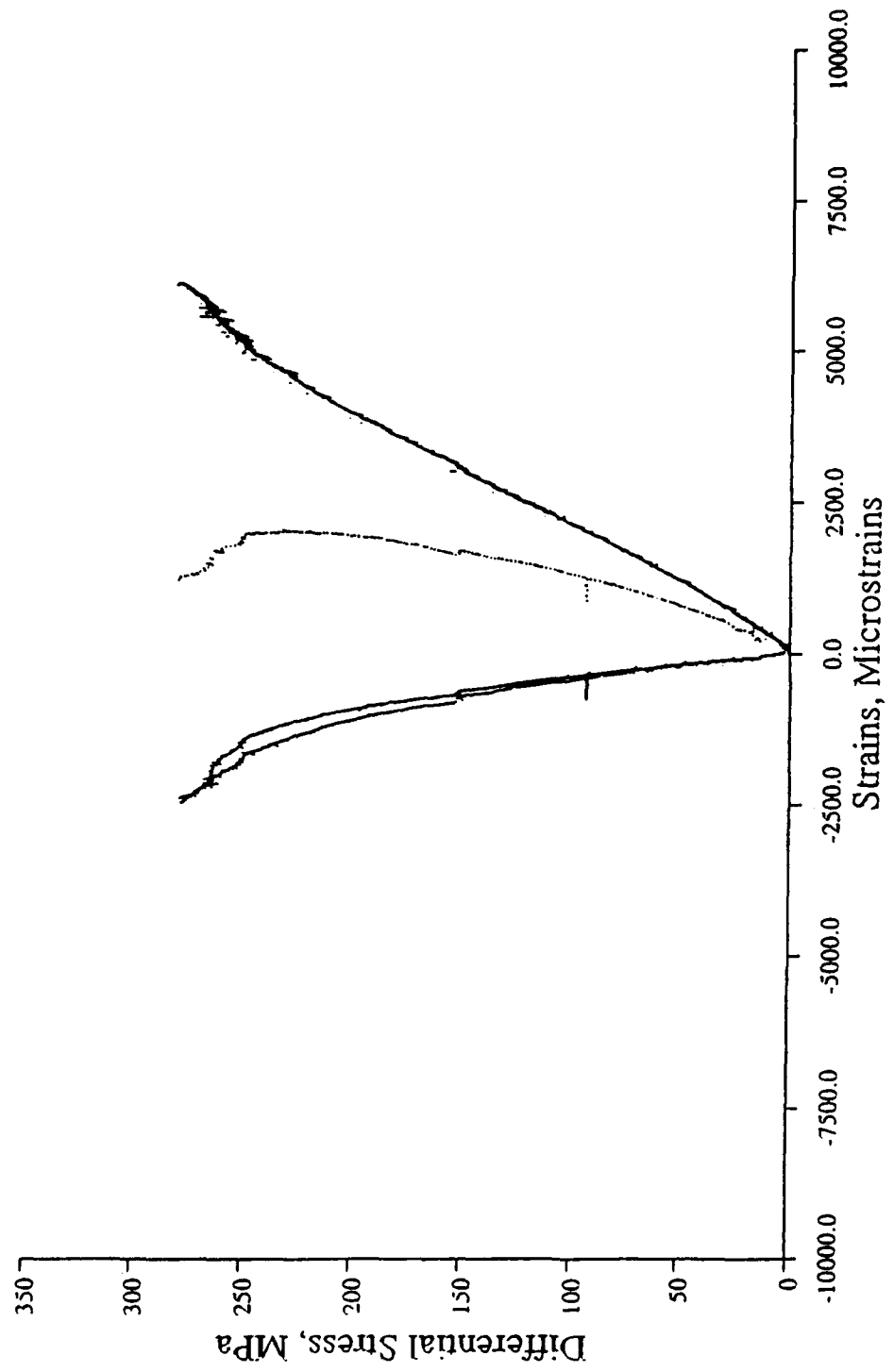


Figure 18

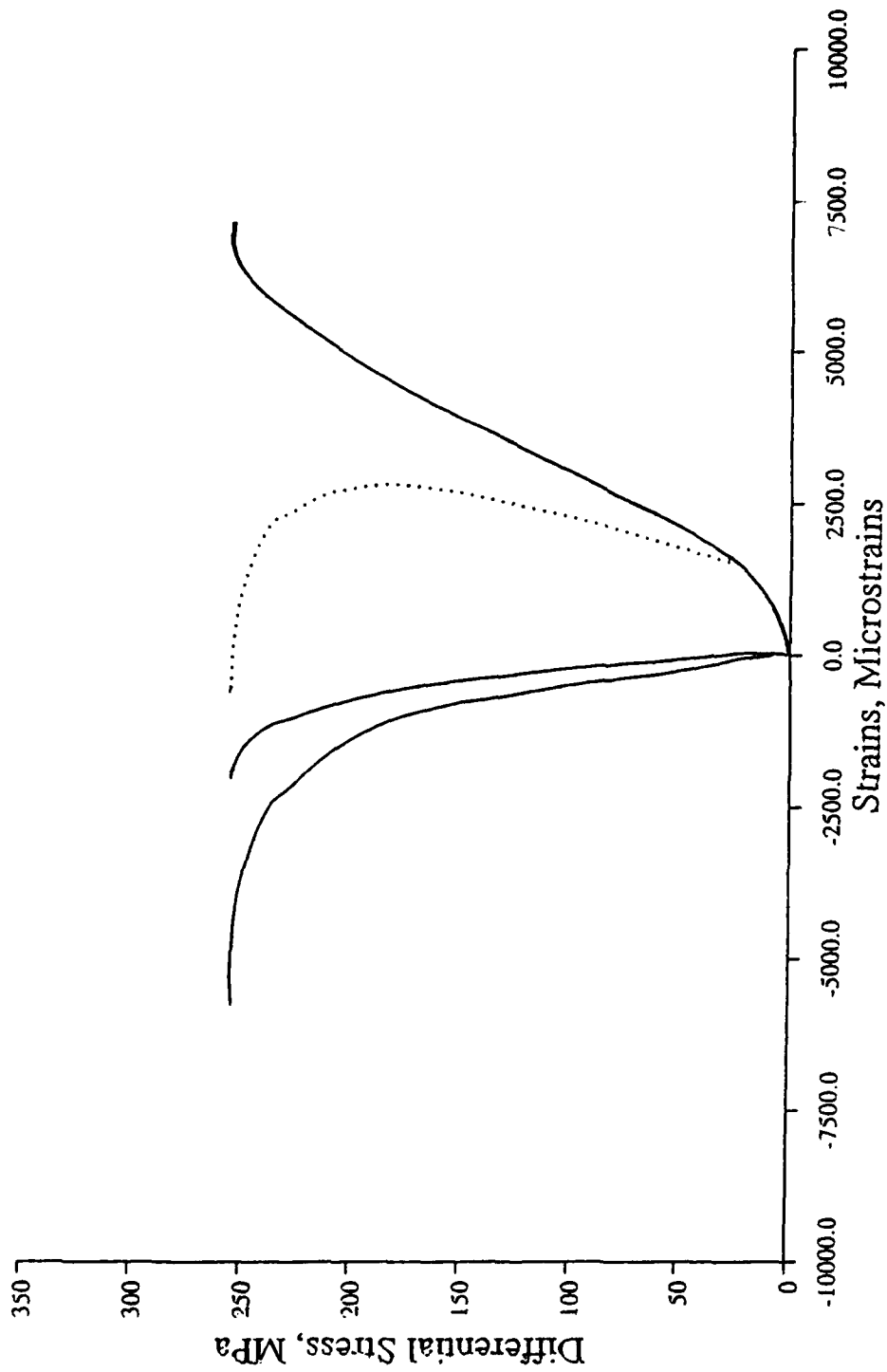


Figure 19

KG 18

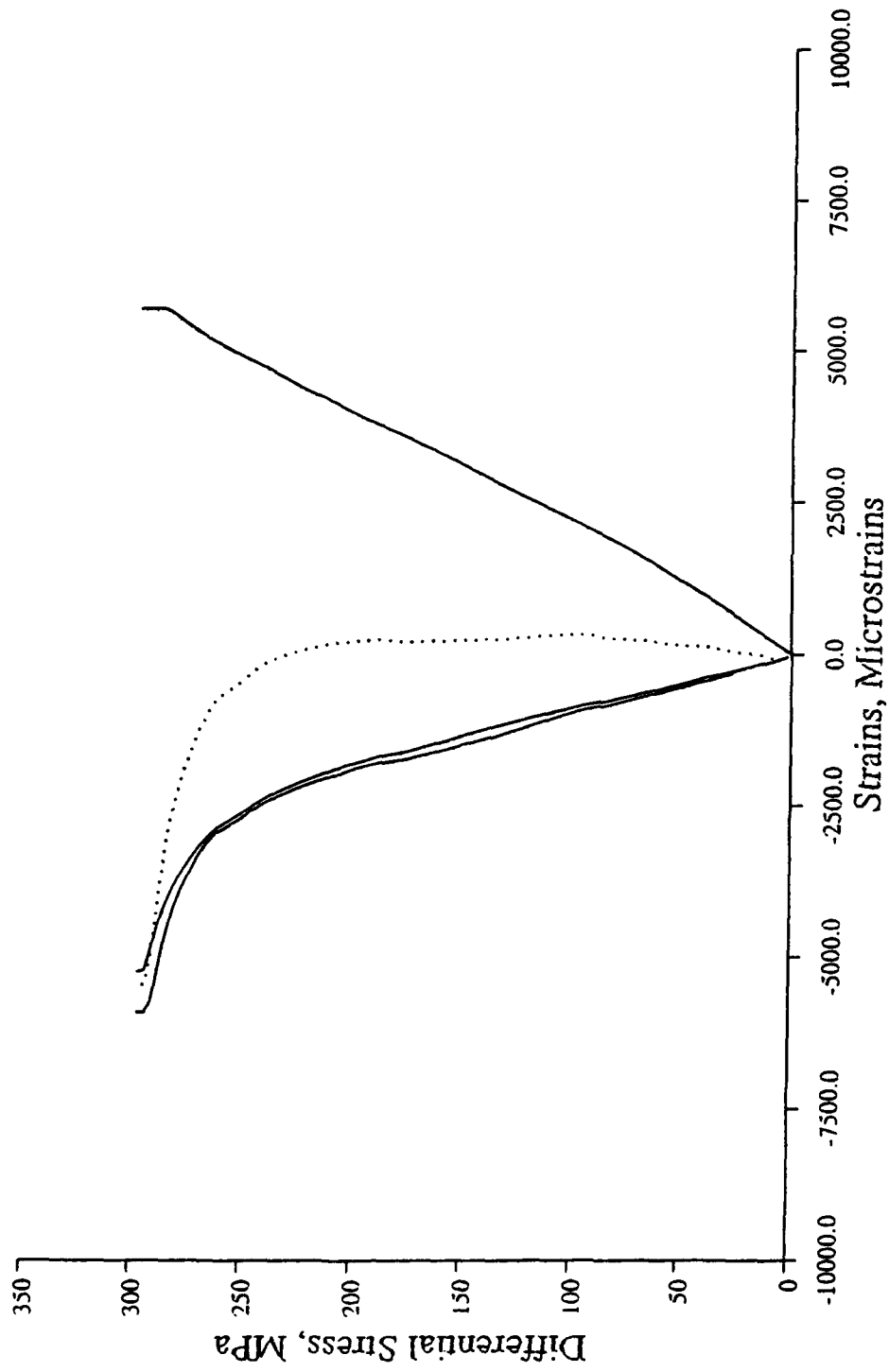


Figure 20

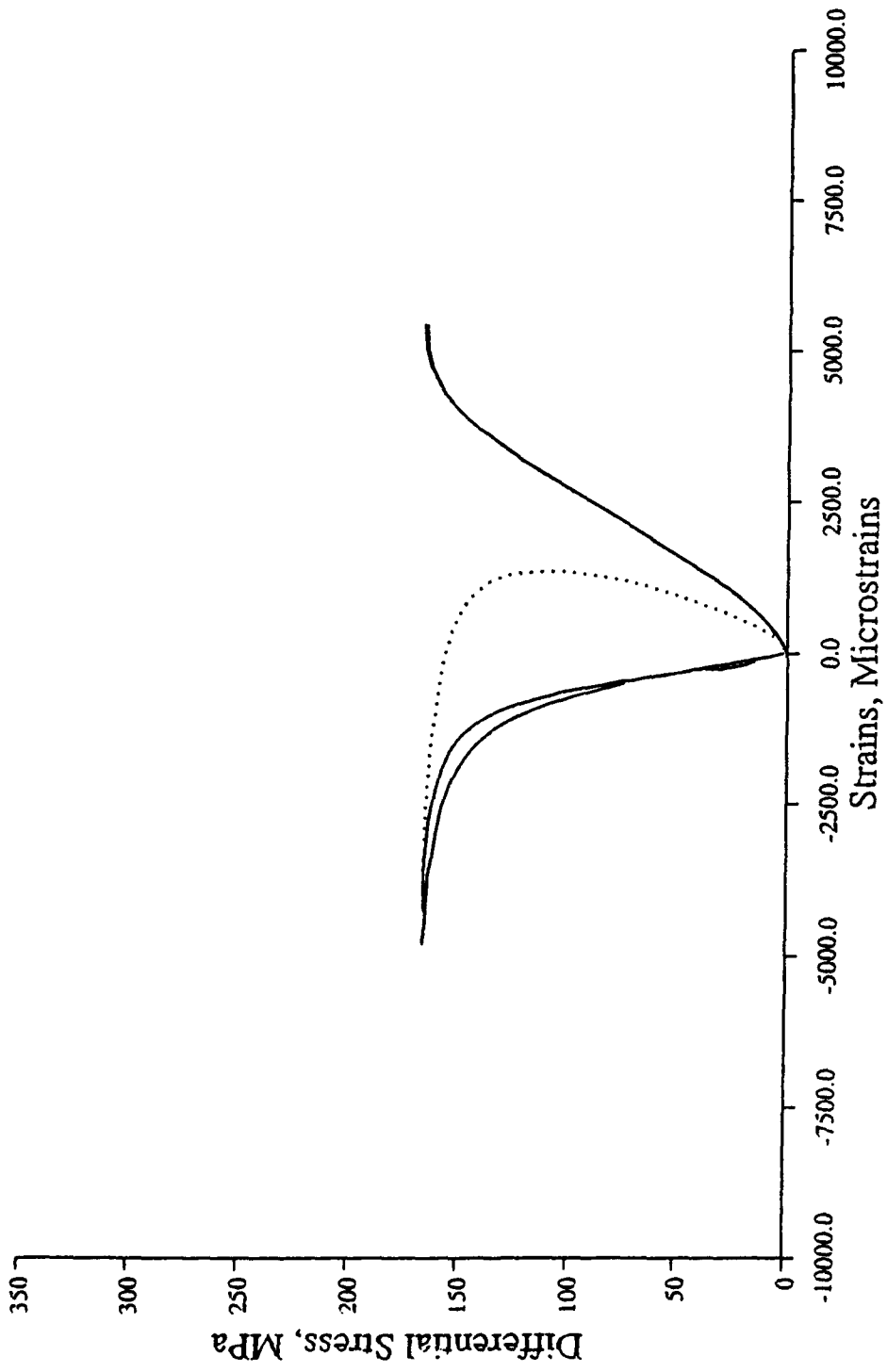


Figure 21

KG 20

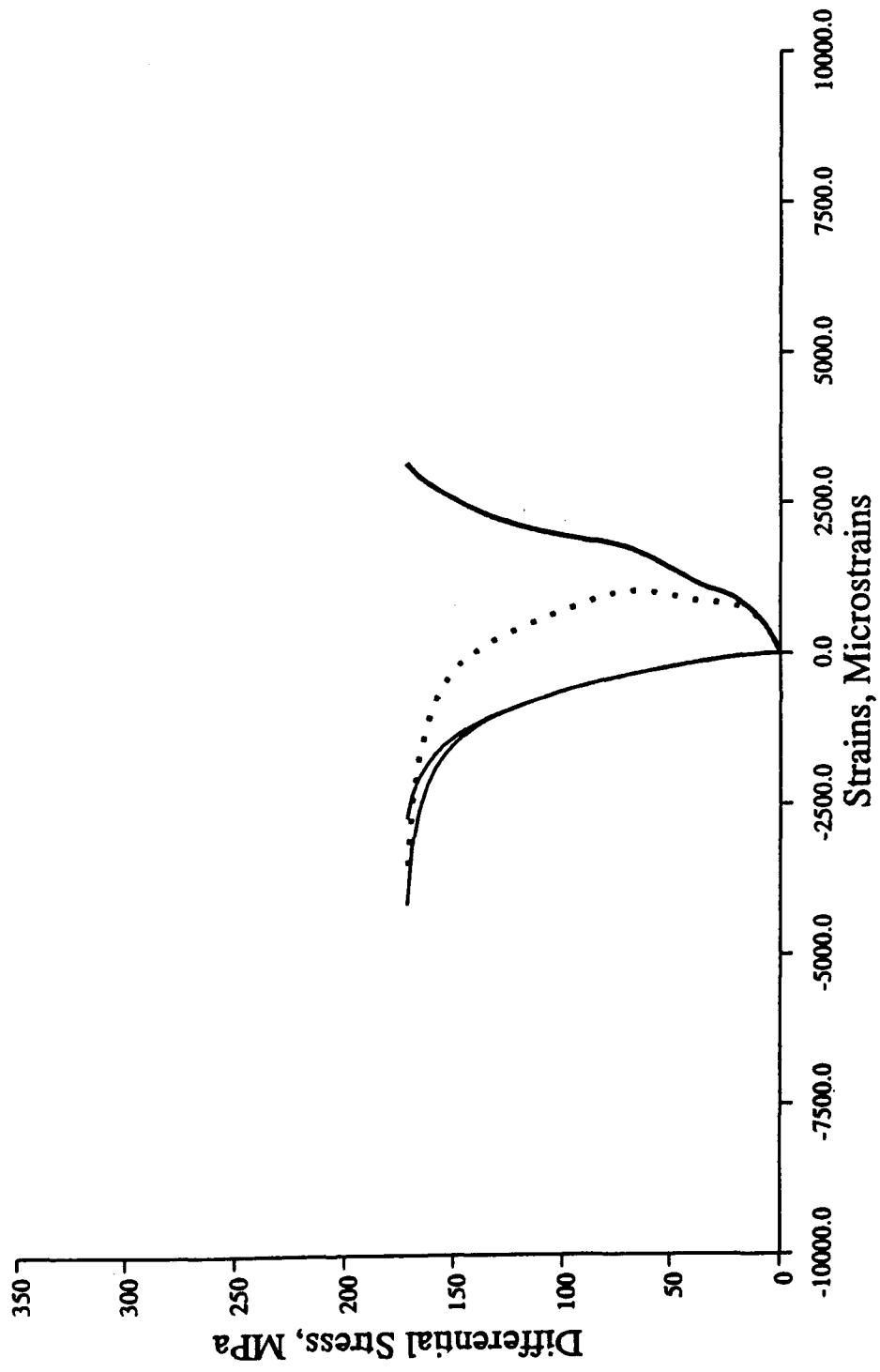


Figure 22

KG 4

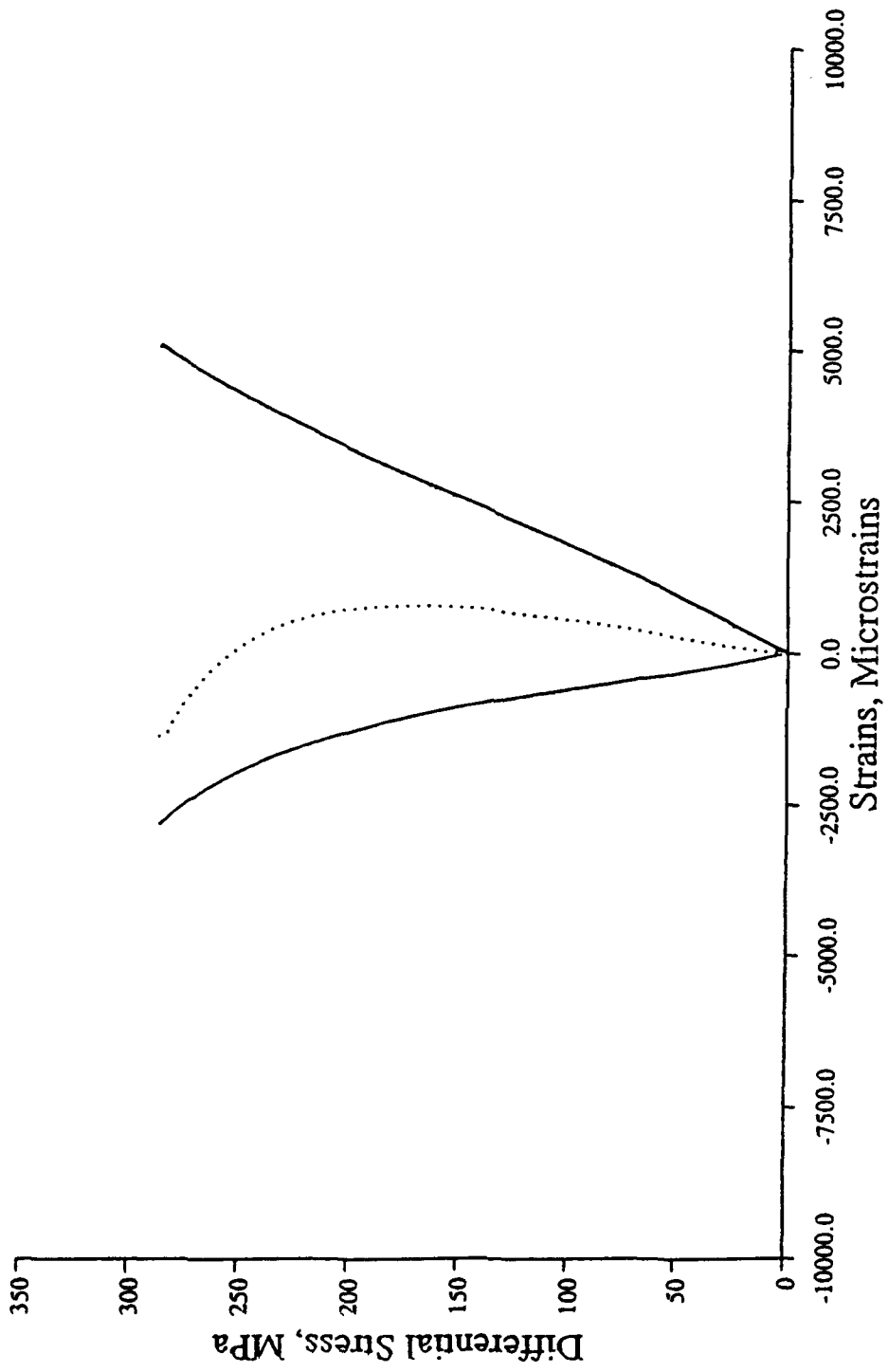


Figure 23

TS 7

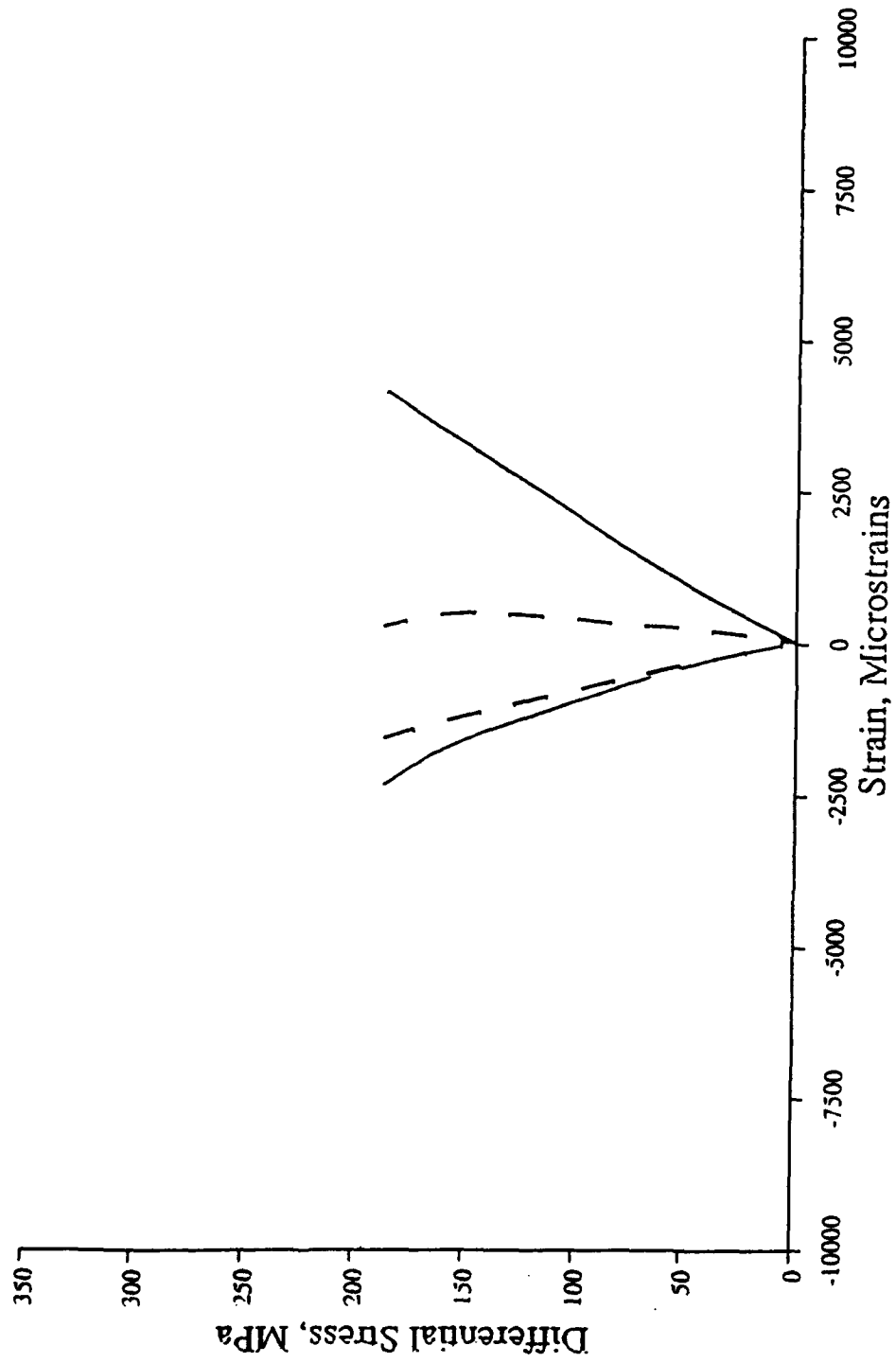


Figure 24

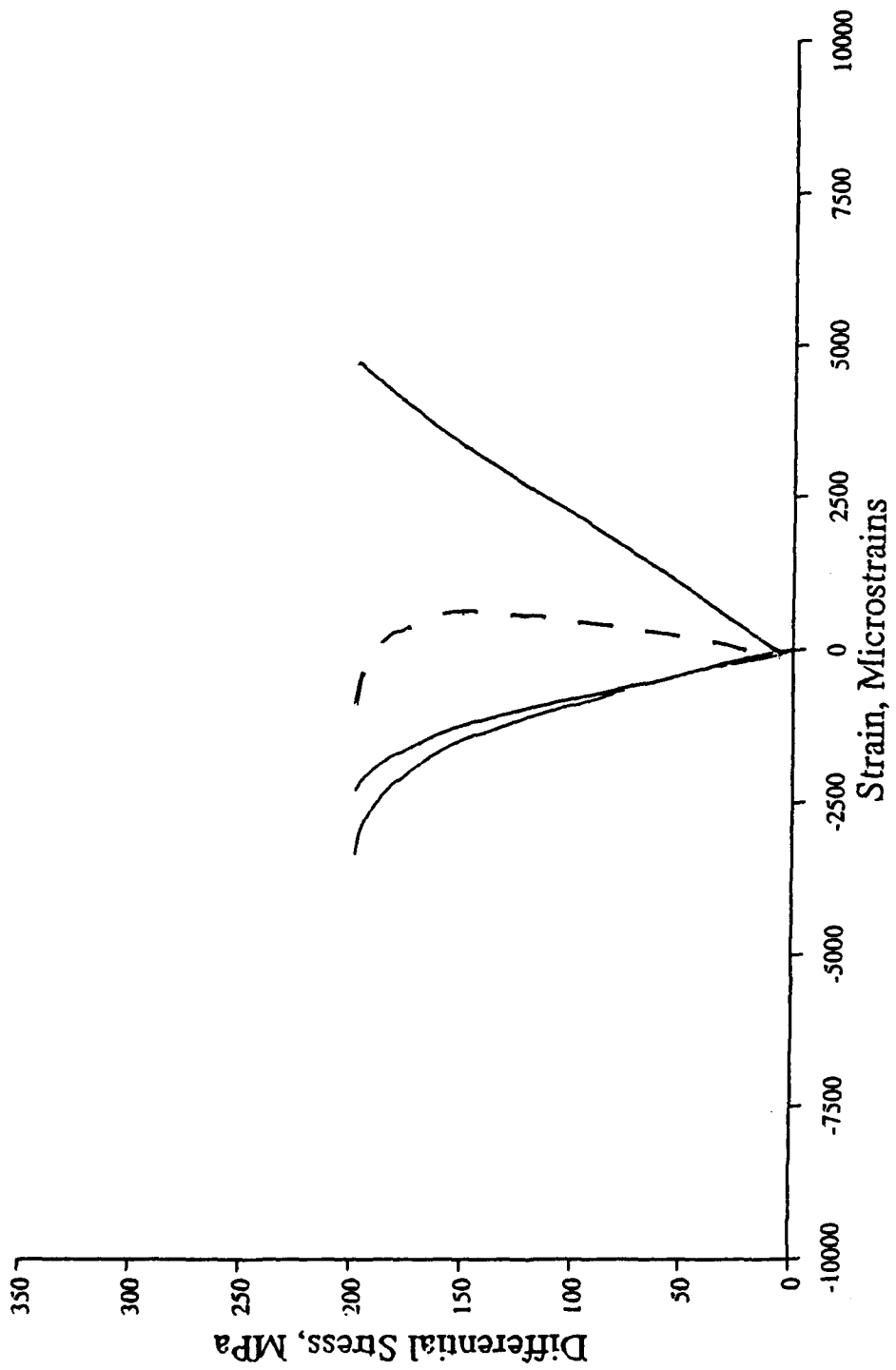


Figure 25

TS 9

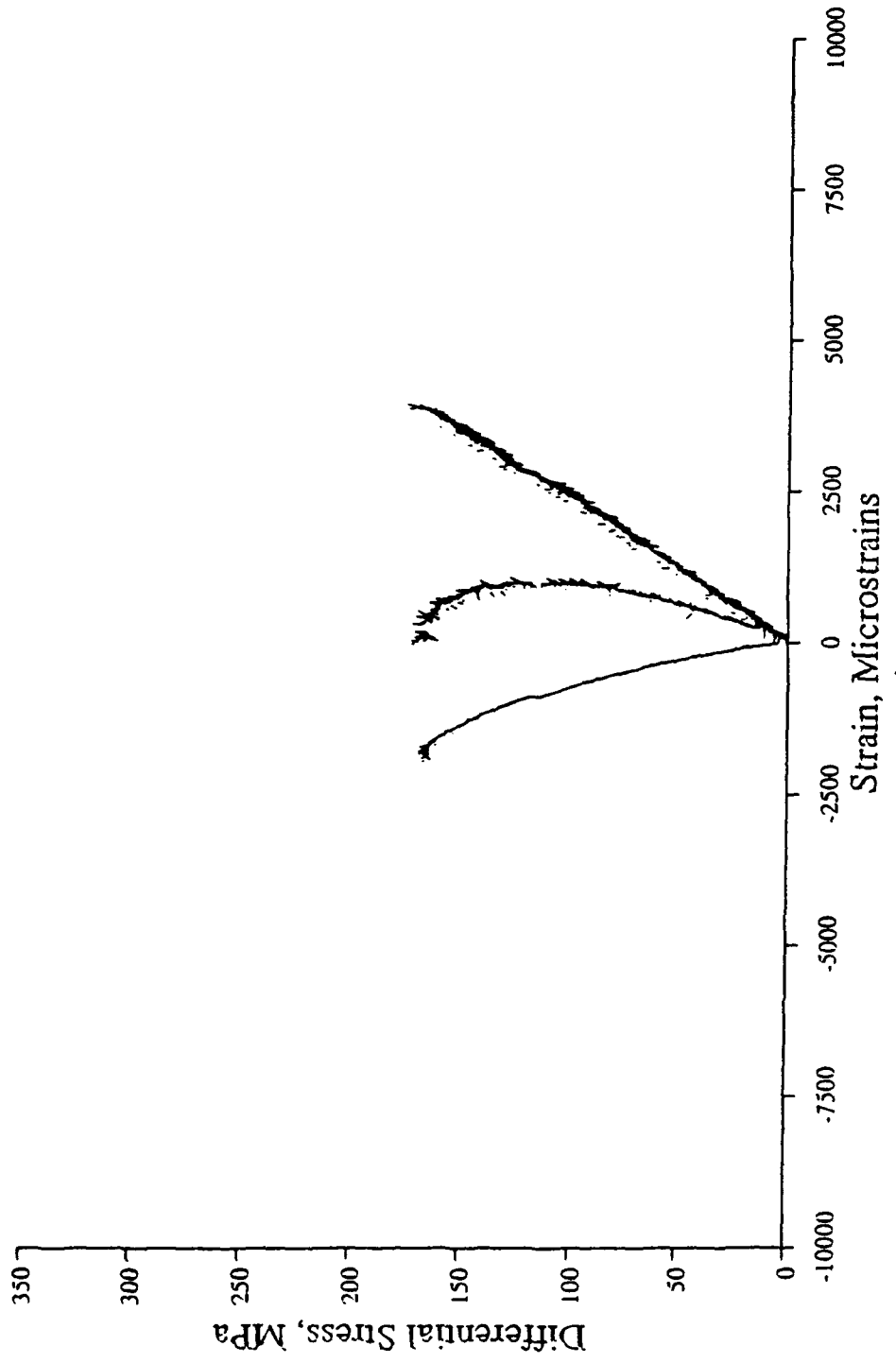


Figure 26

TS 8

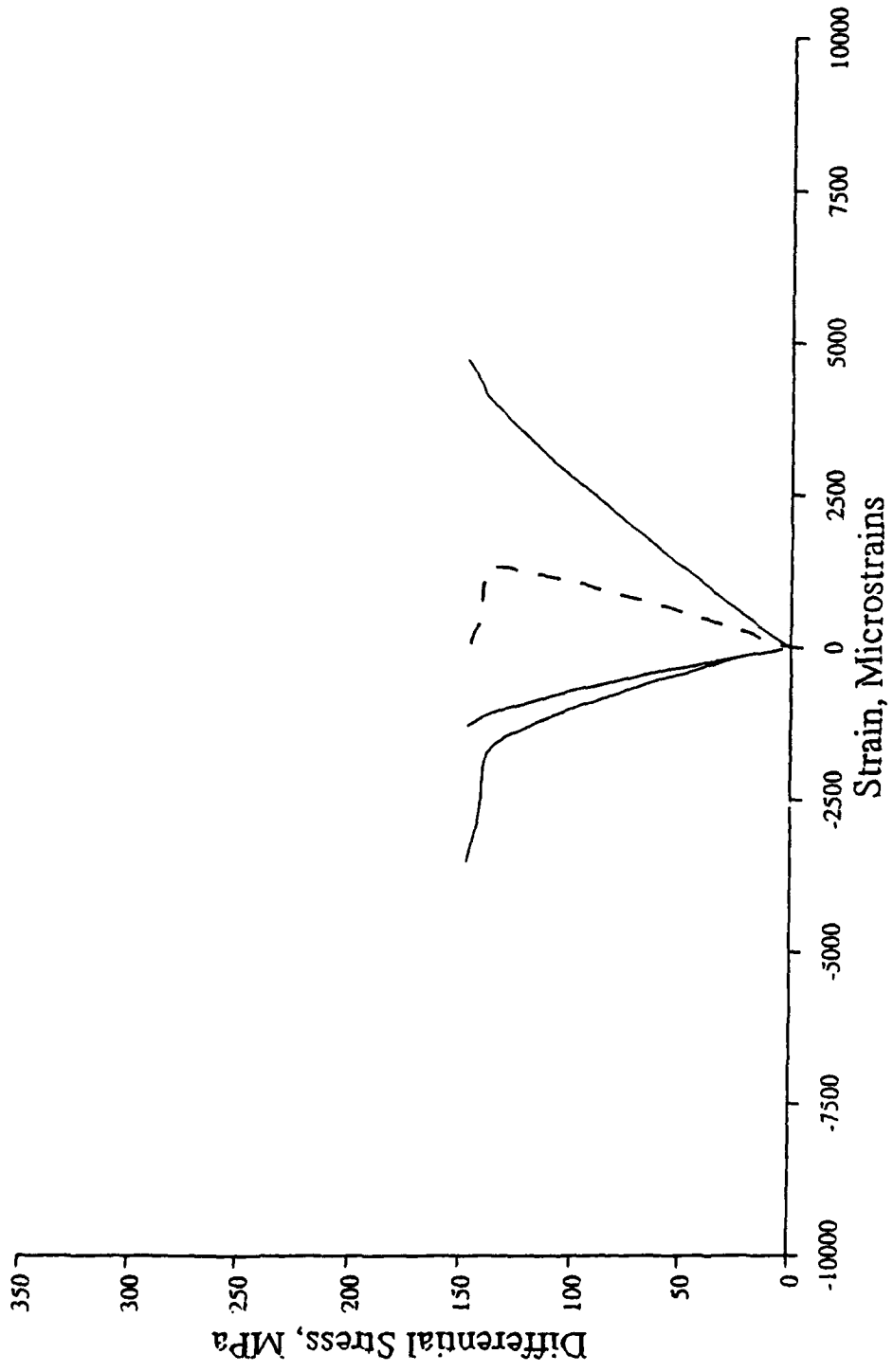


Figure 27

TS 10

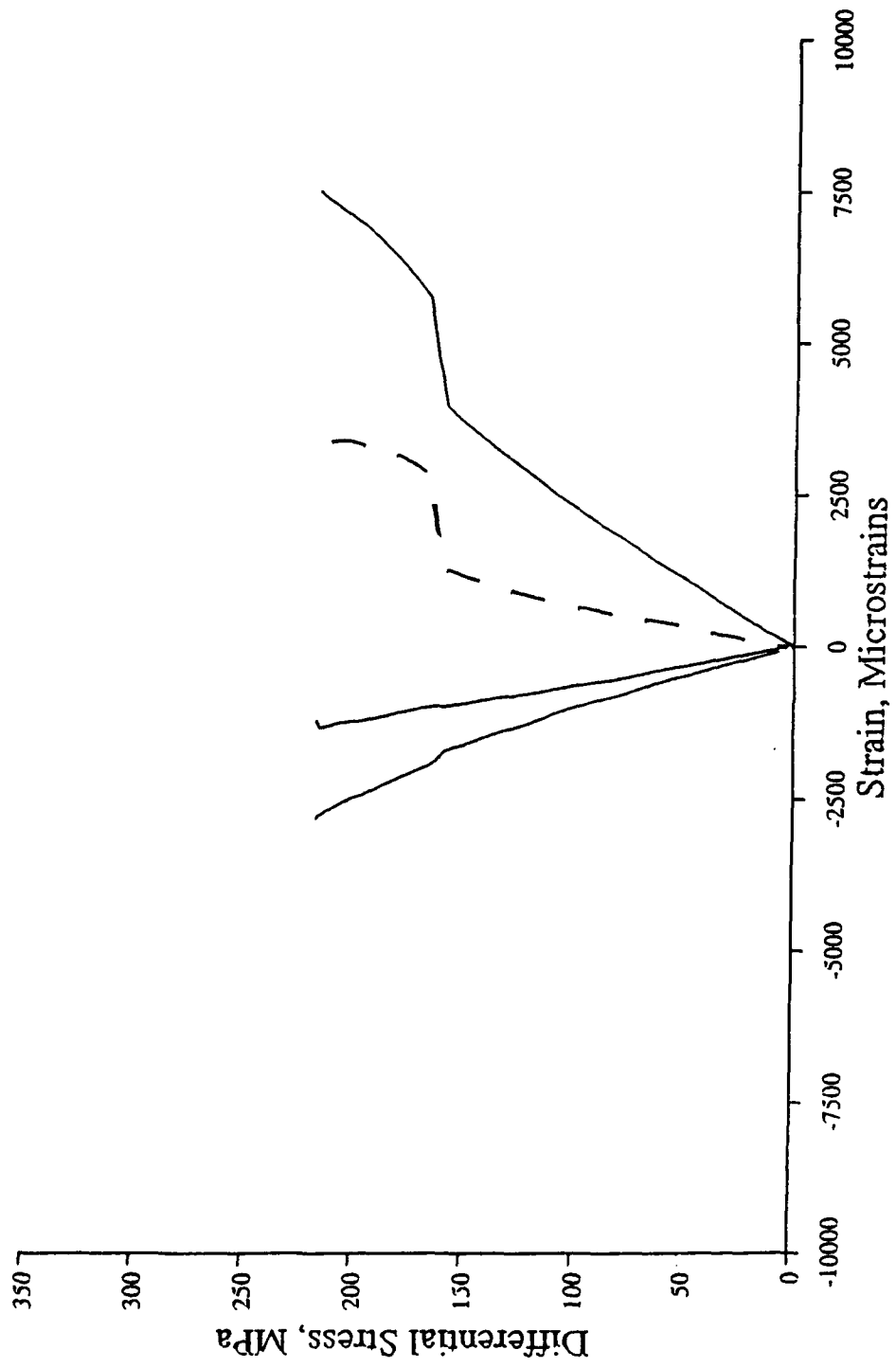


Figure 28

TS 2

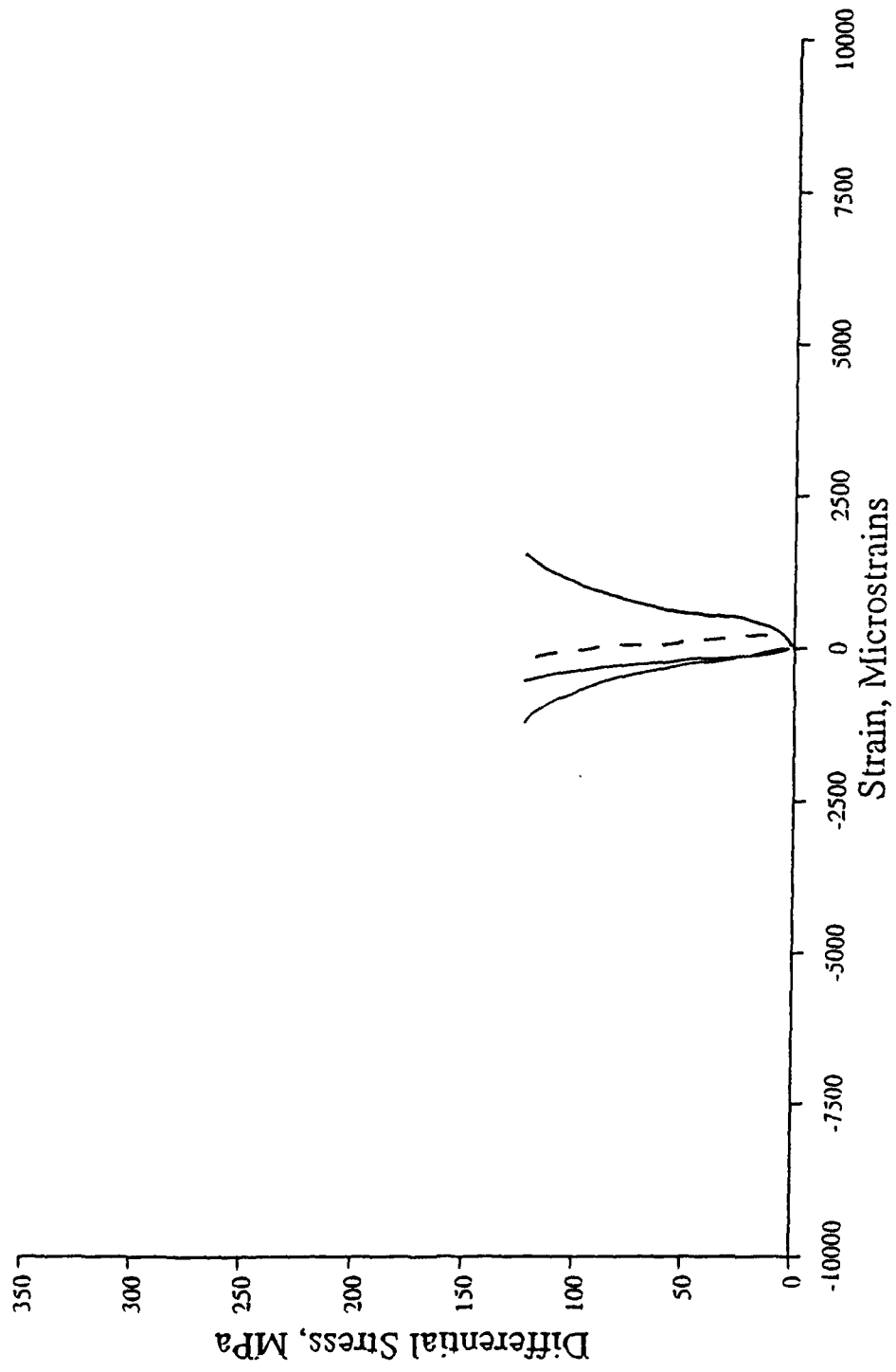


Figure 29

TS 4

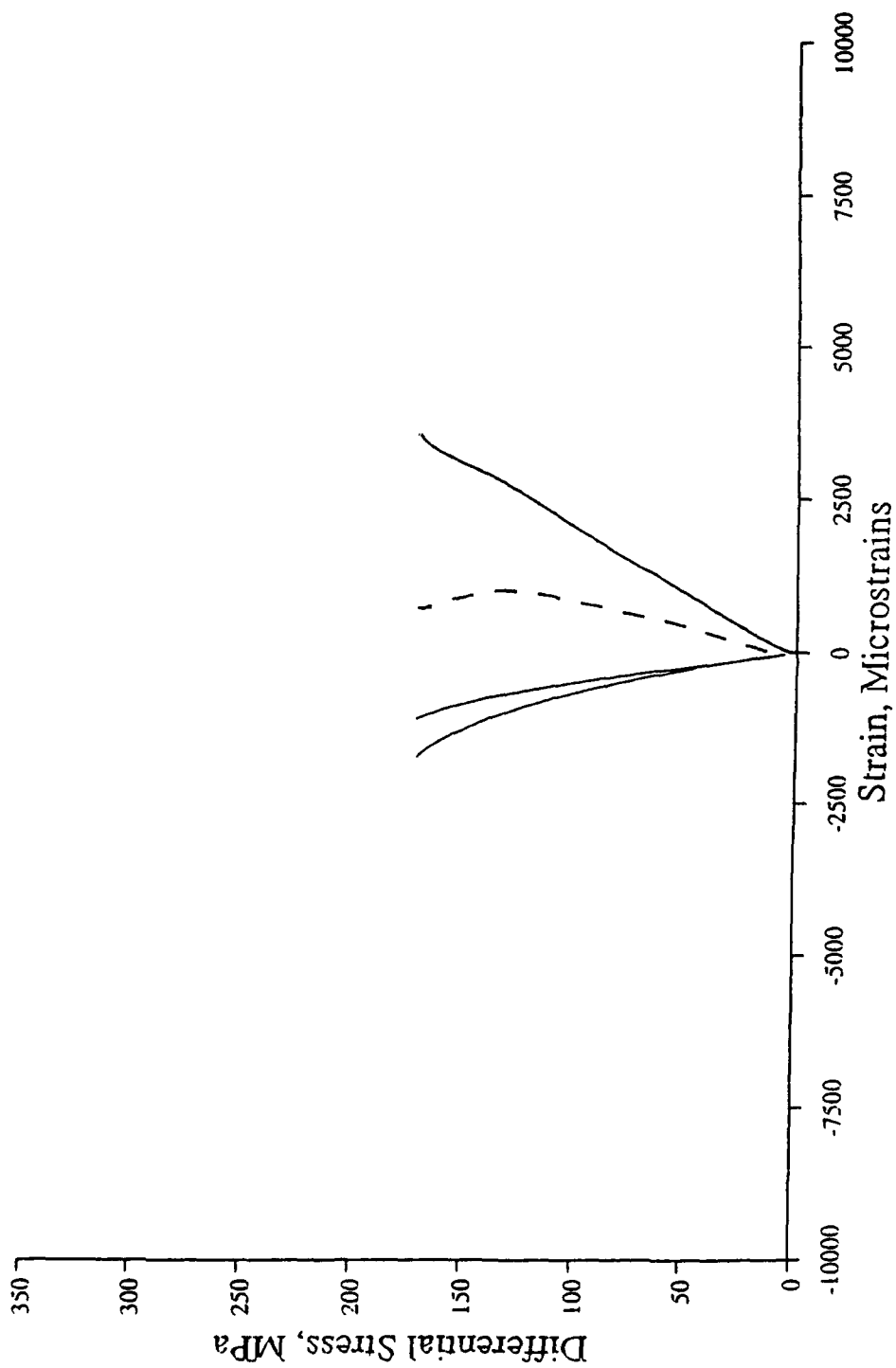


Figure 30

TS 6

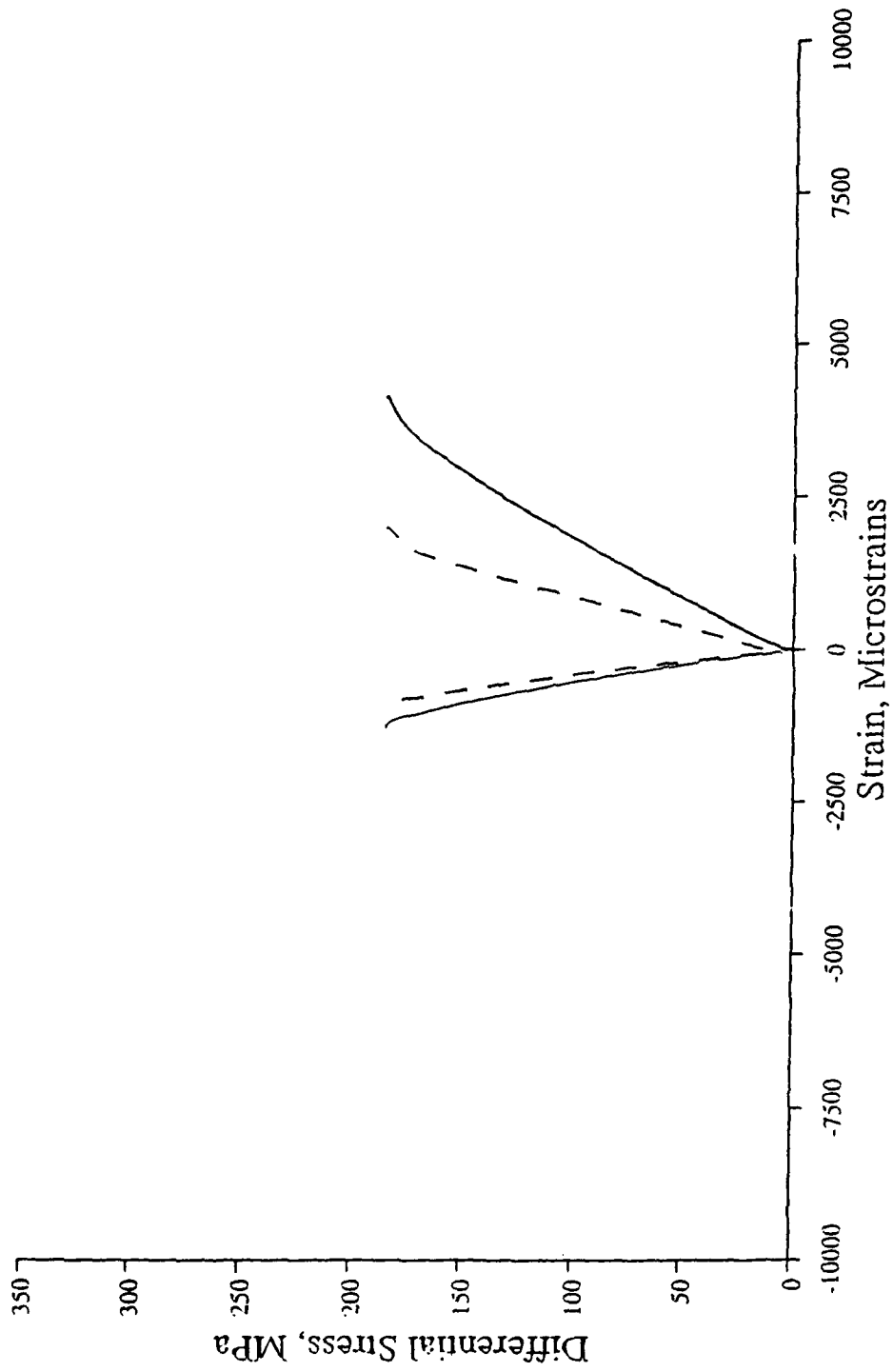


Figure 31

SW 1

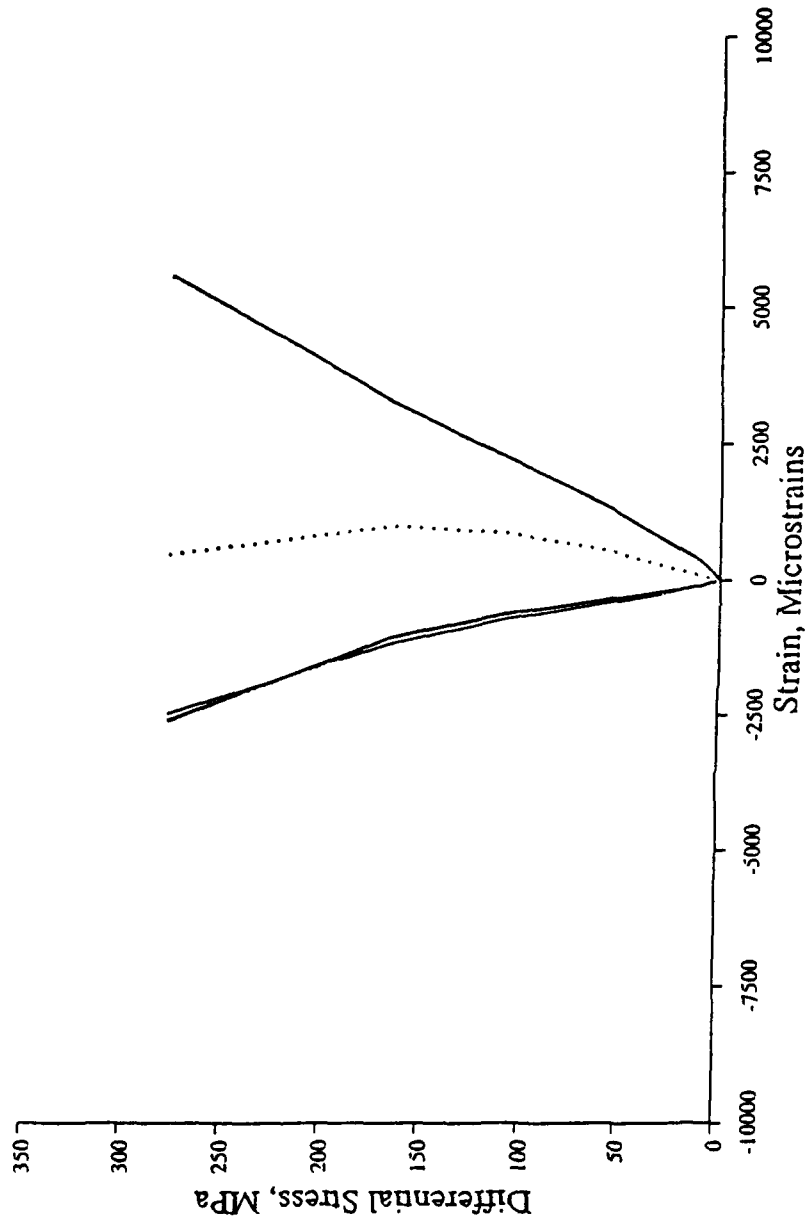


Figure 32

SW 3

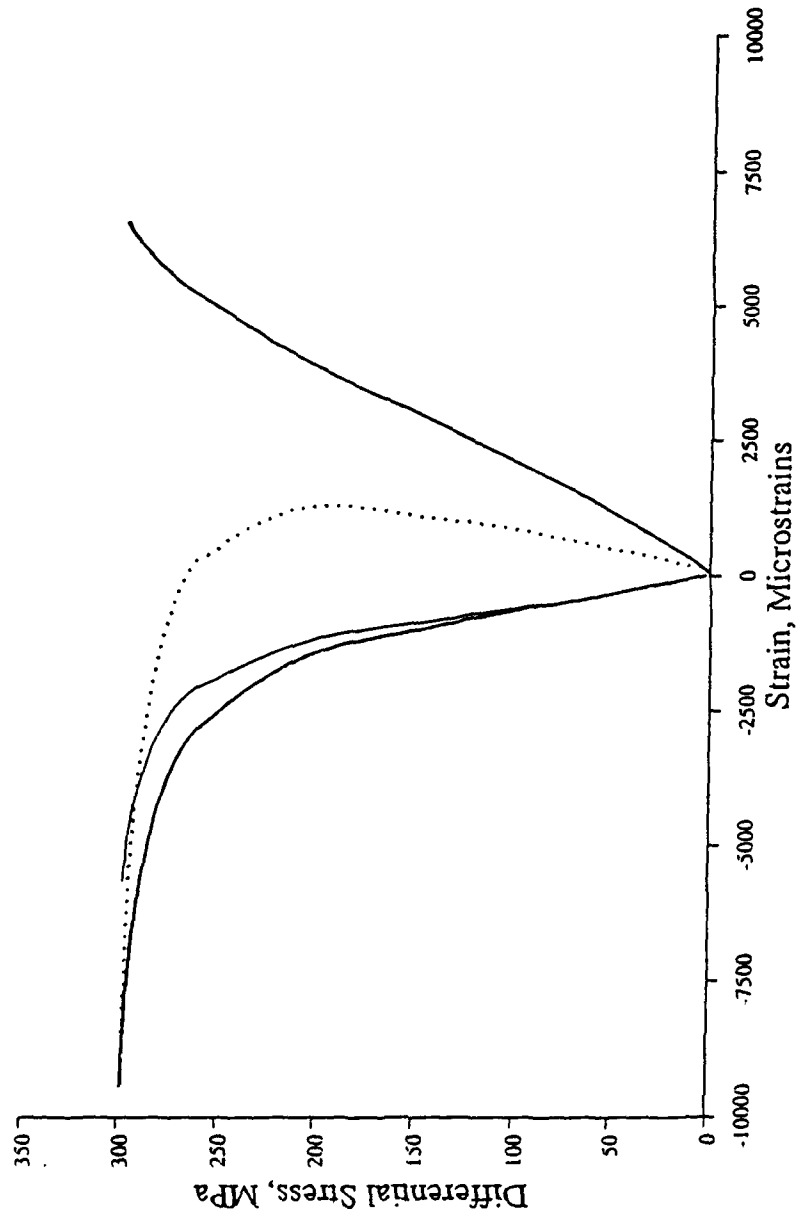


Figure 33

SW 8

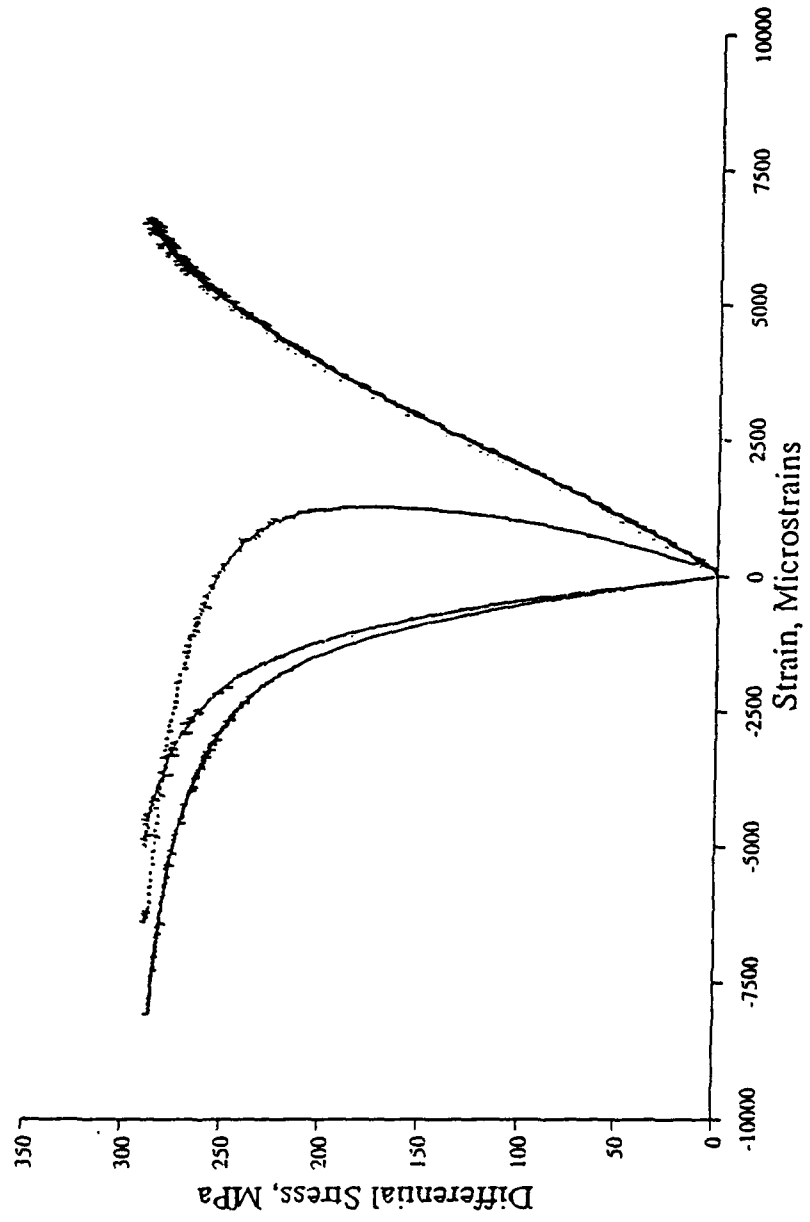


Figure 34

SW 6

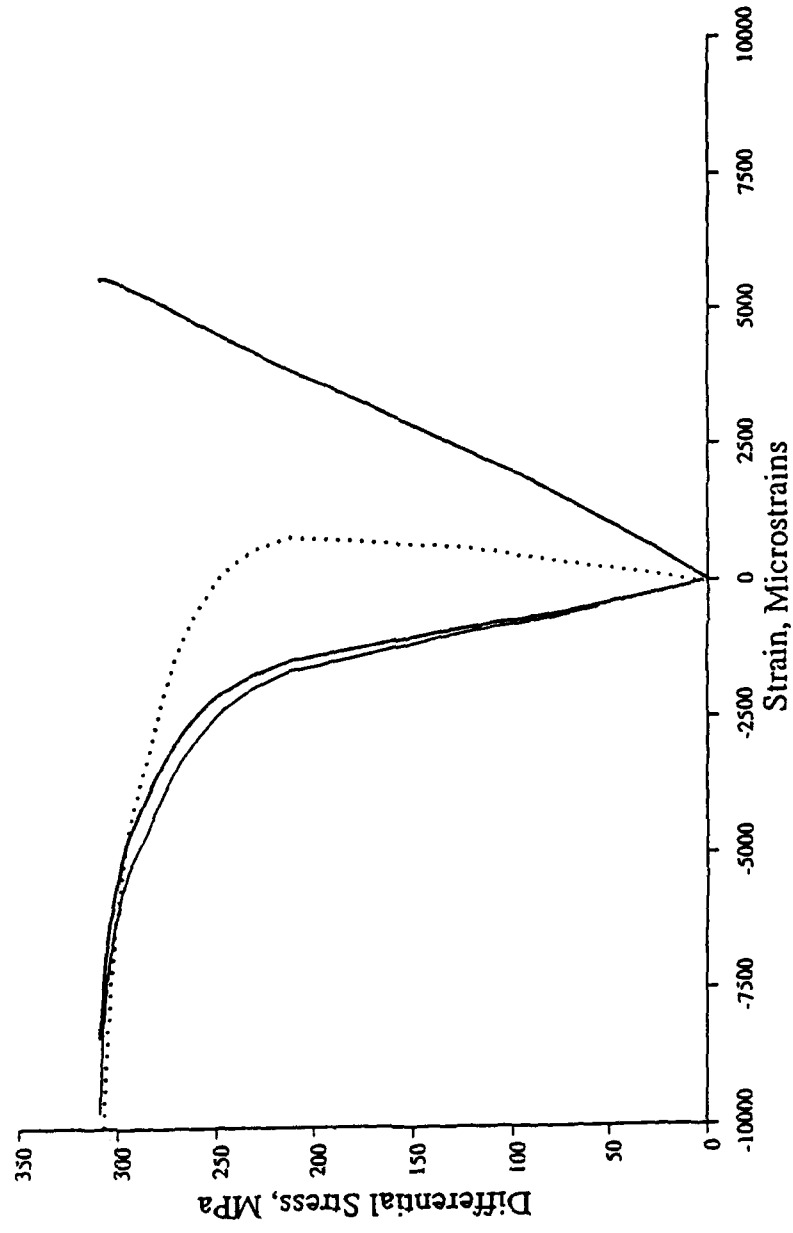


Figure 35

SW 2

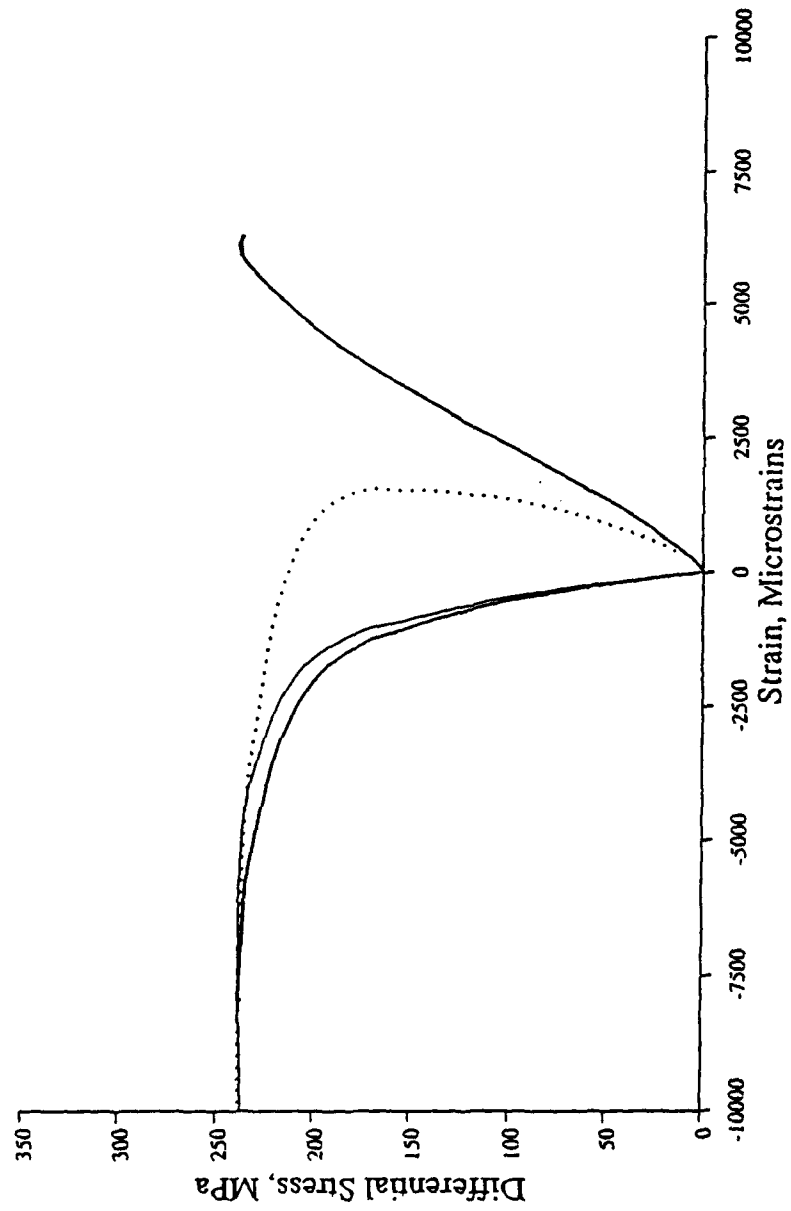


Figure 36

SW 5

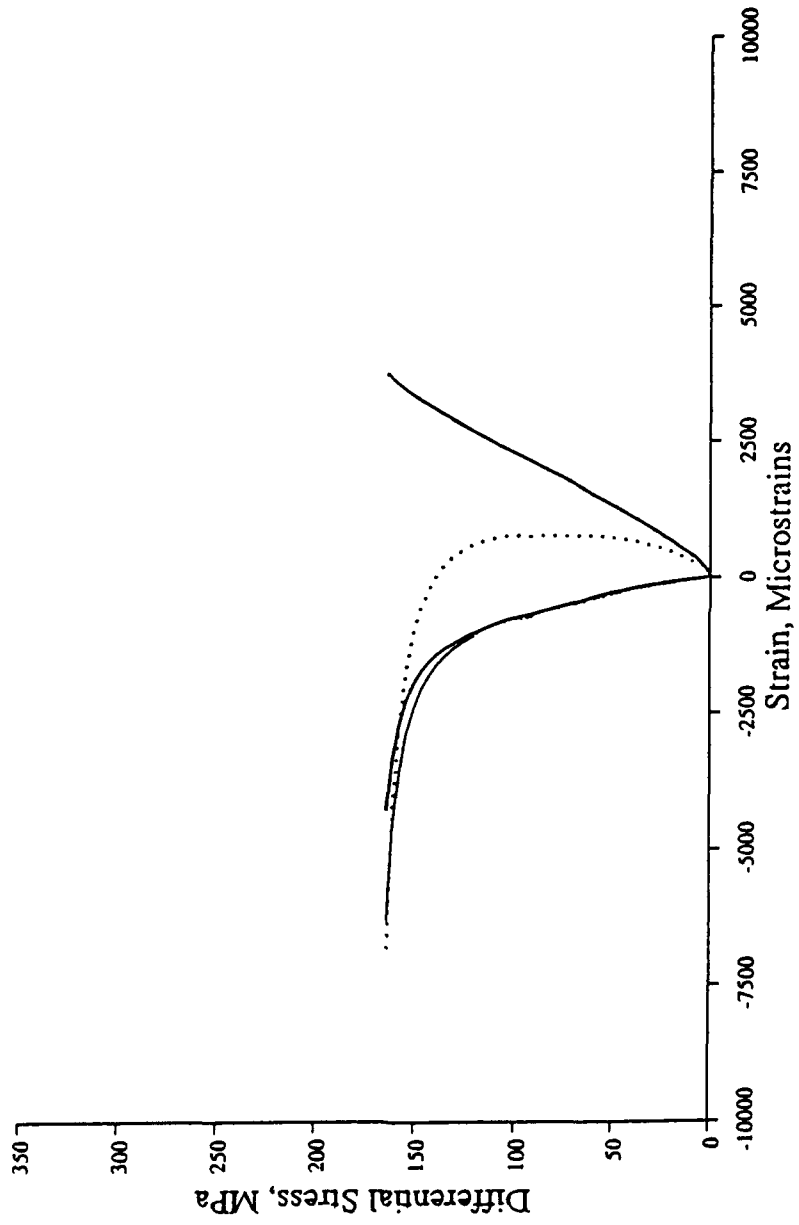


Figure 37

SW 7

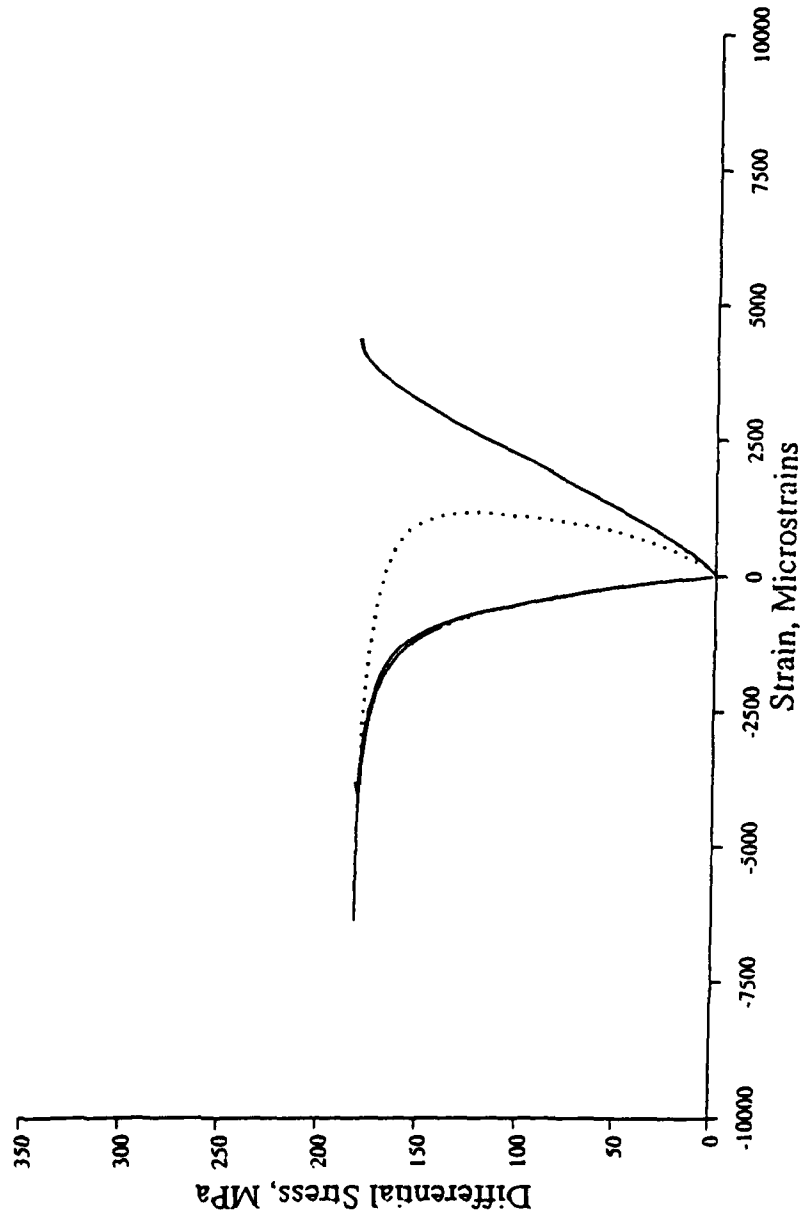


Figure 38

SW 4

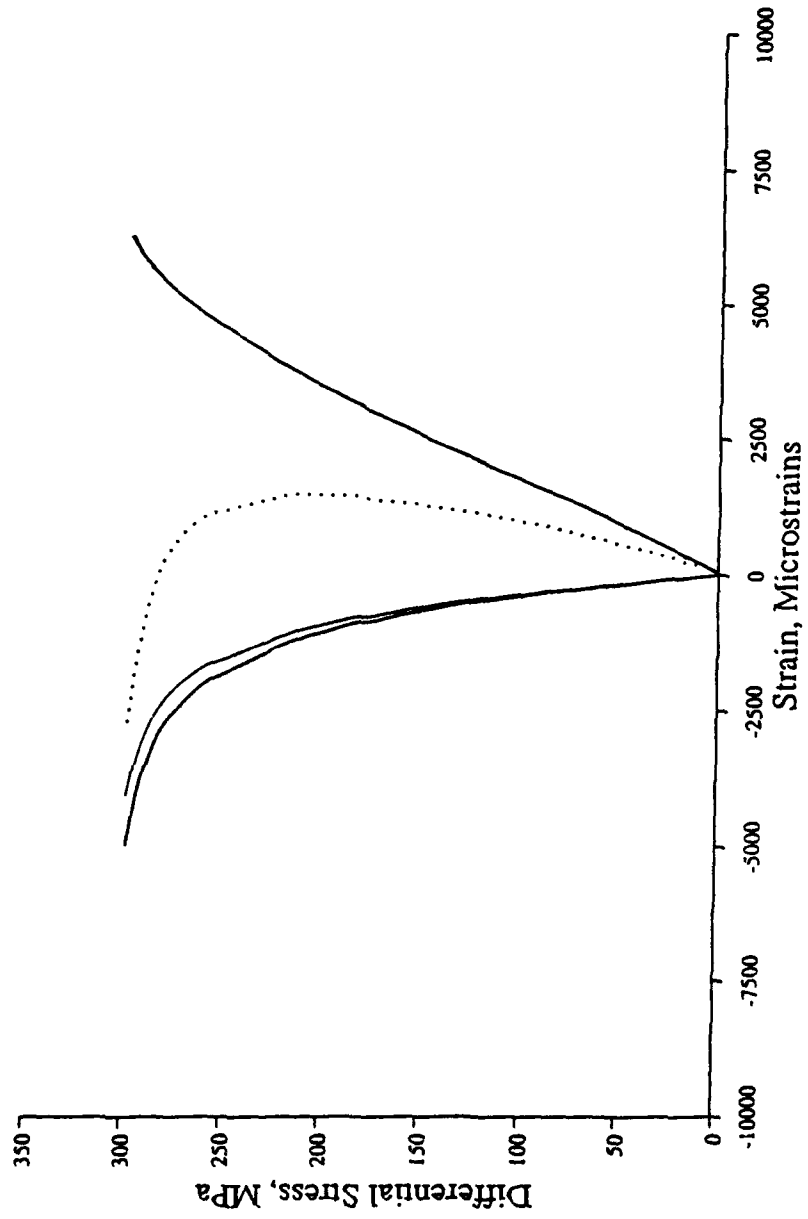


Figure 39

NLI

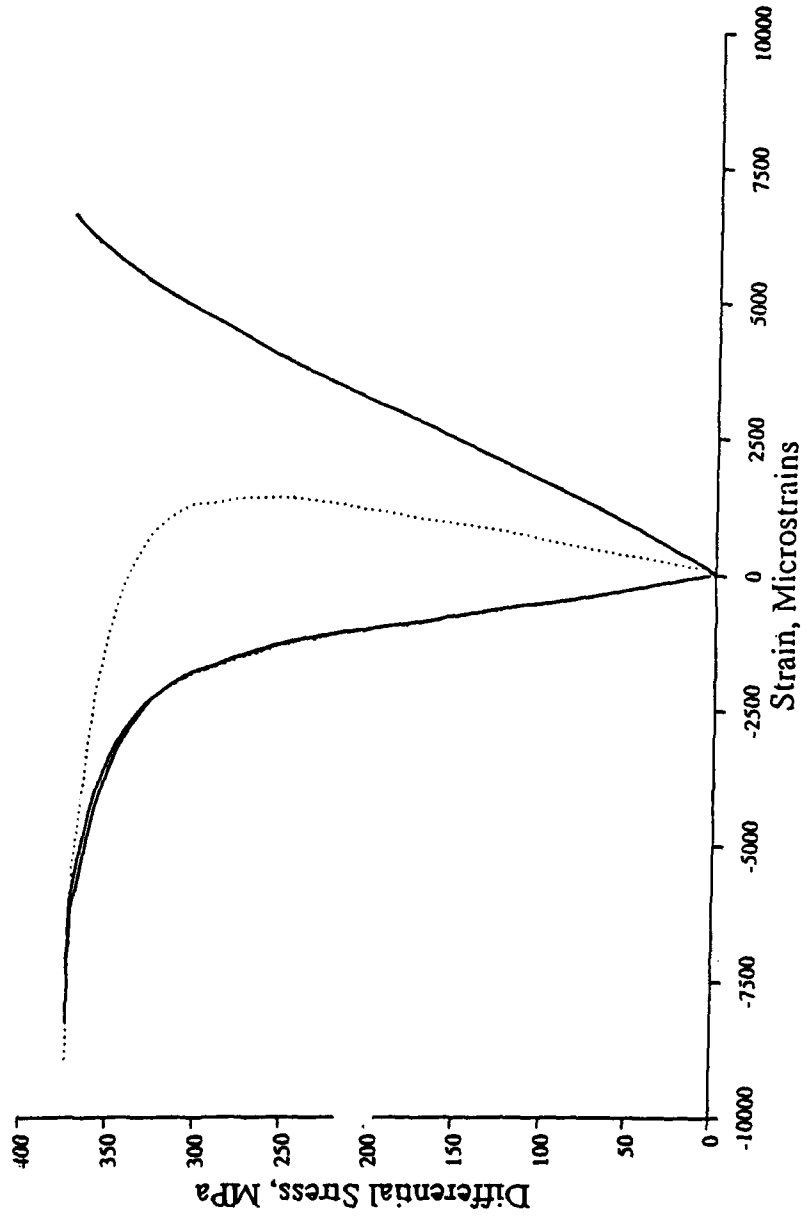


Figure 40

NL2

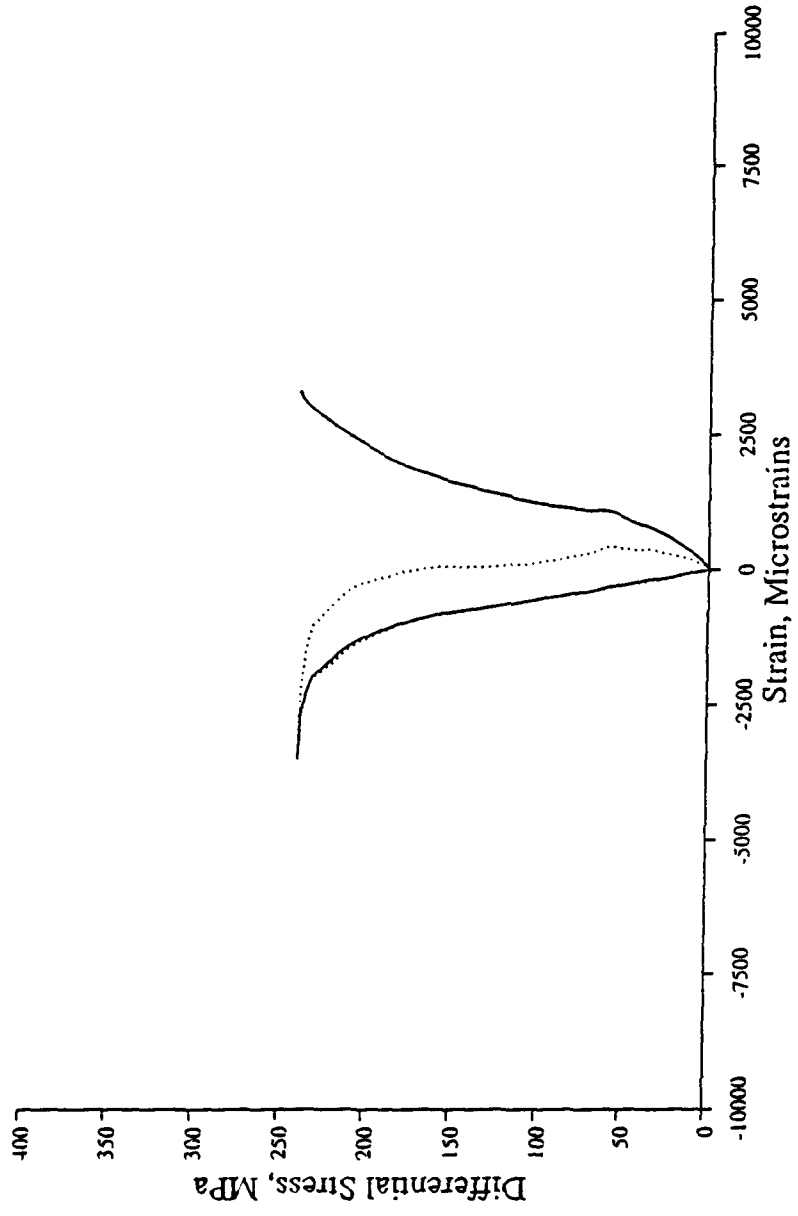


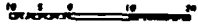
Figure 41

APPENDIX I

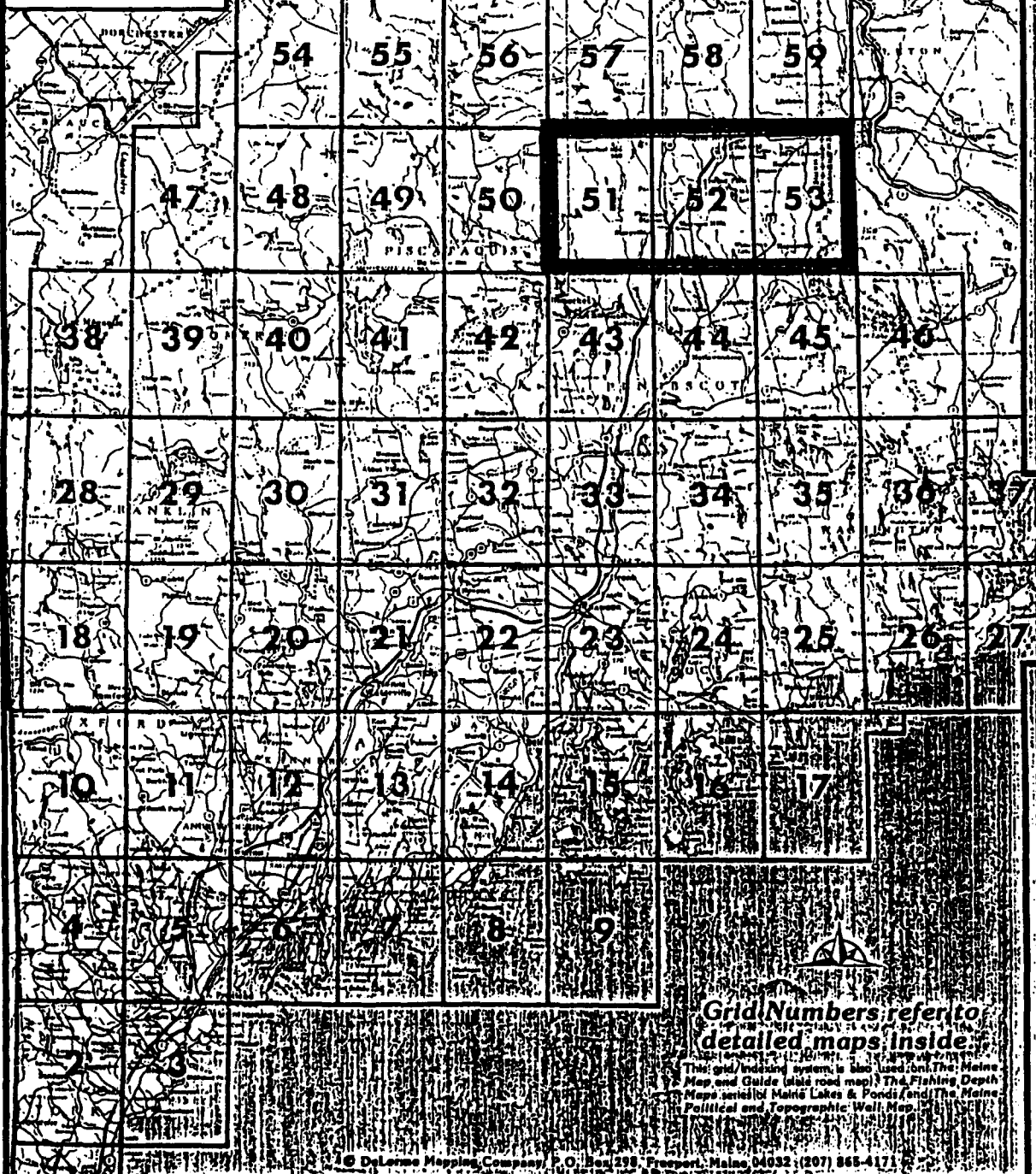
State of Maine map showing location
of analogue test site and sample sites

The Maine Atlas and Gazetteer

Scale of Miles



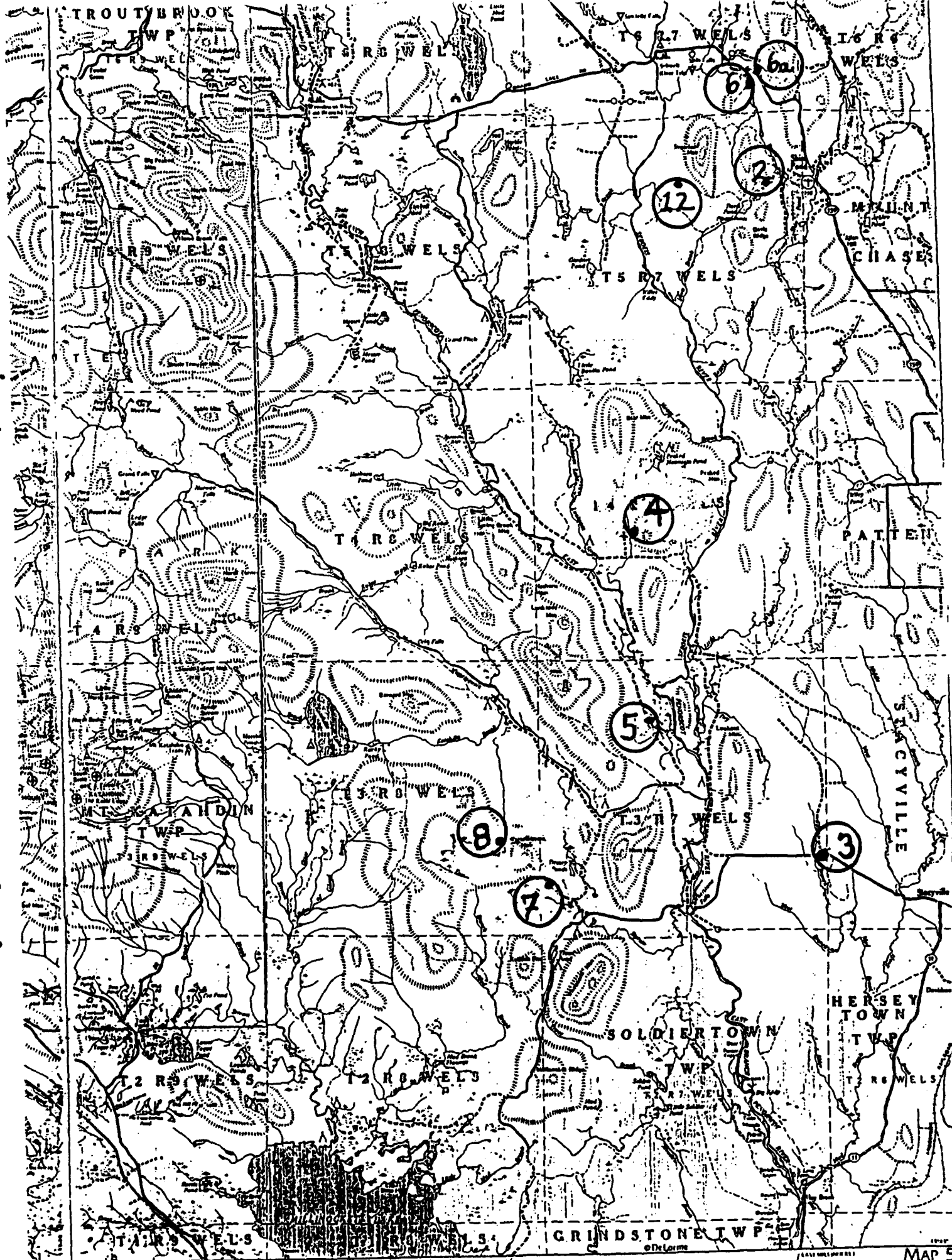
Back Cover Elevations in Meters



Grid Numbers refer to detailed maps inside.

This grid/index system is also used for: The Maine Map and Guide (also road map); The Fishing, Depth, and Tidal Maine Lakes & Ponds; and The Maine Political and Topographic Wall Map.

© DeLorme Mapping Company, P.O. Box 298, Fryeburg, Maine 04932 (207) 865-4171



TROUT BROOK TWP

T 5 R 7 WELS

T 12 R 9 WELS

T 5 R 7 WELS

T 5 R 7 WELS

T 5 R 7 WELS

PATTEN TWP

T 5 R 7 WELS

PATTEN TWP

MILLINT CHASE TWP

T 5 R 7 WELS

T 5 R 7 WELS

STACYVILLE

HERSEY TOWN TWP

T 5 R 7 WELS

SOLDIERTOWN TWP

HERSEY TOWN TWP

T 12 R 9 WELS

T 12 R 9 WELS

GRINDSTONE TWP

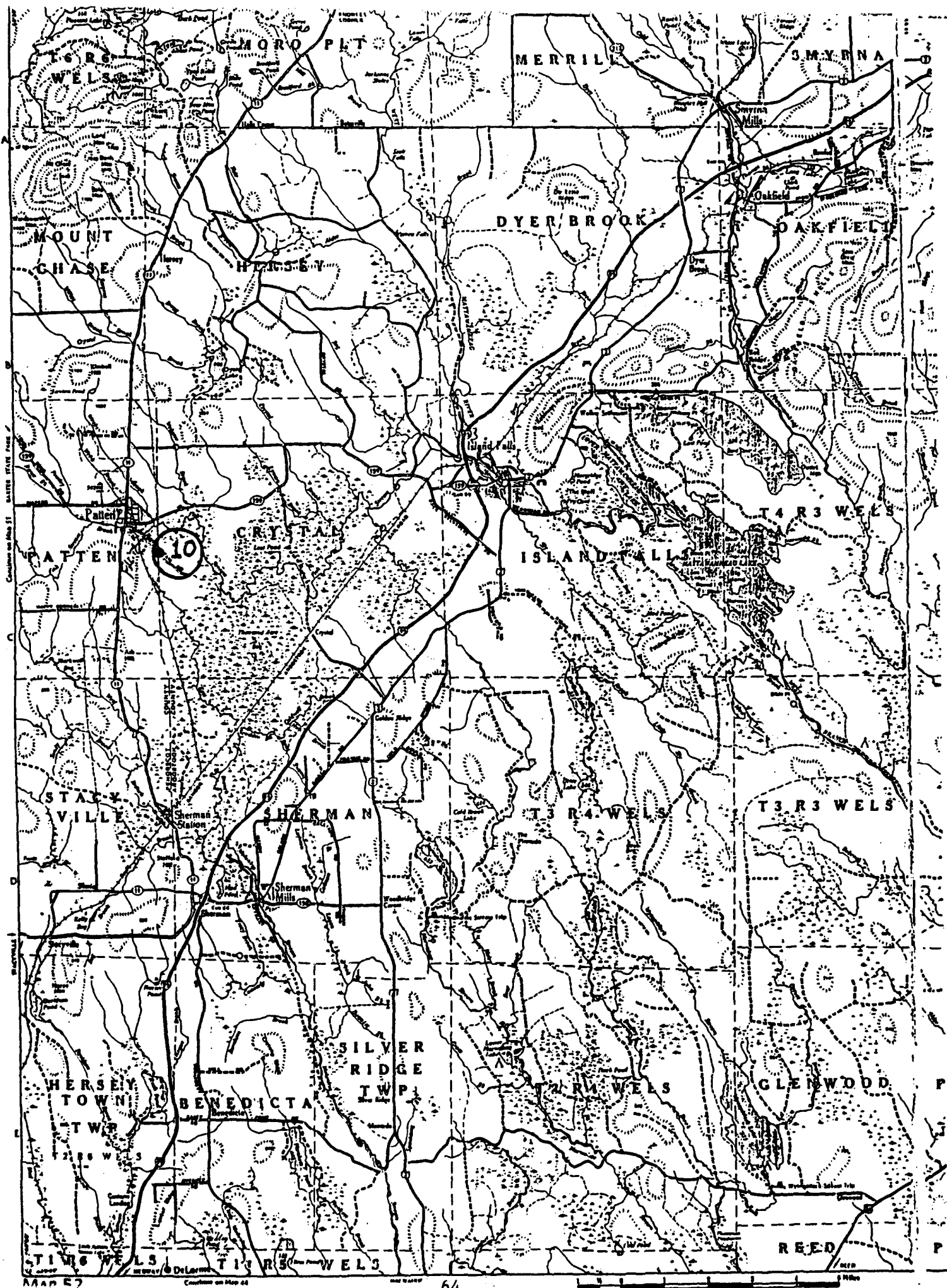
Scale 1" = 1 Mile

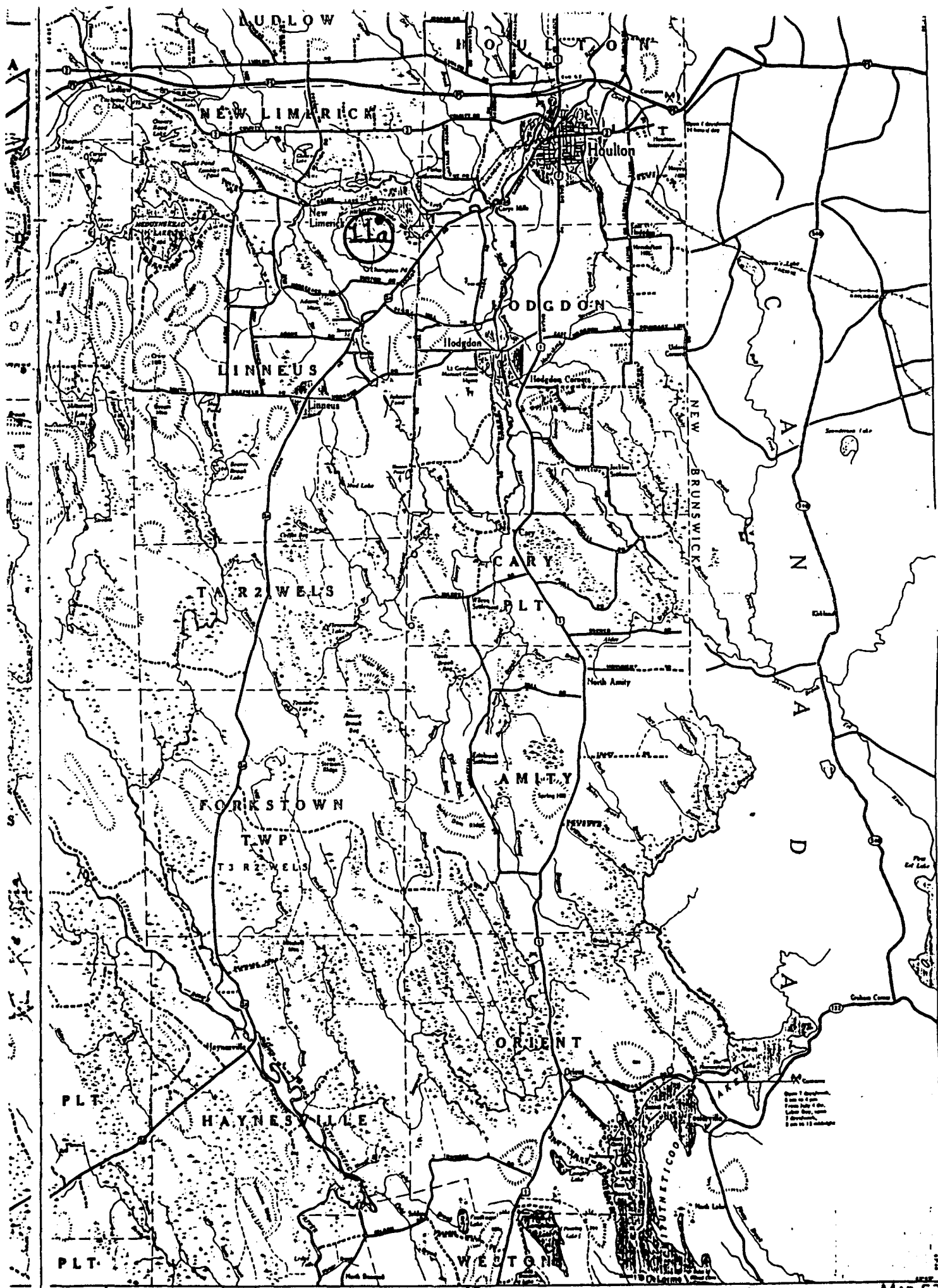
Continued on Map 43

© DeLorme

2000 UNLAWFUL

MAP 51





APPENDIX II

Description of all rock types in analogue test site
(from Neuman, 1967)

Analogue Domestic Samples from Northern Maine

-
- Station 2 - Rockabema Quartz Diorite
Altered quartz diorite. Most of formation is cataclastically sheared, although cataclastic structure is absent around Lower Shin Pond where samples were obtained. Sampled rock showed evidence of severe shearing and jointing. Little chance of intact core recovery.
-
- Station 3 - Allsbury Formation (slate member) [See Station 10]
Medium to dark-gray, fine-grained slate and siltstone. Severe jointing. Intact core recovery will be difficult.
-
- Station 4 - Volcanic Rocks
Altered andesitic and basaltic flows and diabase, in some places intruded by Rockabema quartz diorite. Gray fine-grained igneous rocks. Only mild surface jointing. Good chance of core recovery.
-
- Station 5 - Limestone
Largely reefal and reef detritus. Intensely sheared and penetrated with joints healed with siliceous or calcareous cement. Severe jointing, but healed cracks make core recovery possible.
-
- Station - Shin Brook Formation
Tuffaceous sandstone and conglomerate. Moderate evidence of tectonic shearing or jointing. Core recovery considered possible.
-
- Station 6a - Grand Pitch Formation (quartzite member) [See Station 12]
Oldest rocks in Shin Pond, Stacyville quadrangle (Cambrian). Samples are mostly gray, green, and red quartzite. Intensely jointed. Intact core recovery unlikely. One attempt failed.
-
- Station 7 - Brecciated Katahdin Monzonite (migmatite)
Broad brecciated zone at eastern margin of the Katahdin batholith. This boundary consists of a contact zone of brecciated and partially assimilated sedimentary rocks in a granitic matrix. Mildly jointed samples suggest fair chance of core recovery.
-
- Station 8 - Katahdin Quartz Monzonite (larger grained sample) [See Station 11a]
Medium-gray to light-gray, medium-grained massive granitic rock representing the Katahdin batholith. Mostly massive and structureless. 2/3 feldspar, 1/3 quartz, and 5 to 10% biotite. Beneath weathered layer (≈6 inches) the granite shows excellent potential for core recovery. No significant evidence of shearing, jointing.
-

Station 10 - Allsbury Formation (sandstone member) [See Station 3]
Sandstone and graywacke member of the Allsbury, consisting of sandstone and minor amounts of pebble conglomerate. Thin sections of several beds show nearly 90% of clast are quartz; the remainder are feldspar, quartzite, muscovite and carbonate grains. Samples from coring showed evidence of slight to moderate shearing and jointing. Core recovery may be possible beneath the weathered layer.

Station 11a - Katahdin Quartz Monzonite (finer grained sample) [See Station 8]
Same as Station 8, but this is finer grained member. Samples were retrieved from a tailing pile on the south side of Nickerson Lake. Core recovery from abandoned quarry should be excellent, although actual quarry was not located on this trip.

Station 12 - Grand Pitch Formation (siltstone member) [See Station 6a]
Intensely sheared and jointed rock with poor chance of intact core recovery. This member consists of gray, dark-gray, green and red slate and siltstone with small amounts of vitreous quartzite, graywacke, and tuff.

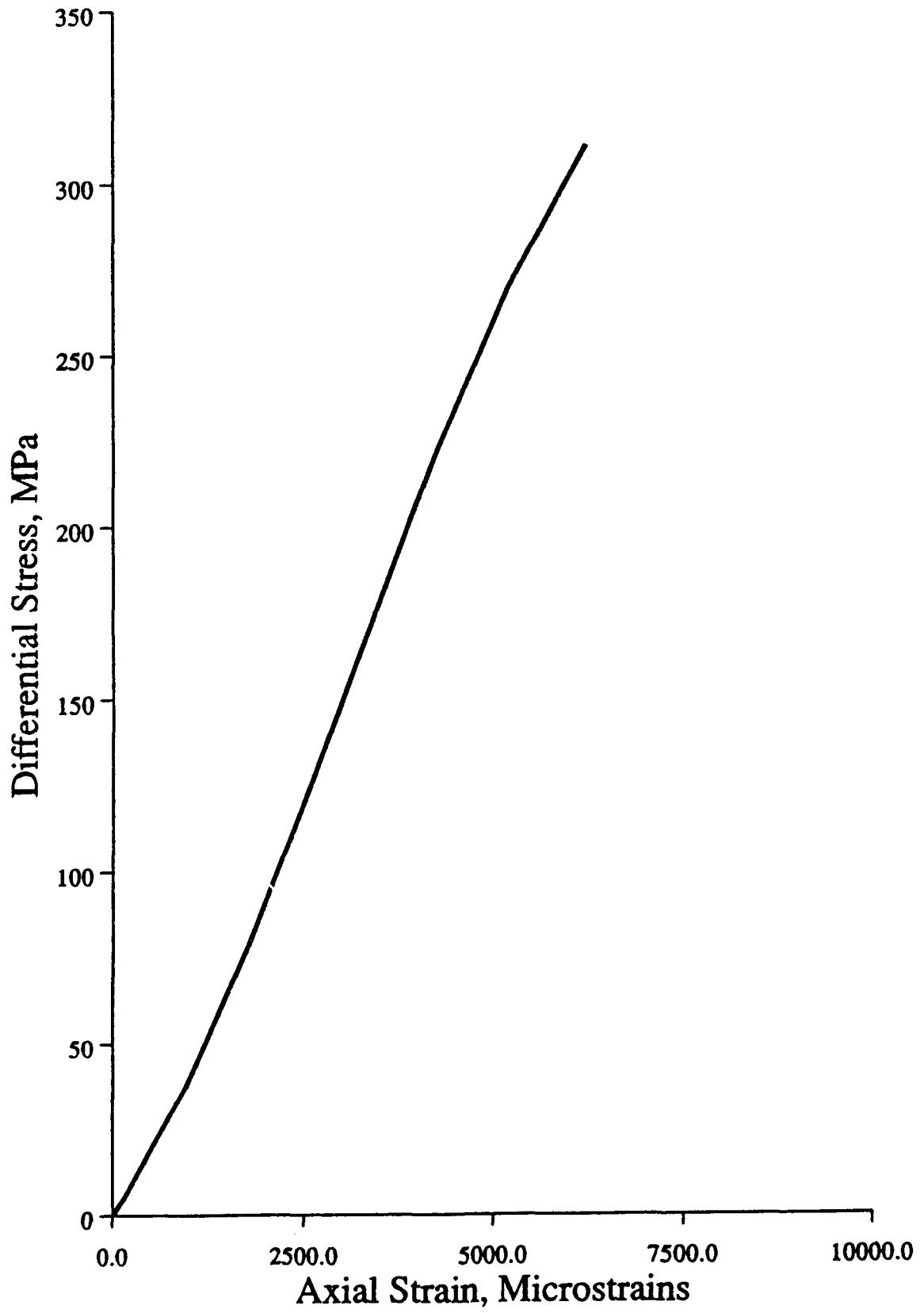
Maine Analogue Rock Samples

Formation	Station	Rock Type	Jointing and Shearing	Chance of Intact Core Recovery		
				1 inch	3 inch	10 inch
Grand Pitch	6a	quartzite member	moderate	fair	fair	poor
	12	siltstone member	severe	fair	poor	poor
Allsbury	10	sandstone member	slight	good	fair	fair
	3	slate member	moderate	fair	fair	poor
Shin Brook	6	tuffaceous sandstone	moderate	good	fair	fair
Rockabema	2	cataclastic quartz diorite	severe	fair	poor	poor
Katahdin	8	large-grain quartz monzonite	almost none	excellent	good	good
	11a	moderate-grain quartz monzonite	almost none	excellent	good	good
Migmatite	7	brecciated sed. rocks in granitic matrix	moderate	good	fair	fair
Limestone	5	fossiliferous l.s. jointed with siliceous and calcareous cement	severe	good	fair	fair
Volcanics	4	andesitic, basaltic flows	slight	good	fair	fair

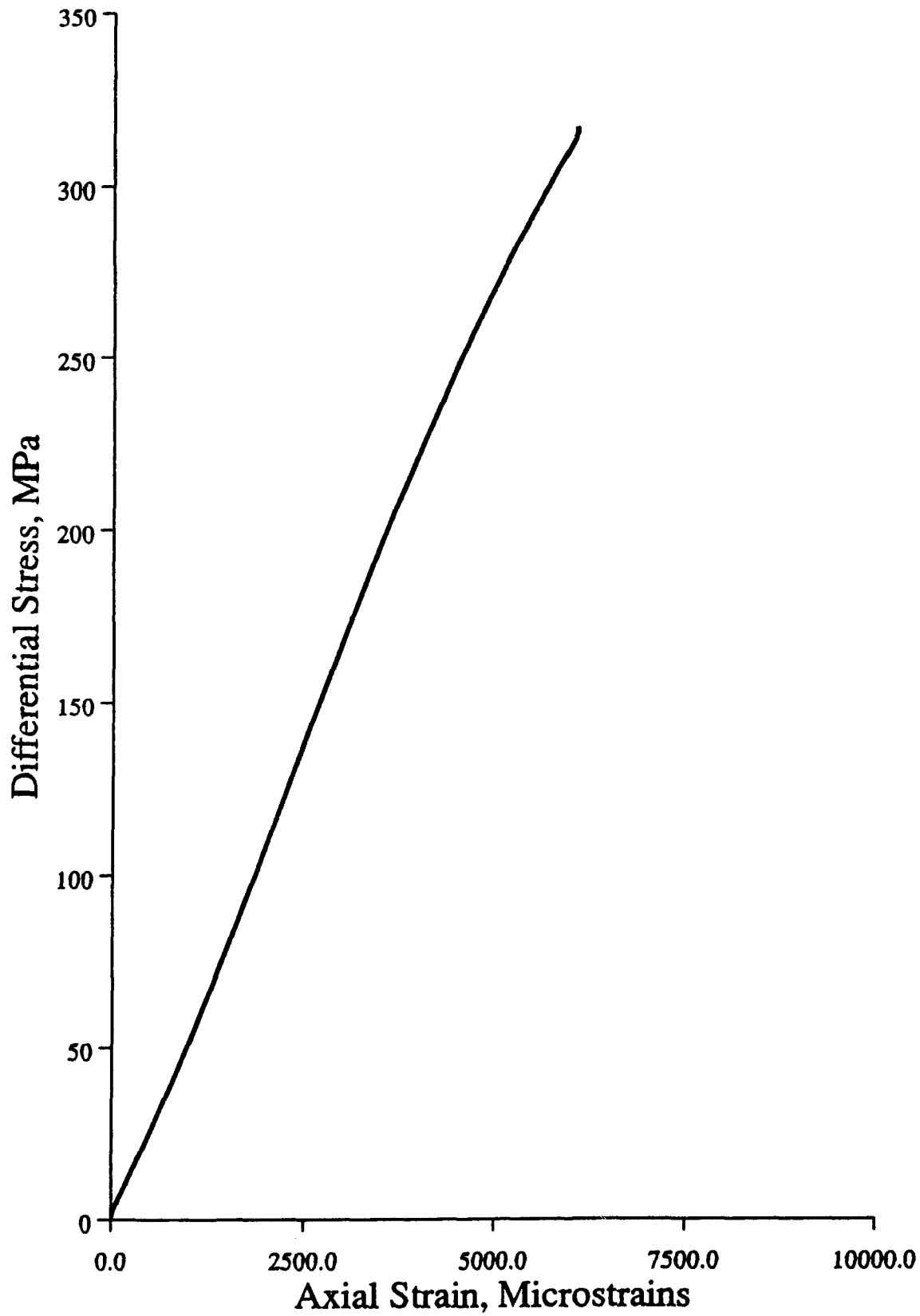
APPENDIX III

Stress-Axial strain and stress-radial strain
plots from all experiments

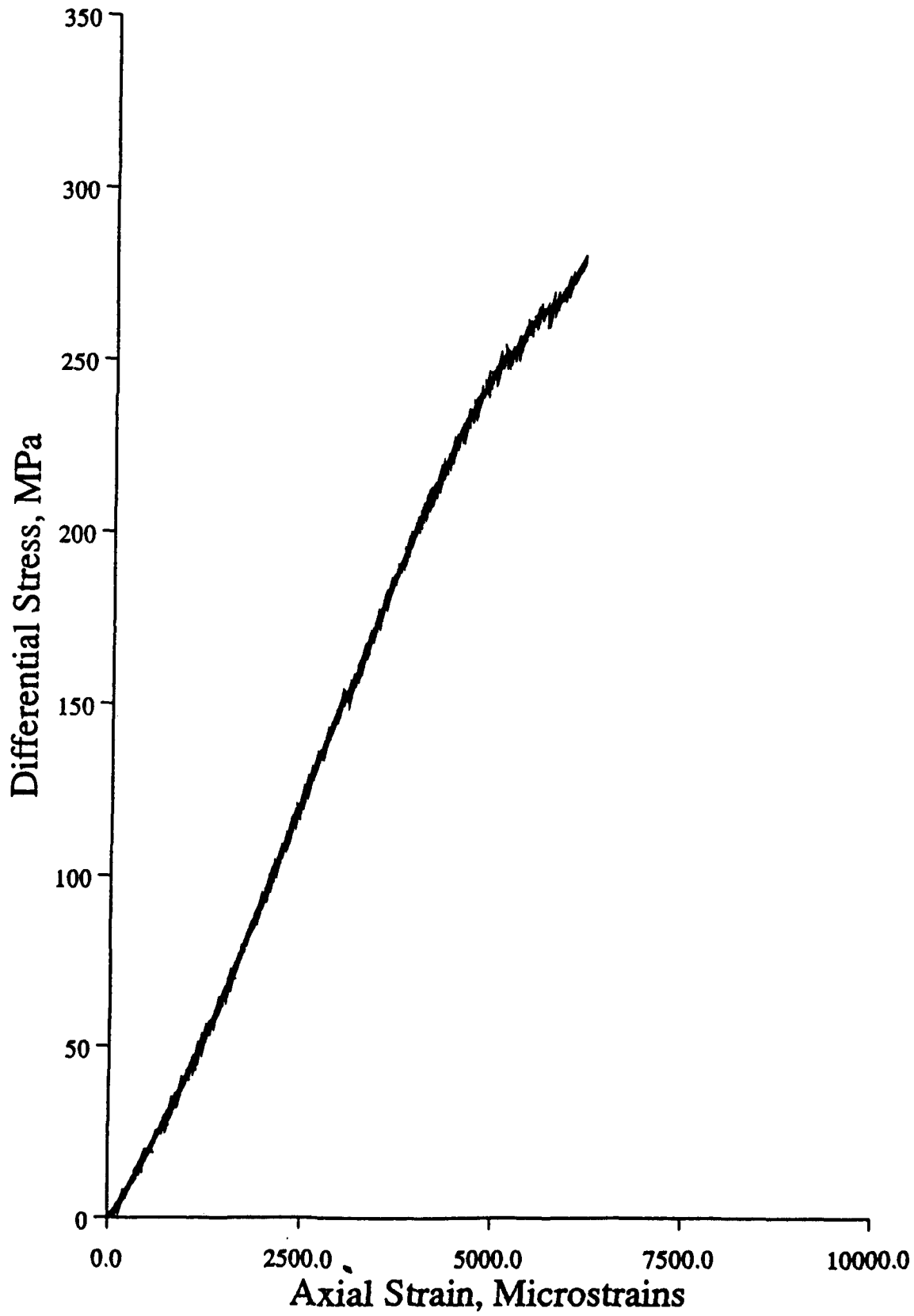
KG 5



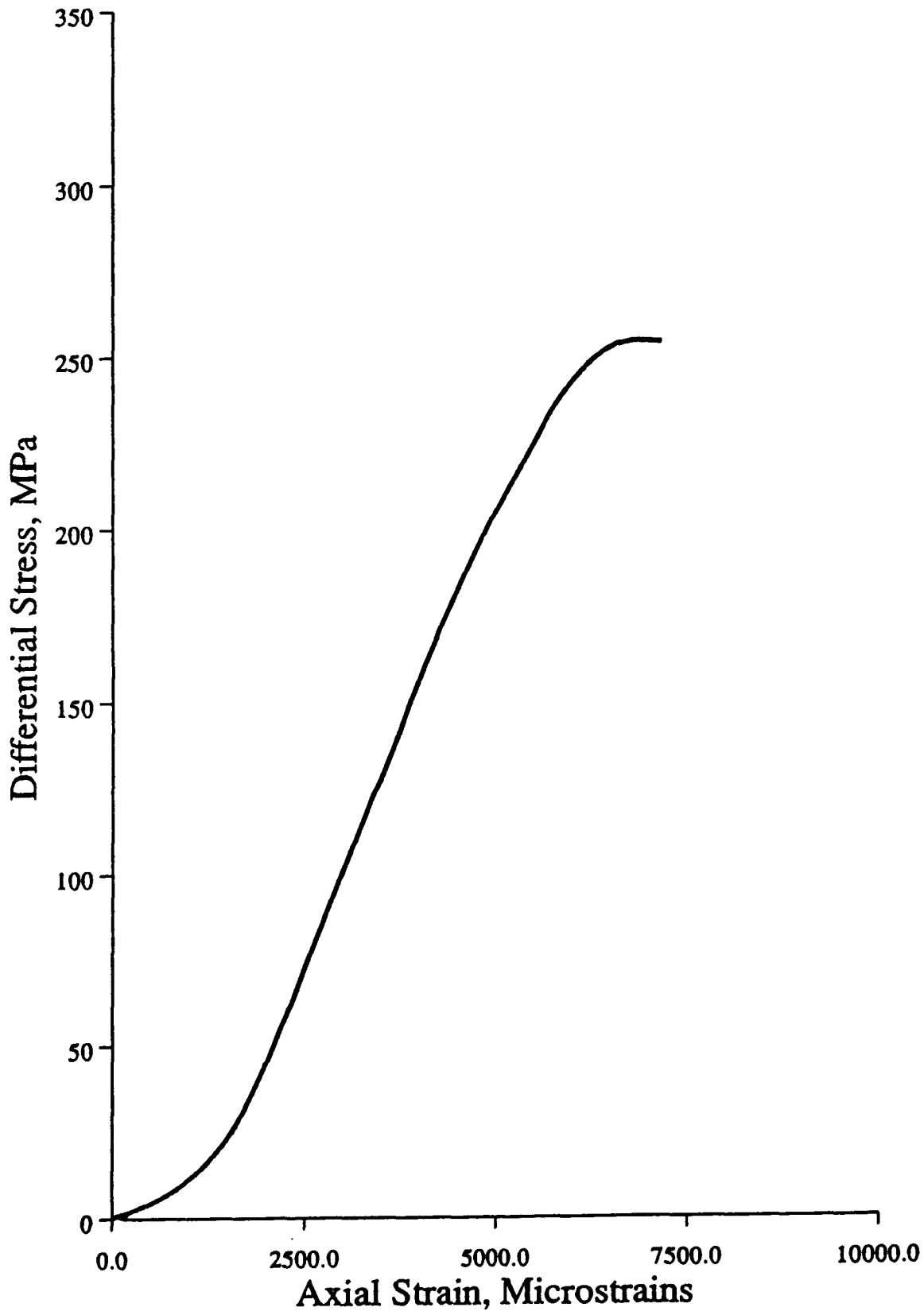
KG 15



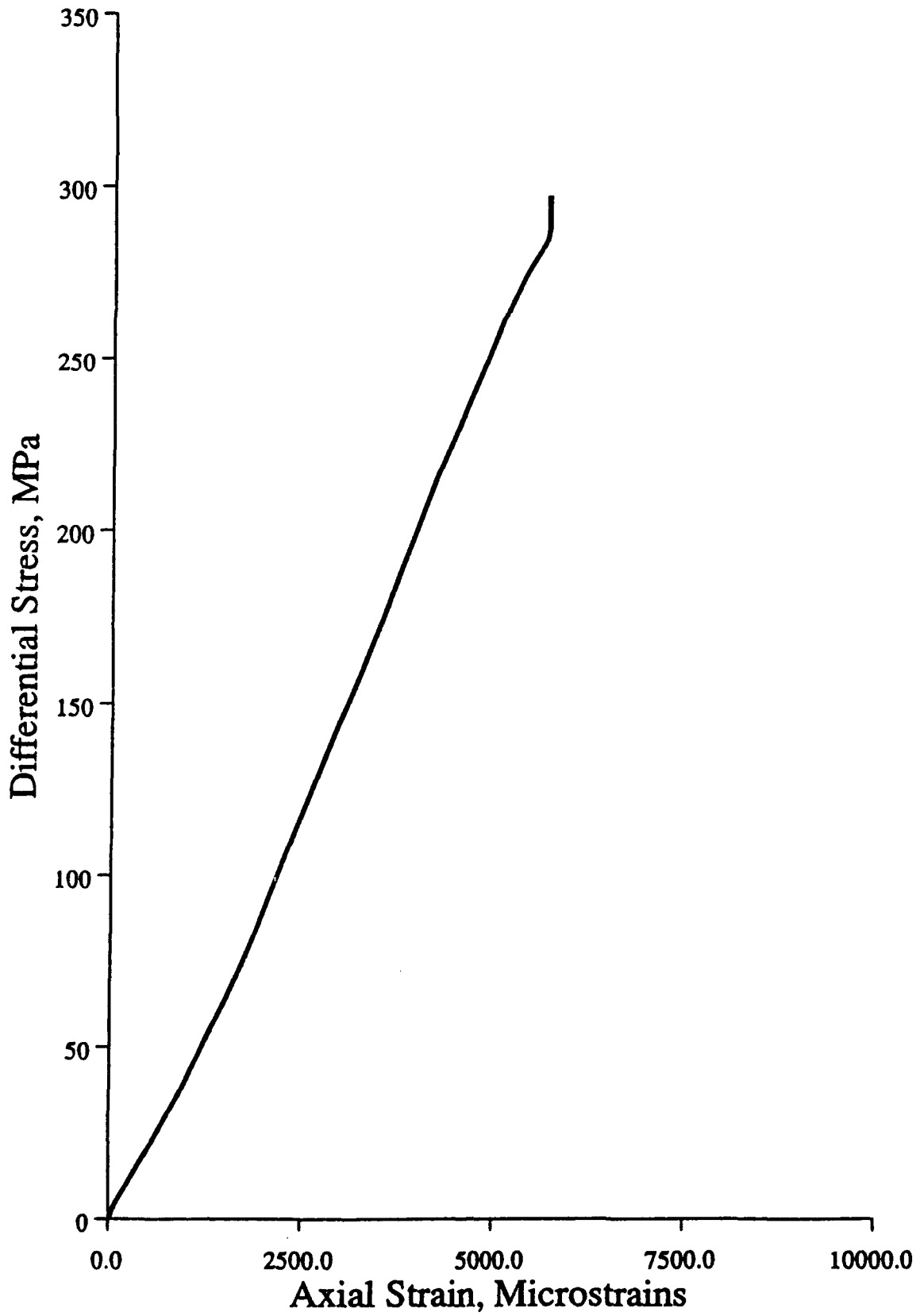
KG 6



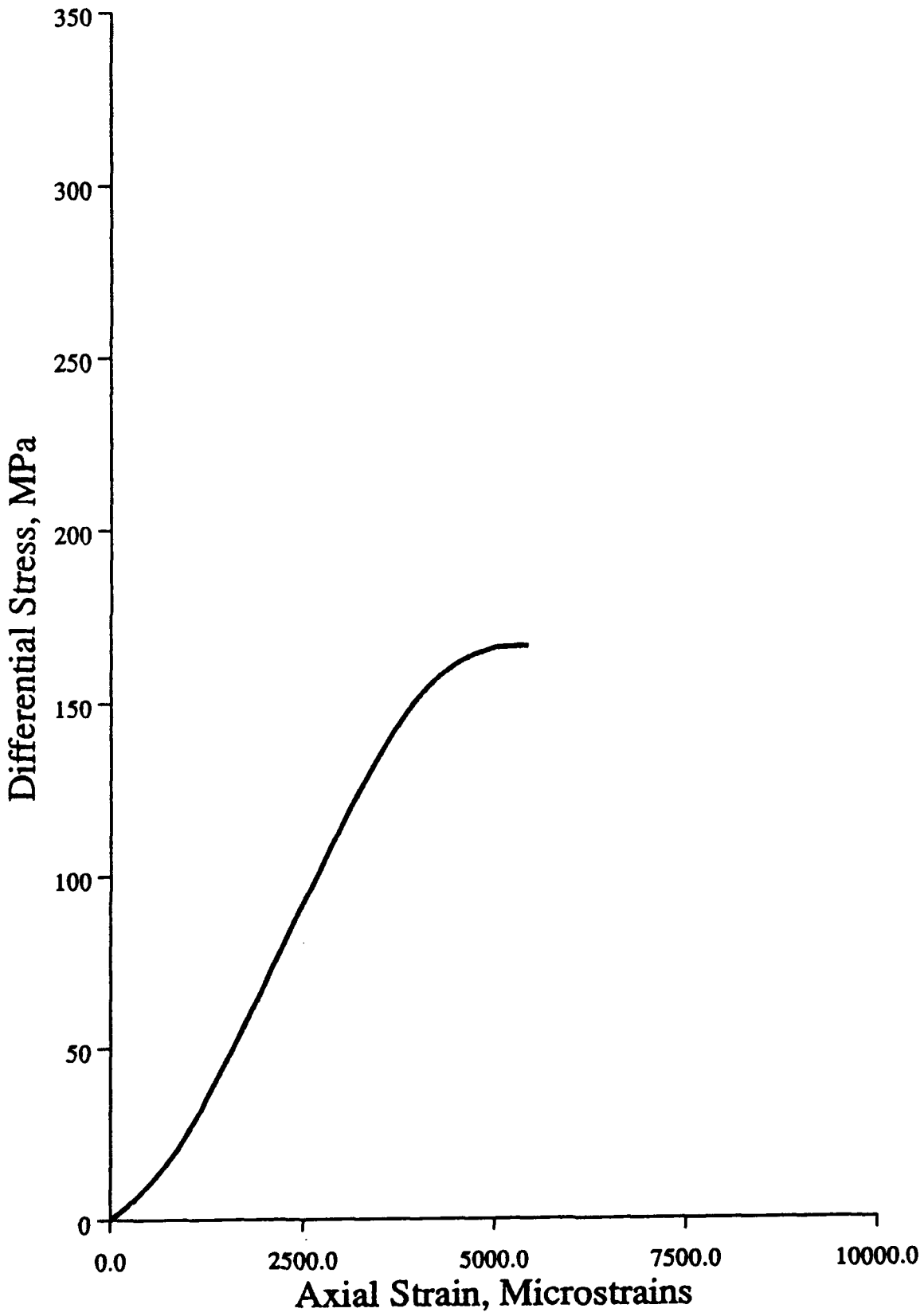
KG 17



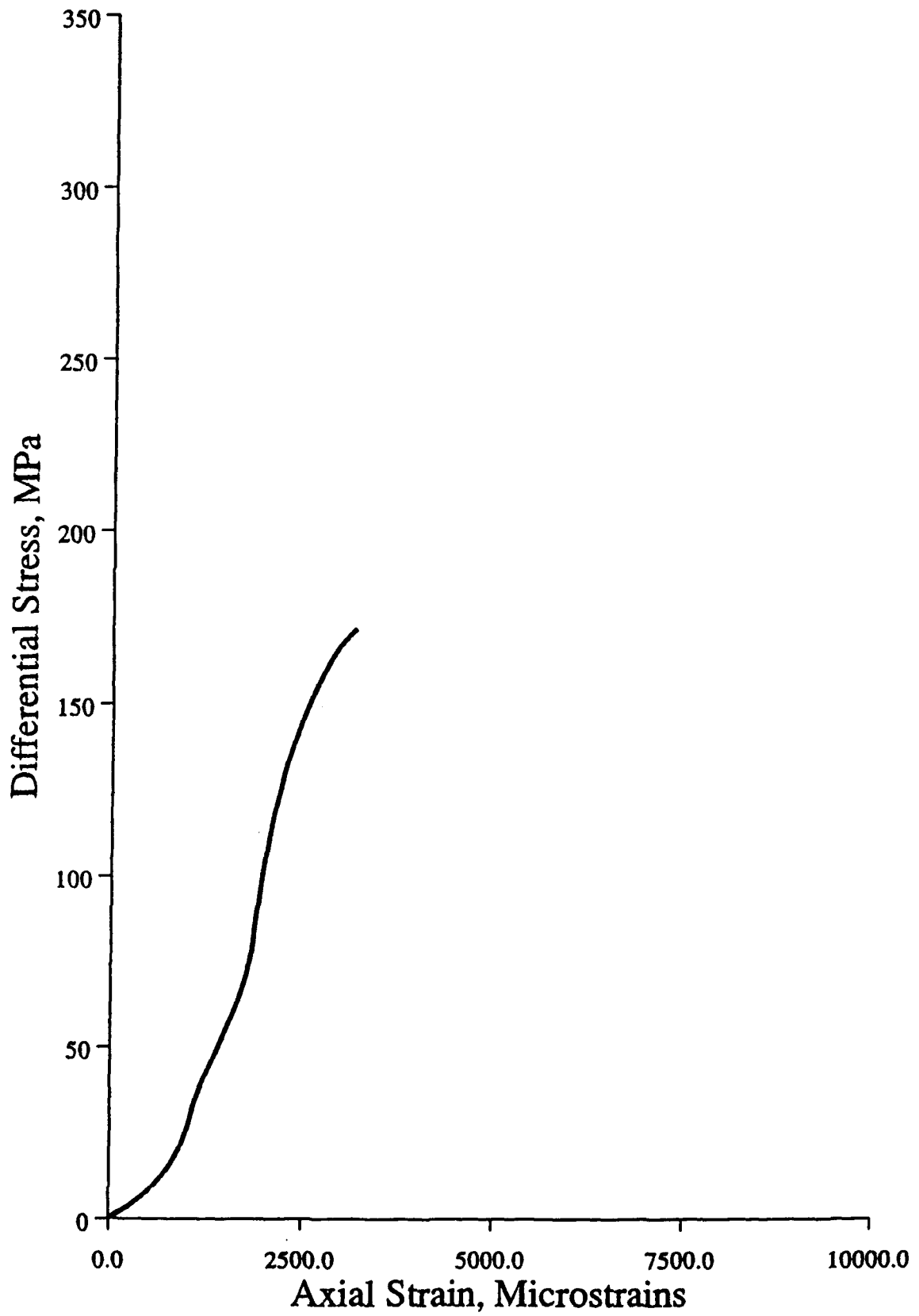
KG 18



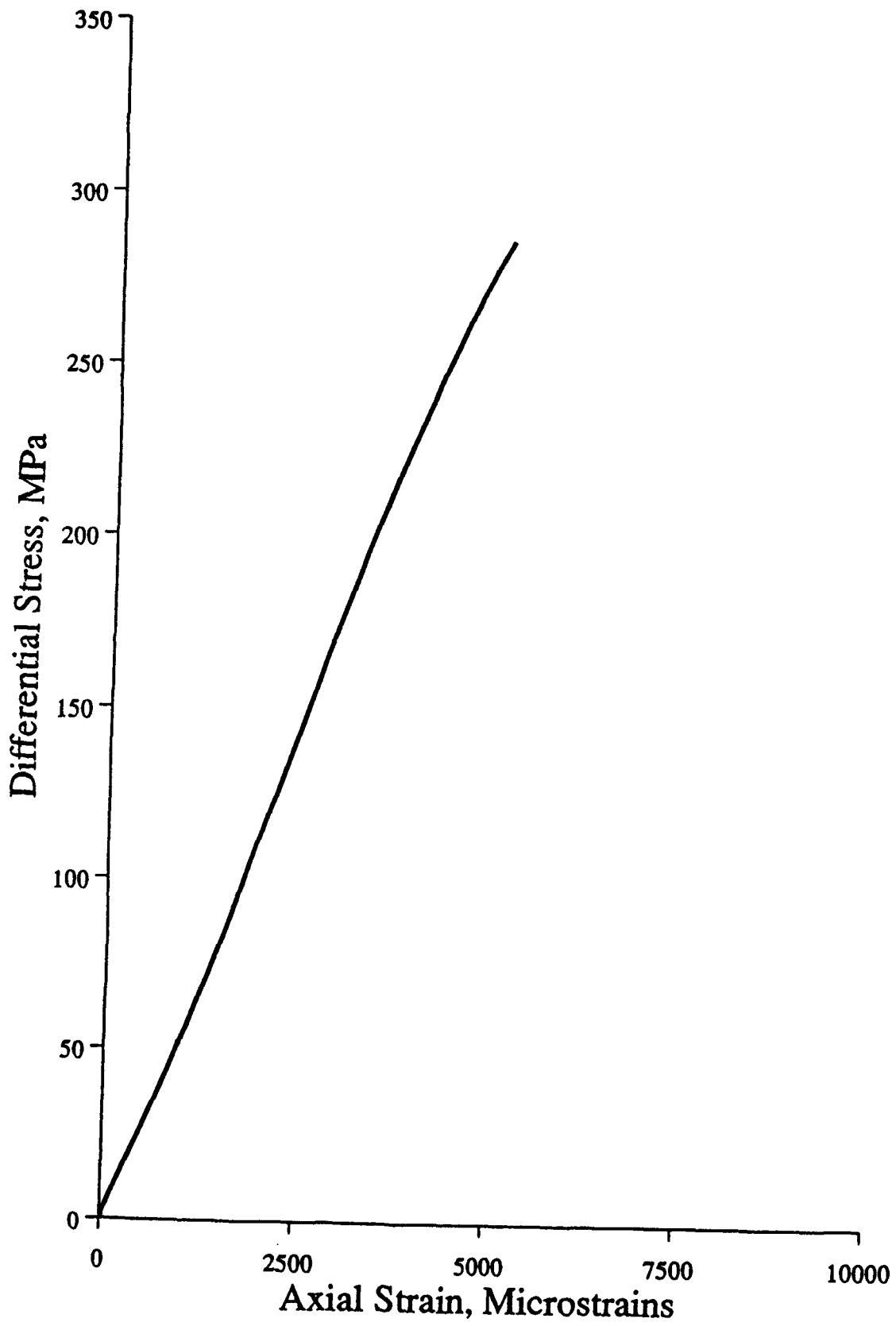
KG 19



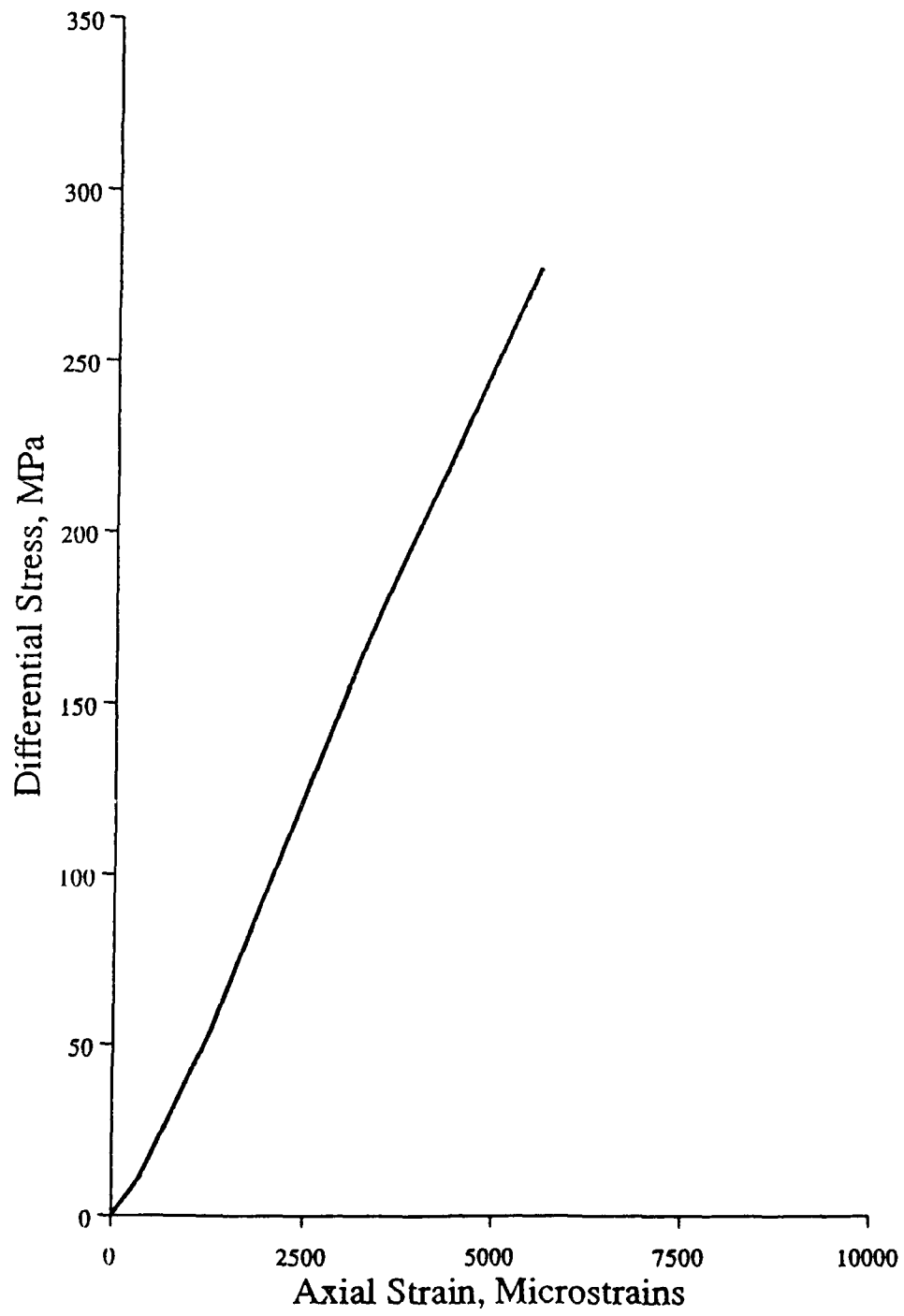
KG 20



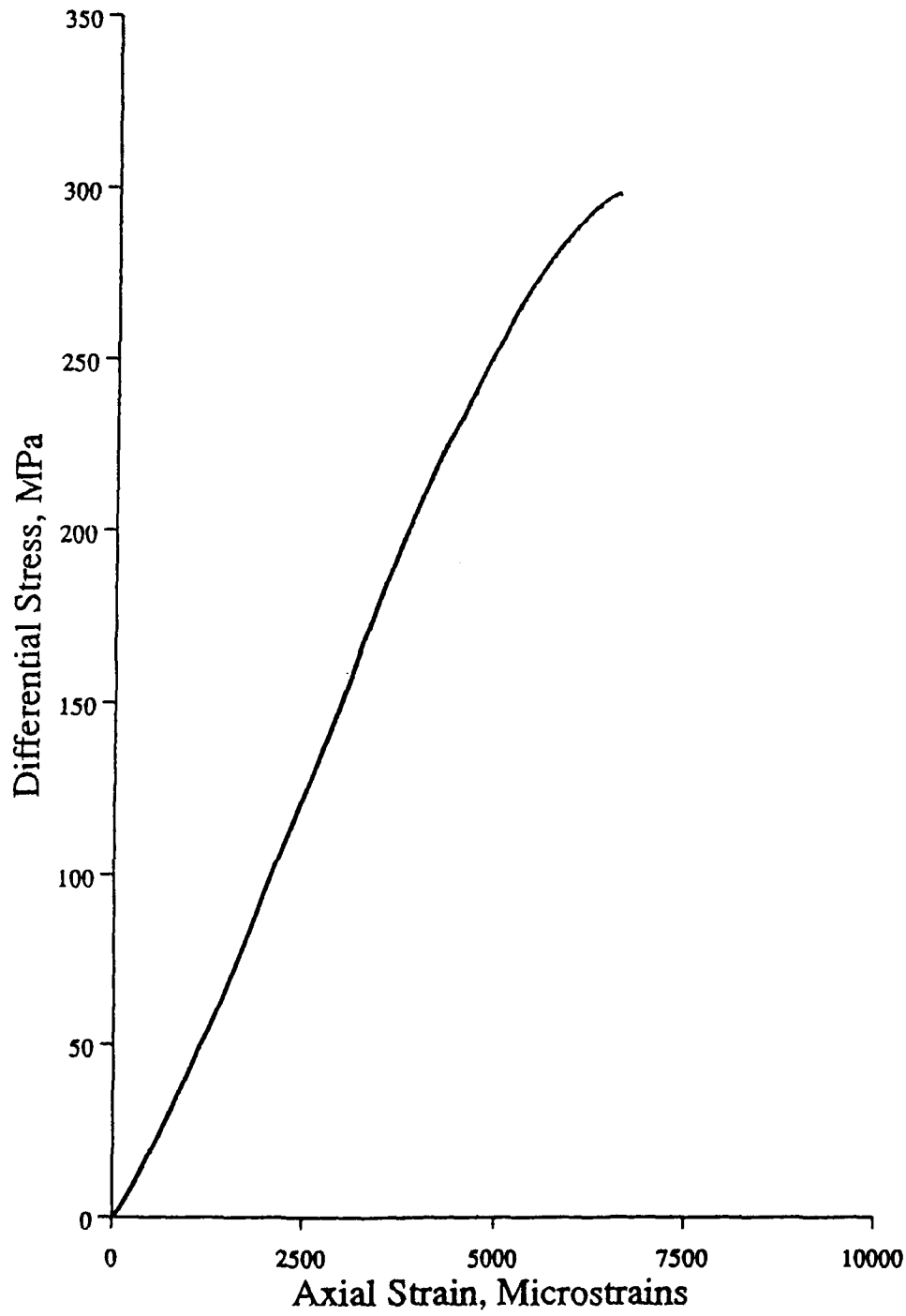
KG 4



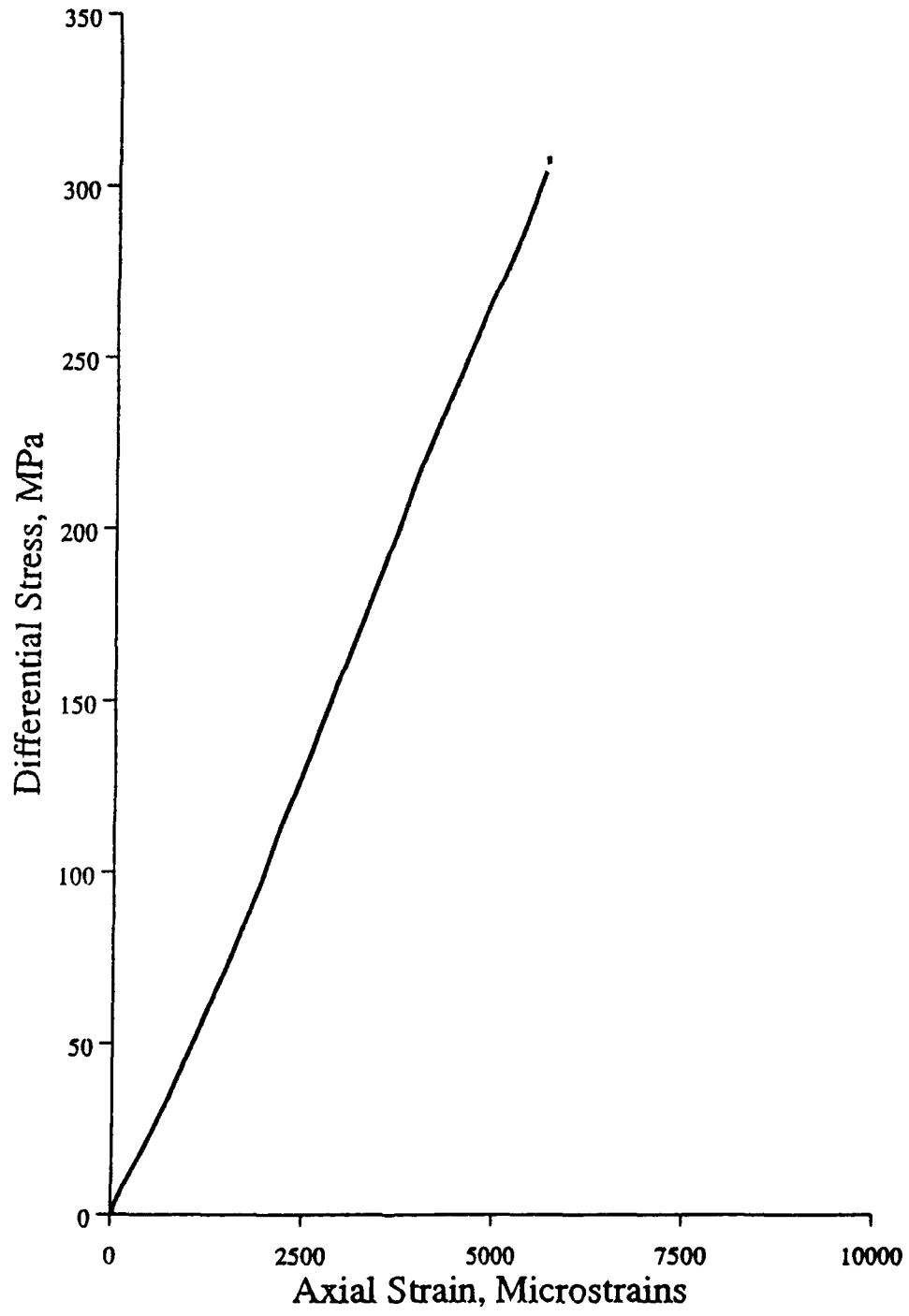
SW 1



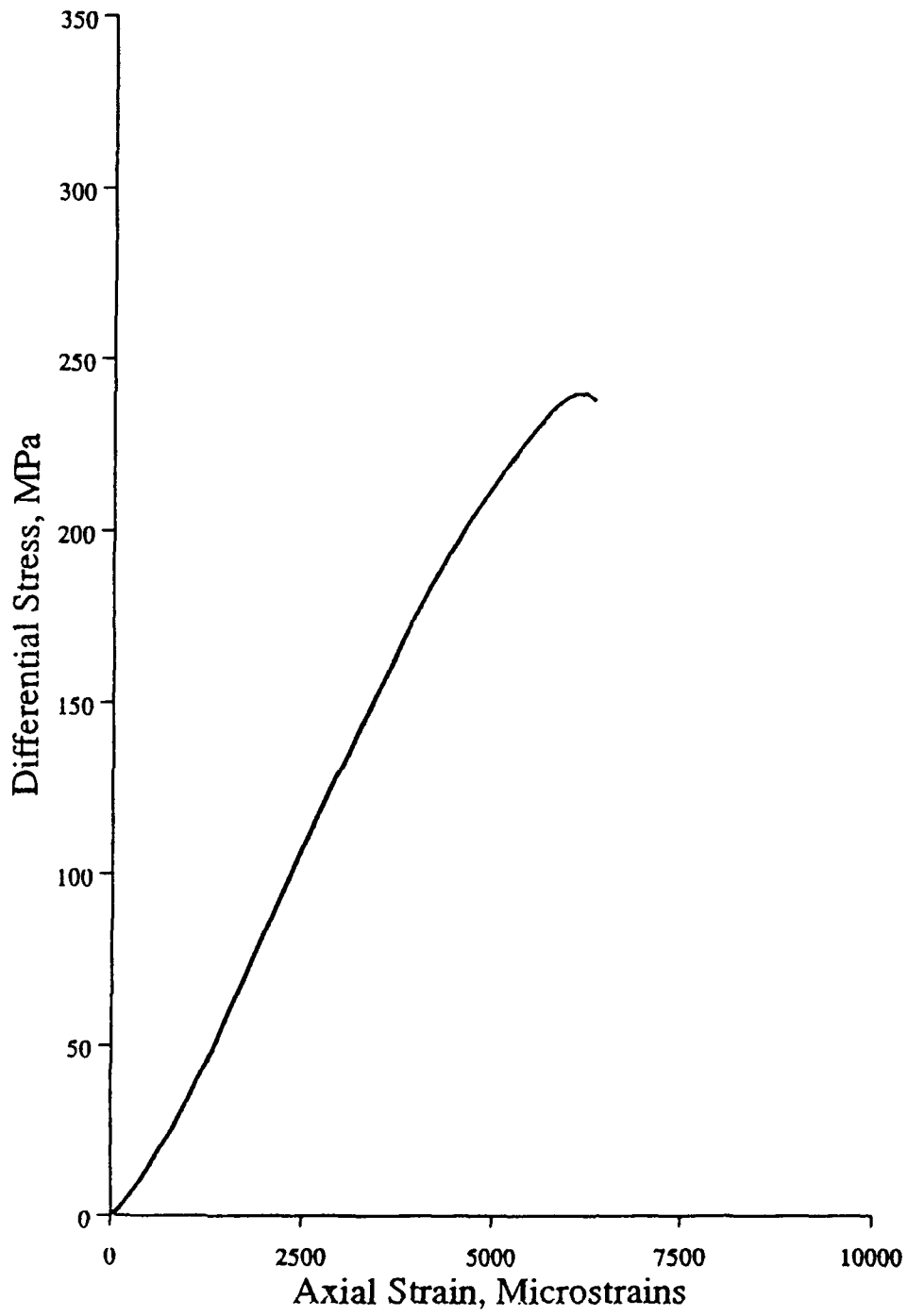
SW 3



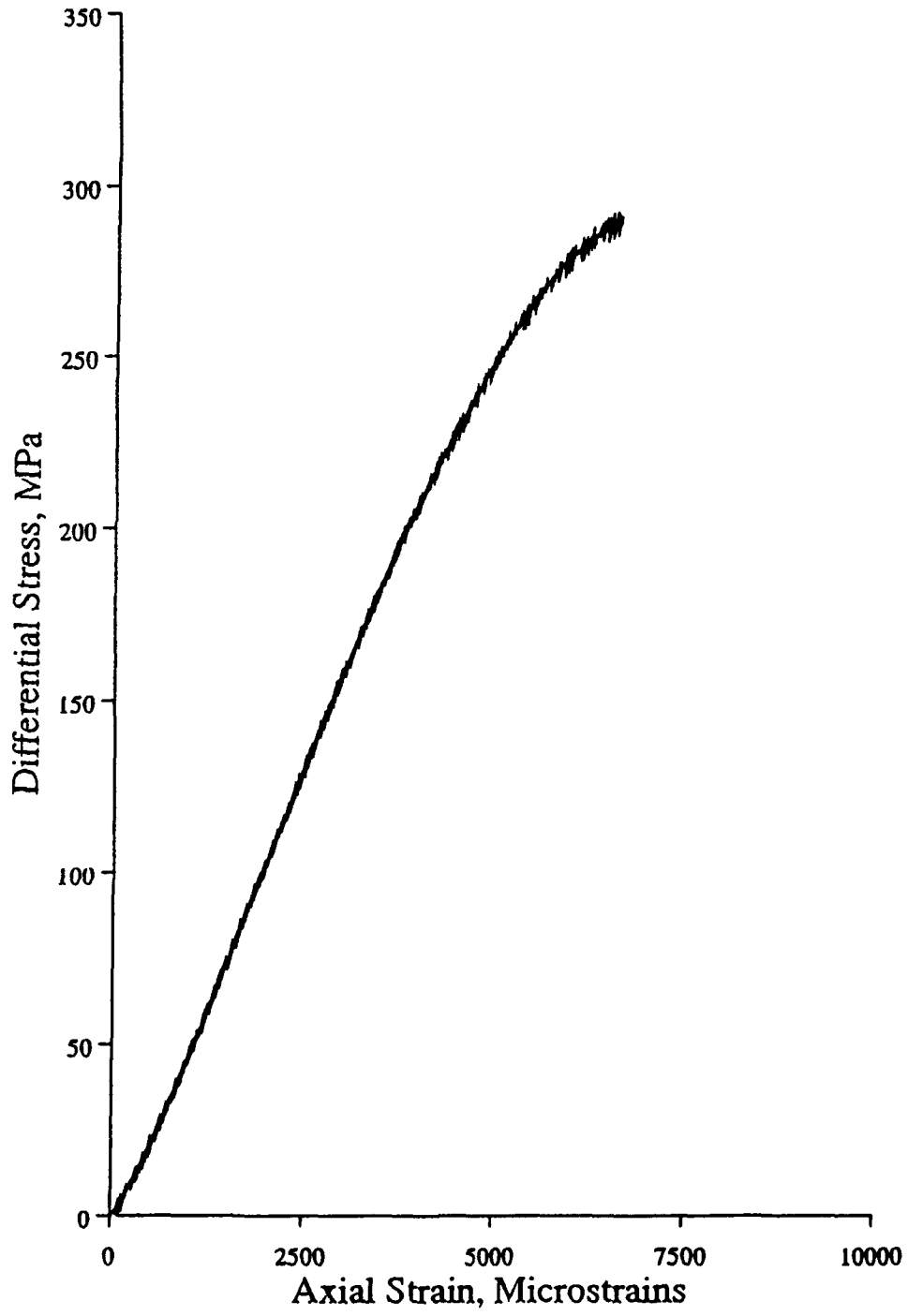
SW 6



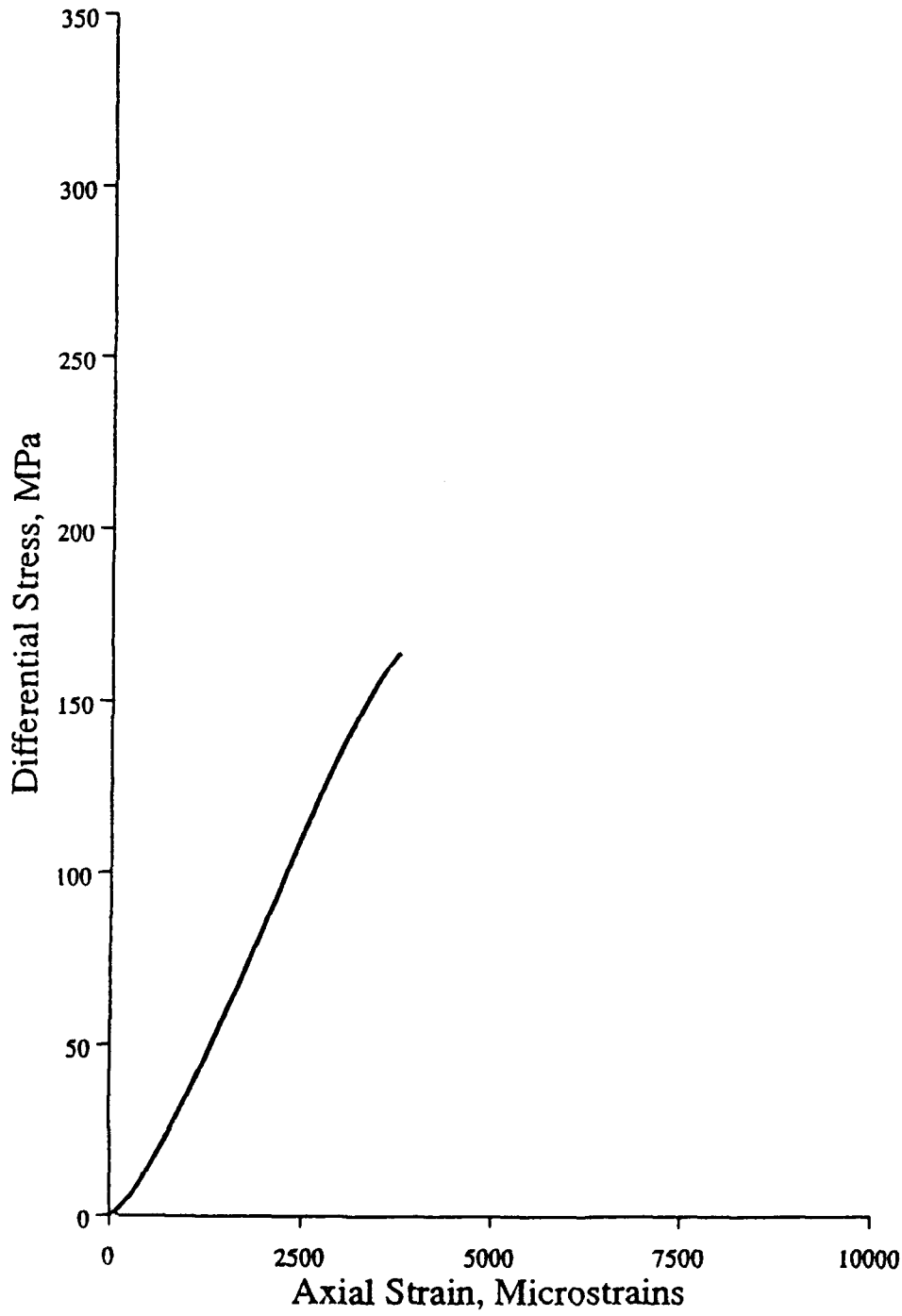
SW 2



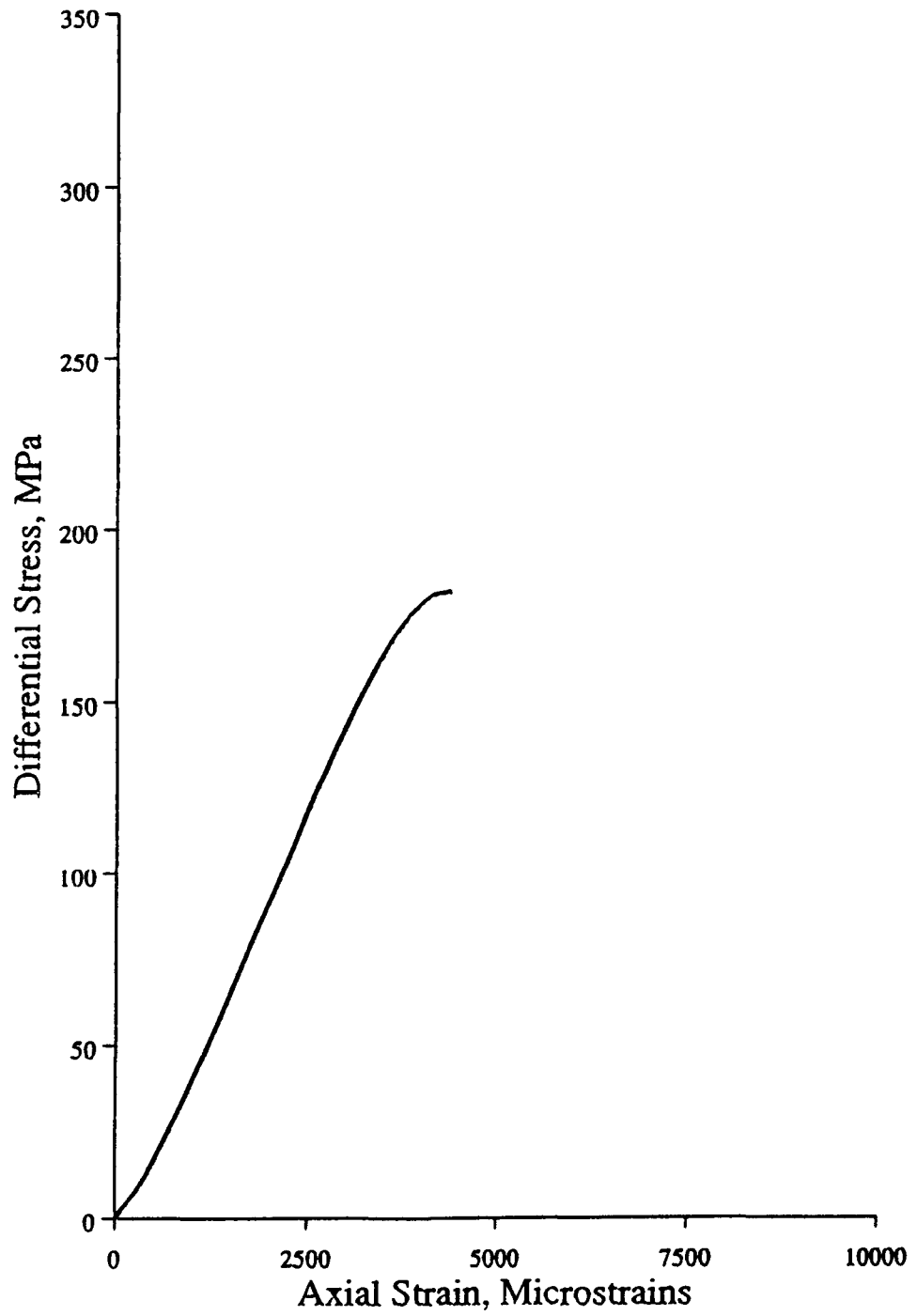
SW 8



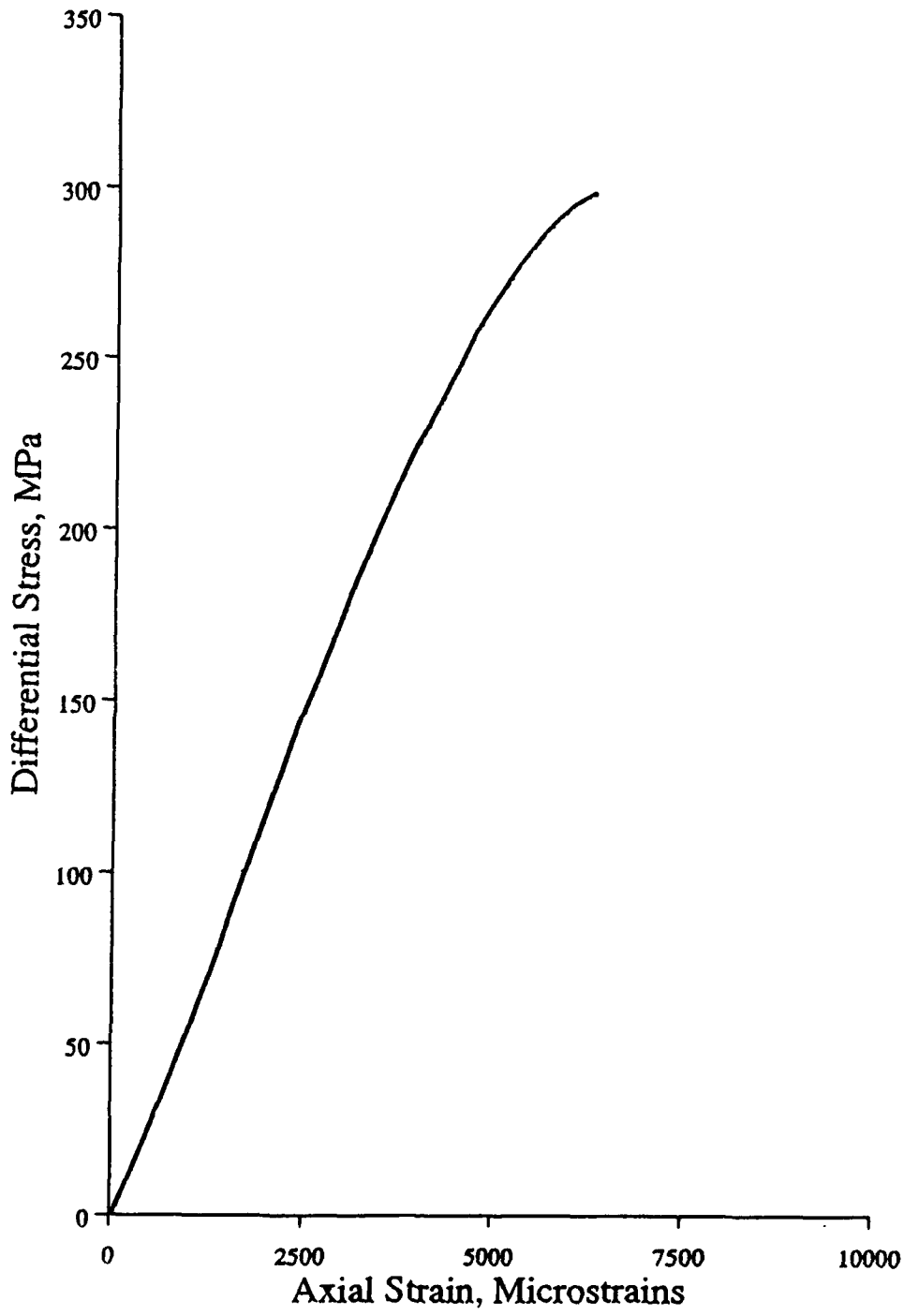
SW 5



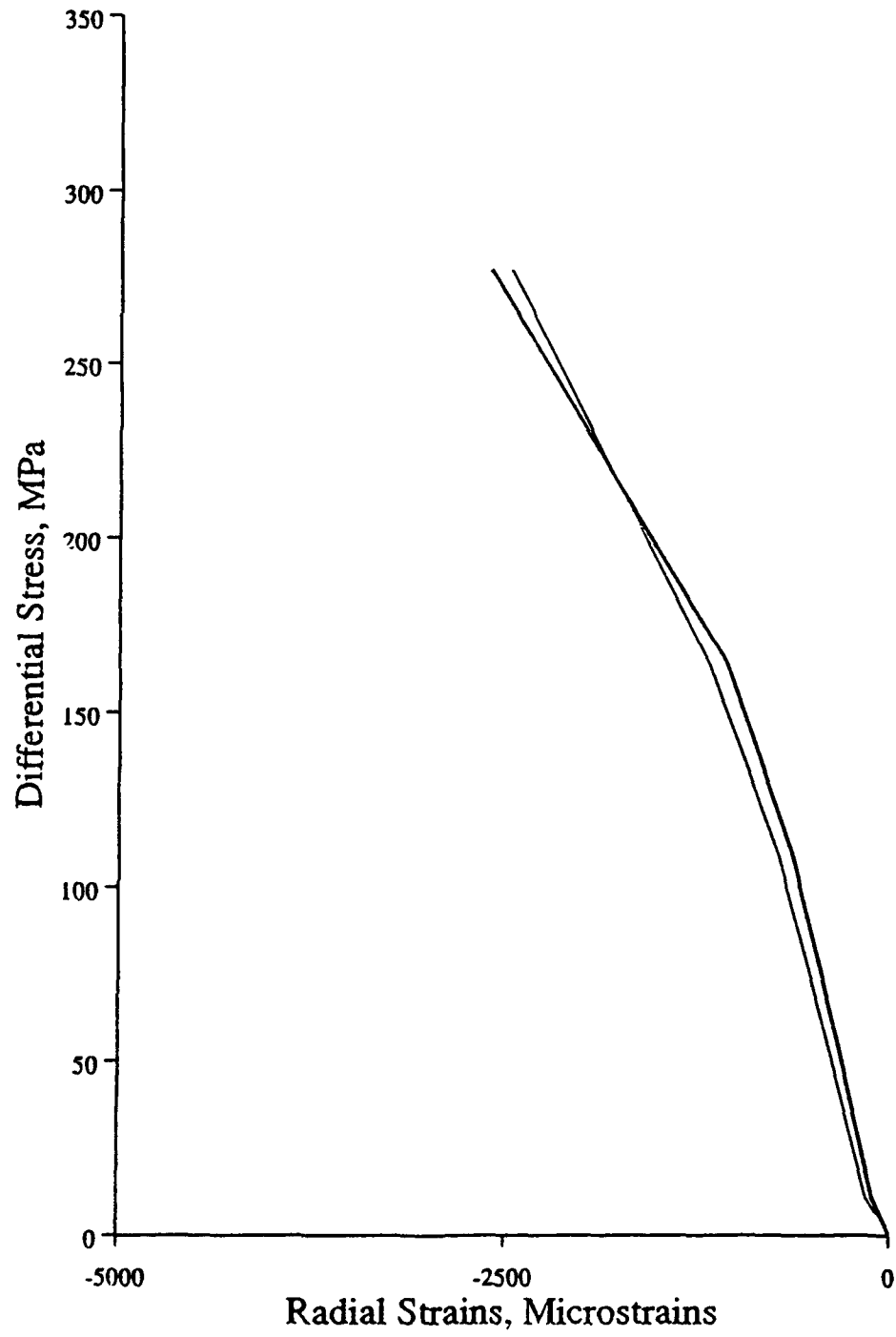
SW 7



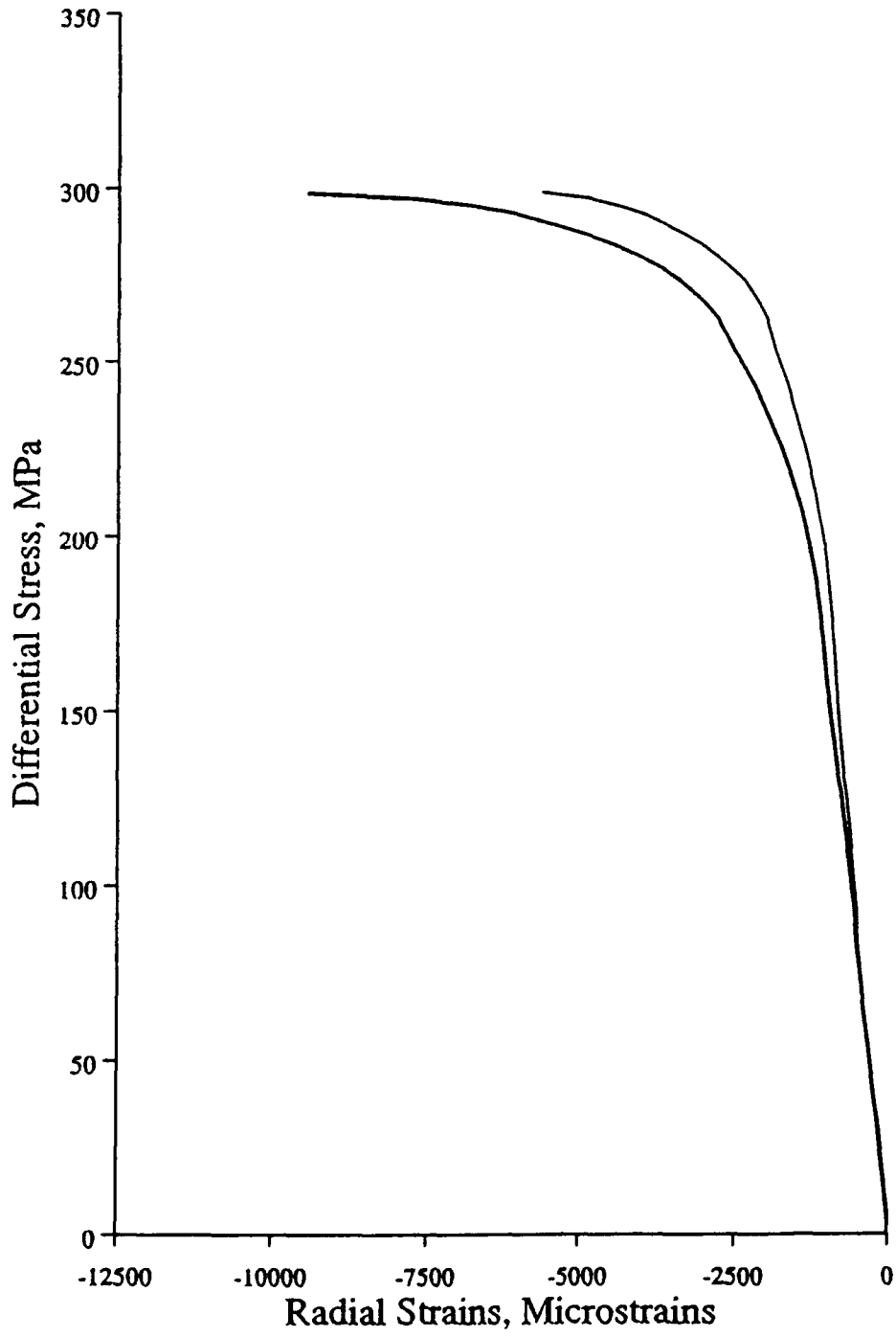
SW 4



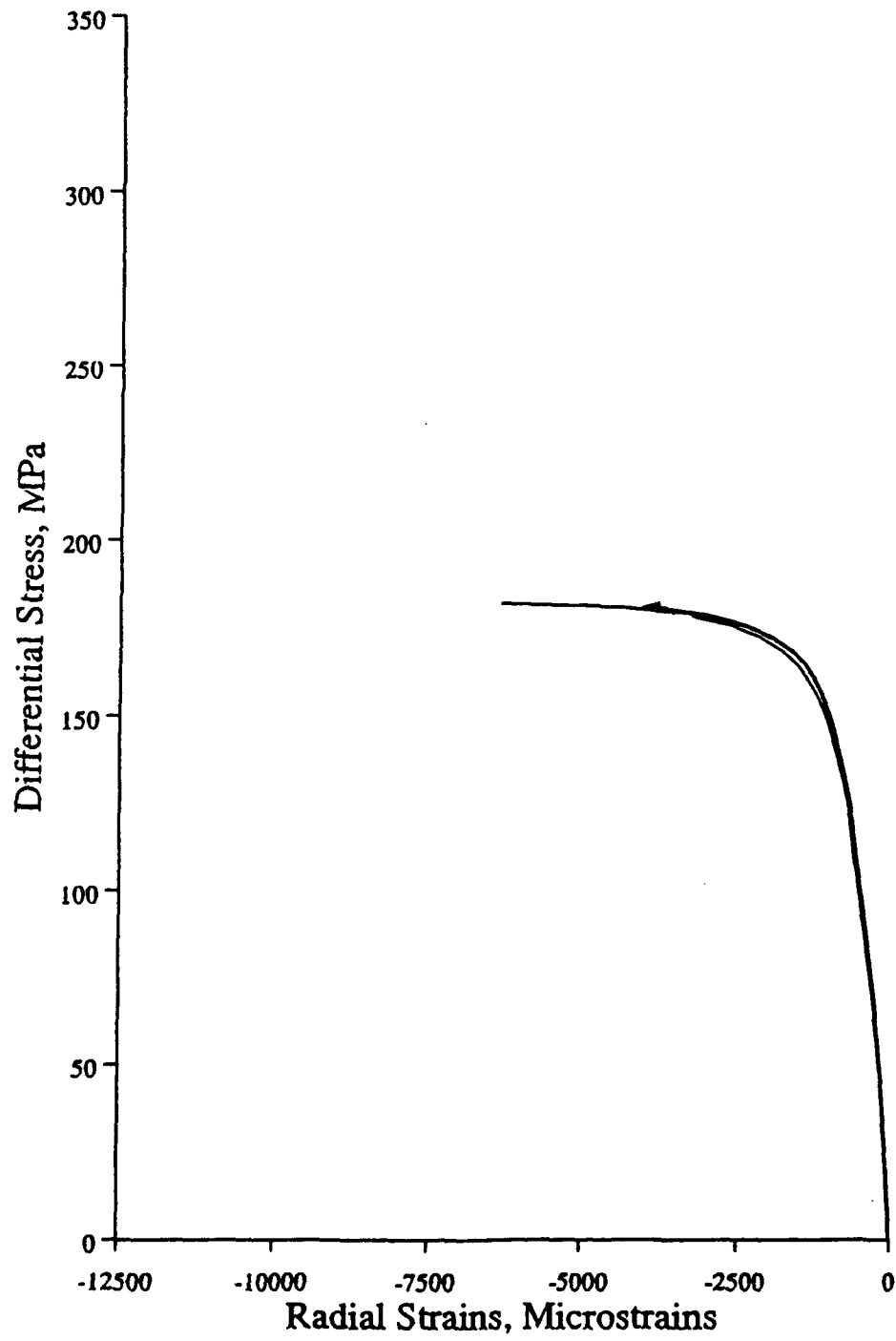
SW 1



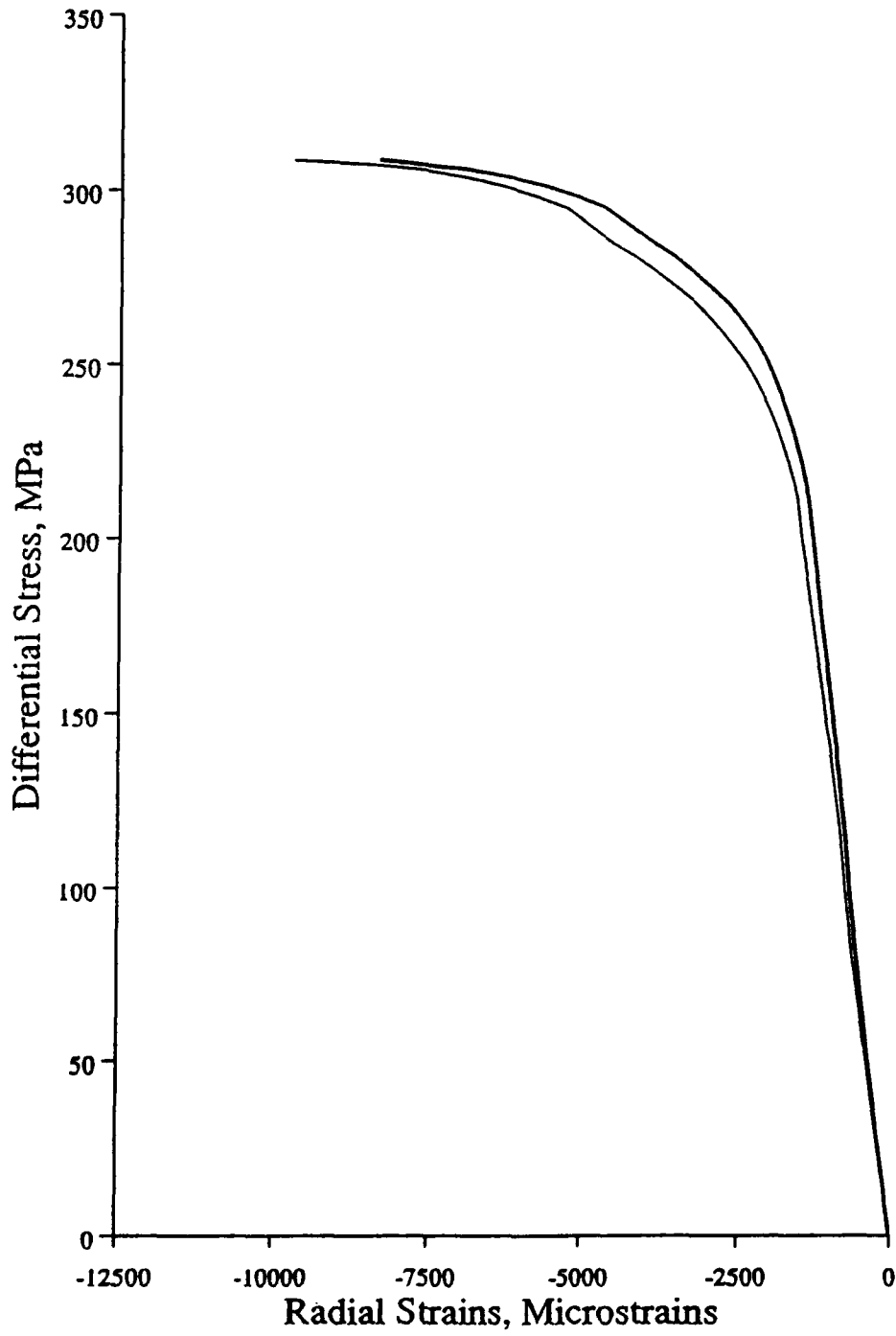
SW 3



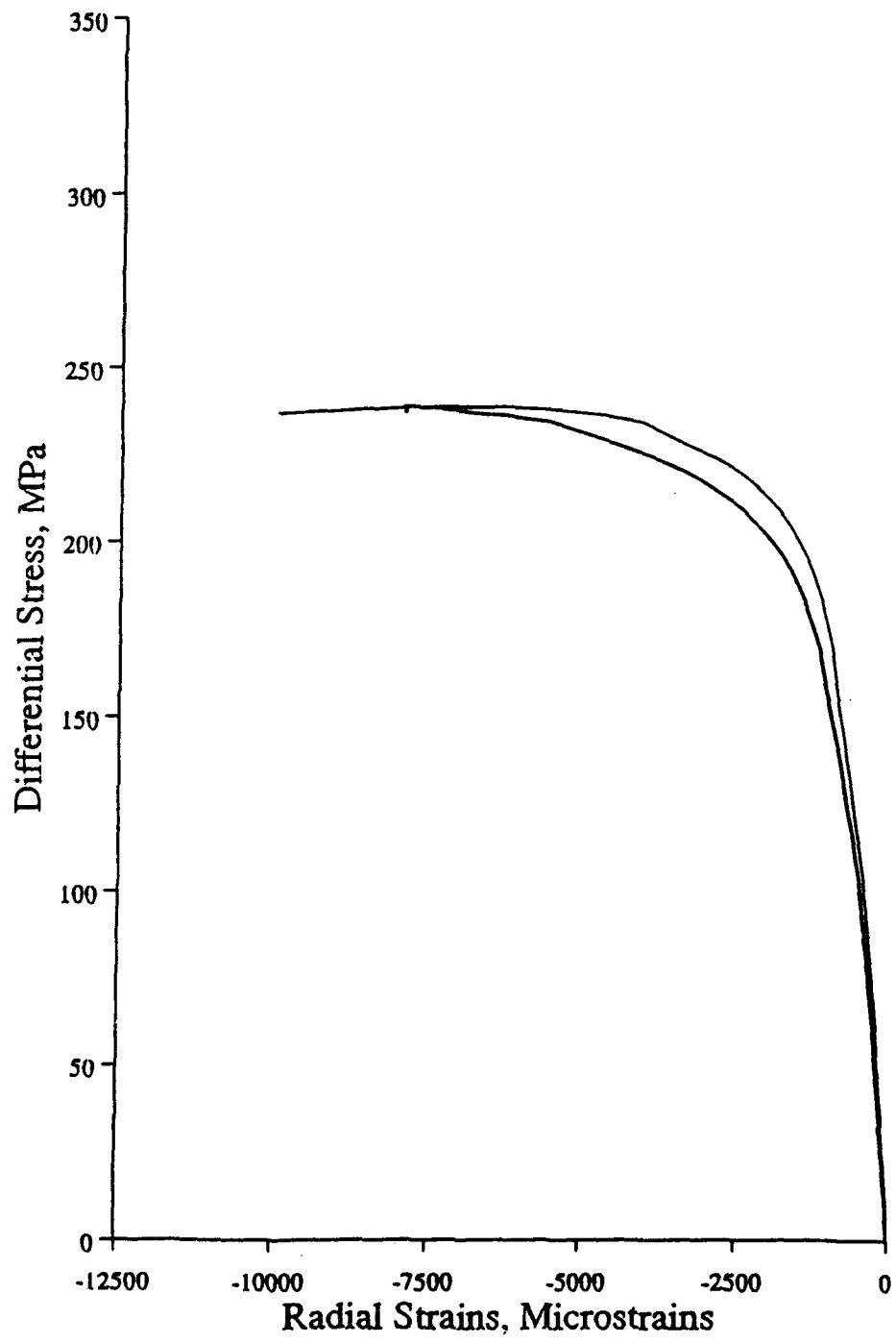
SW 8



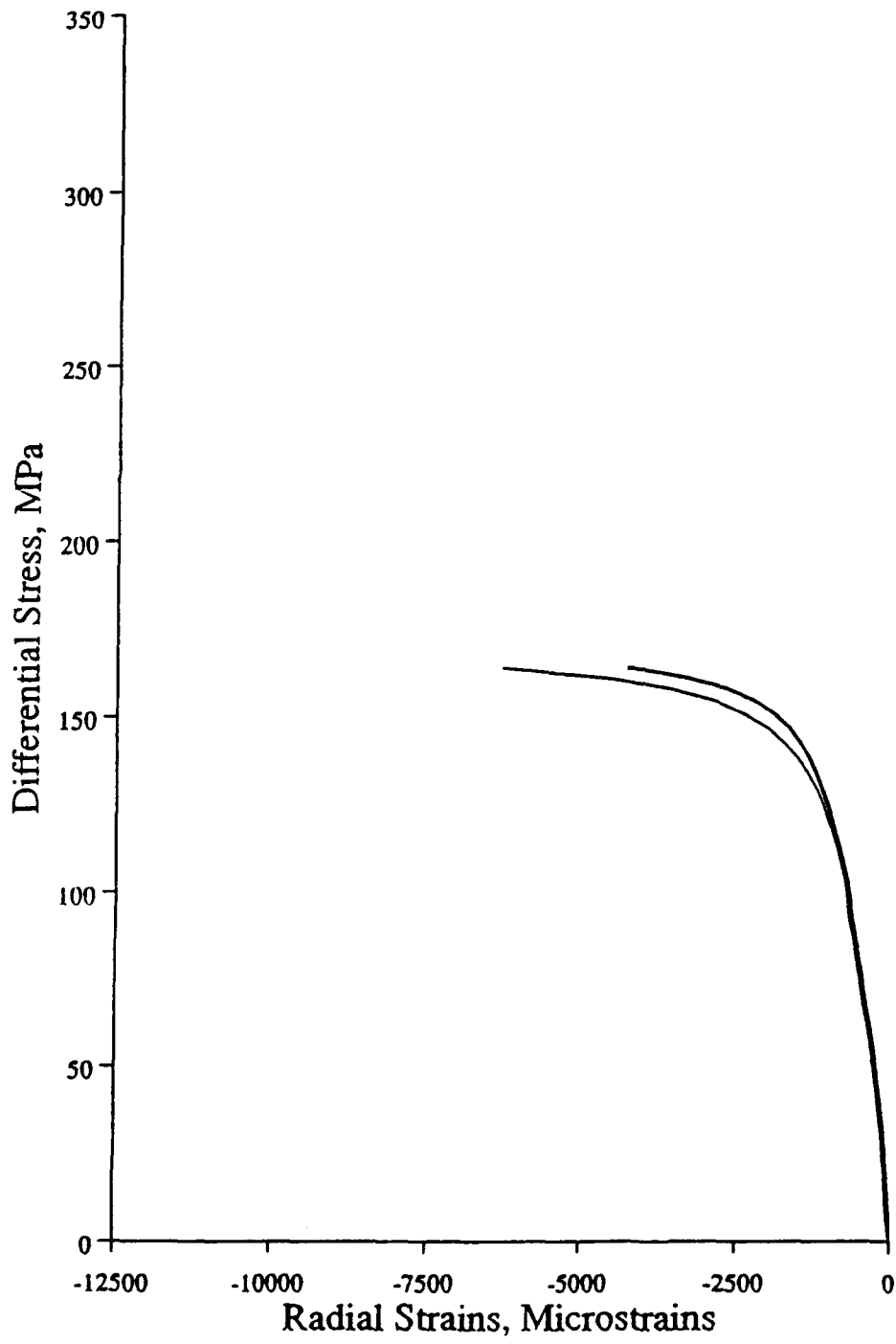
SW 6



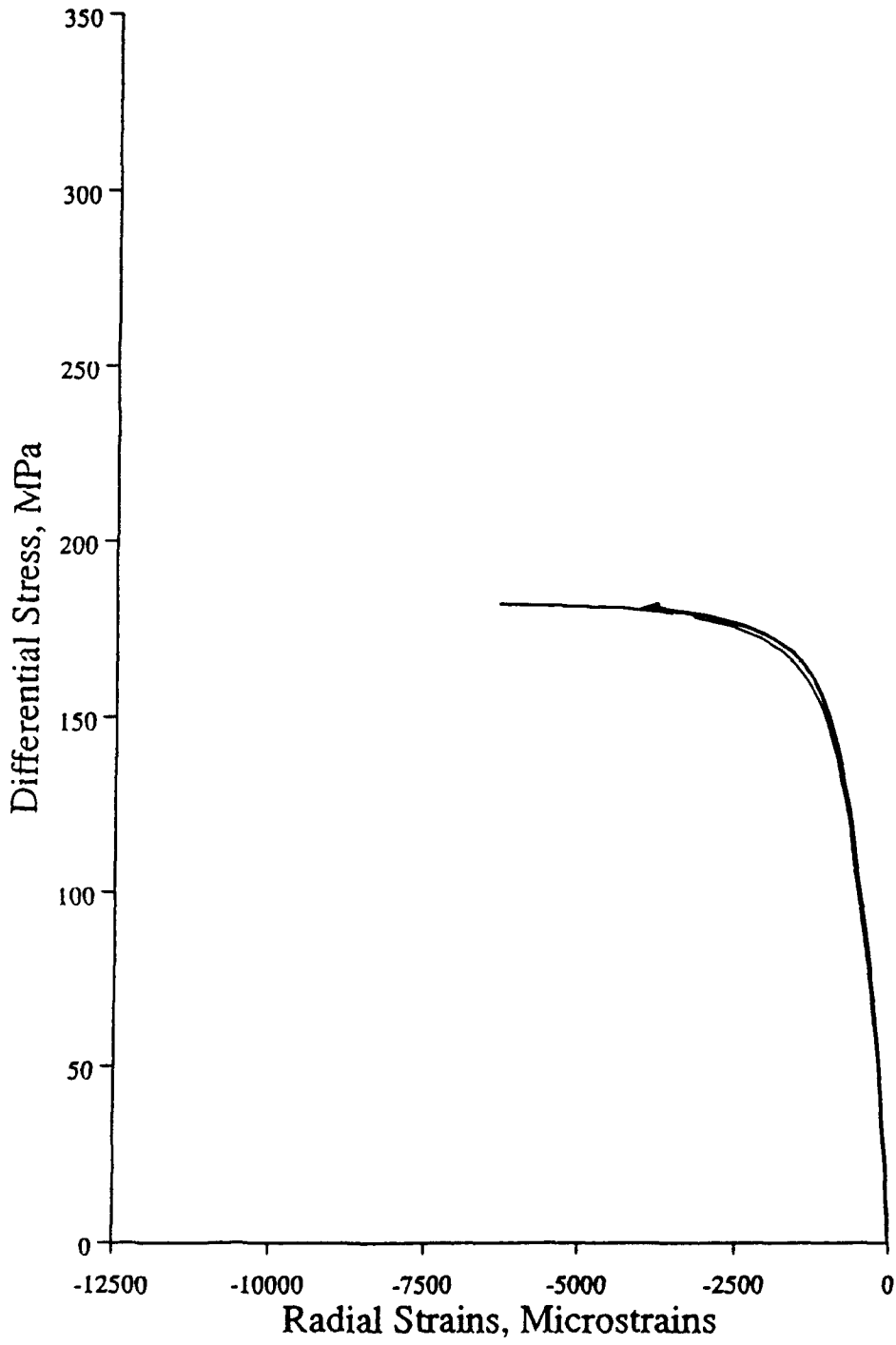
SW 2



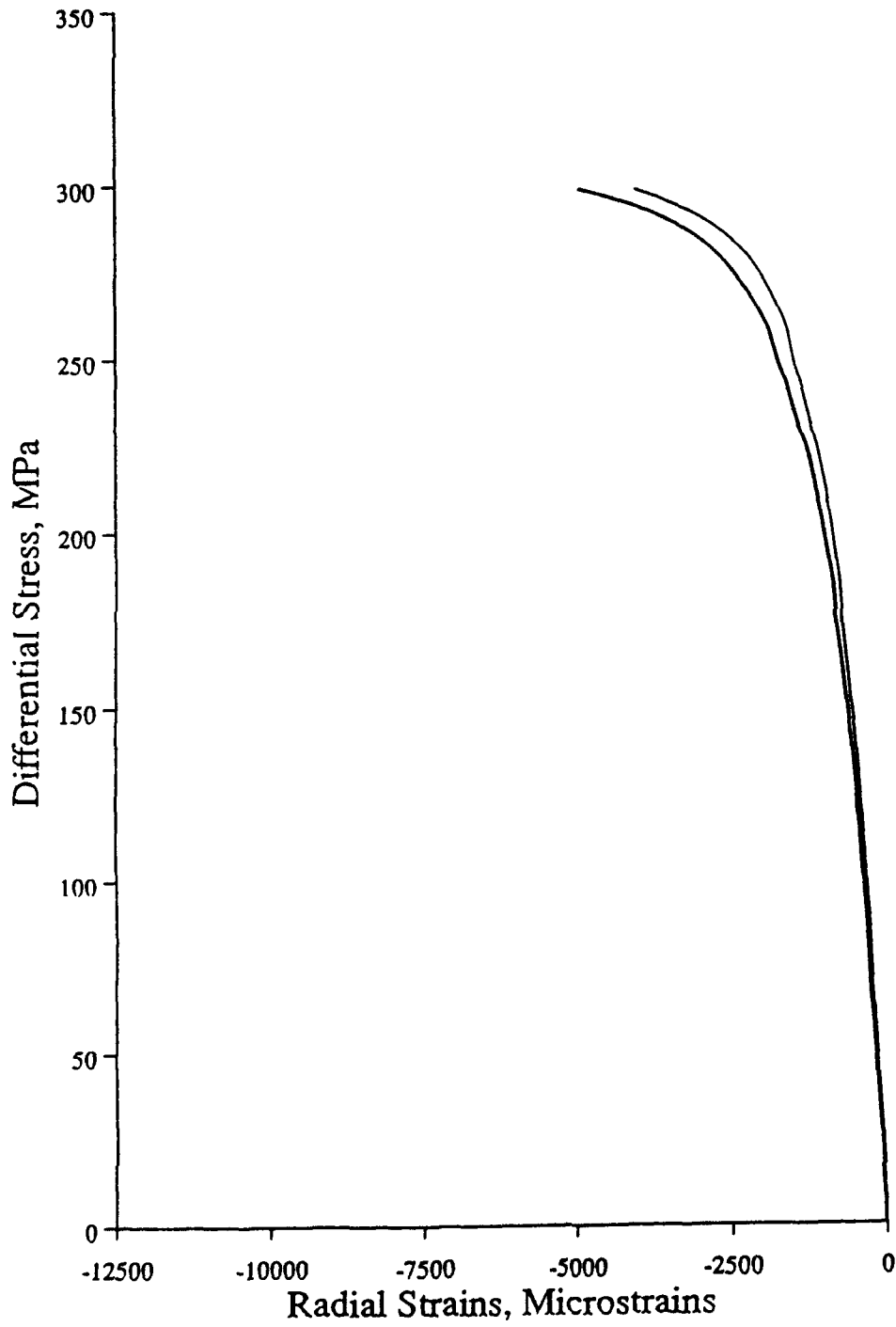
SW 5



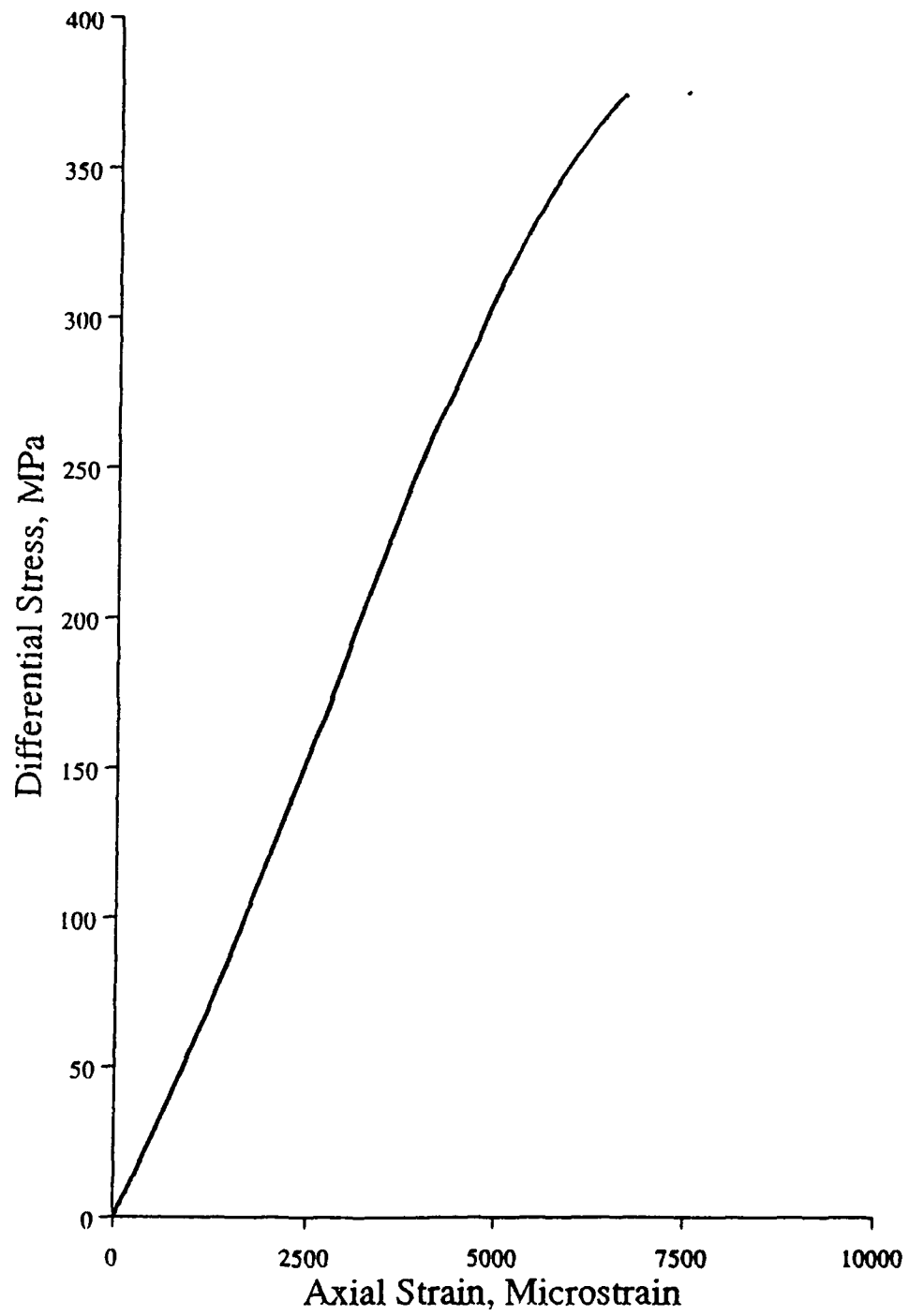
SW 7



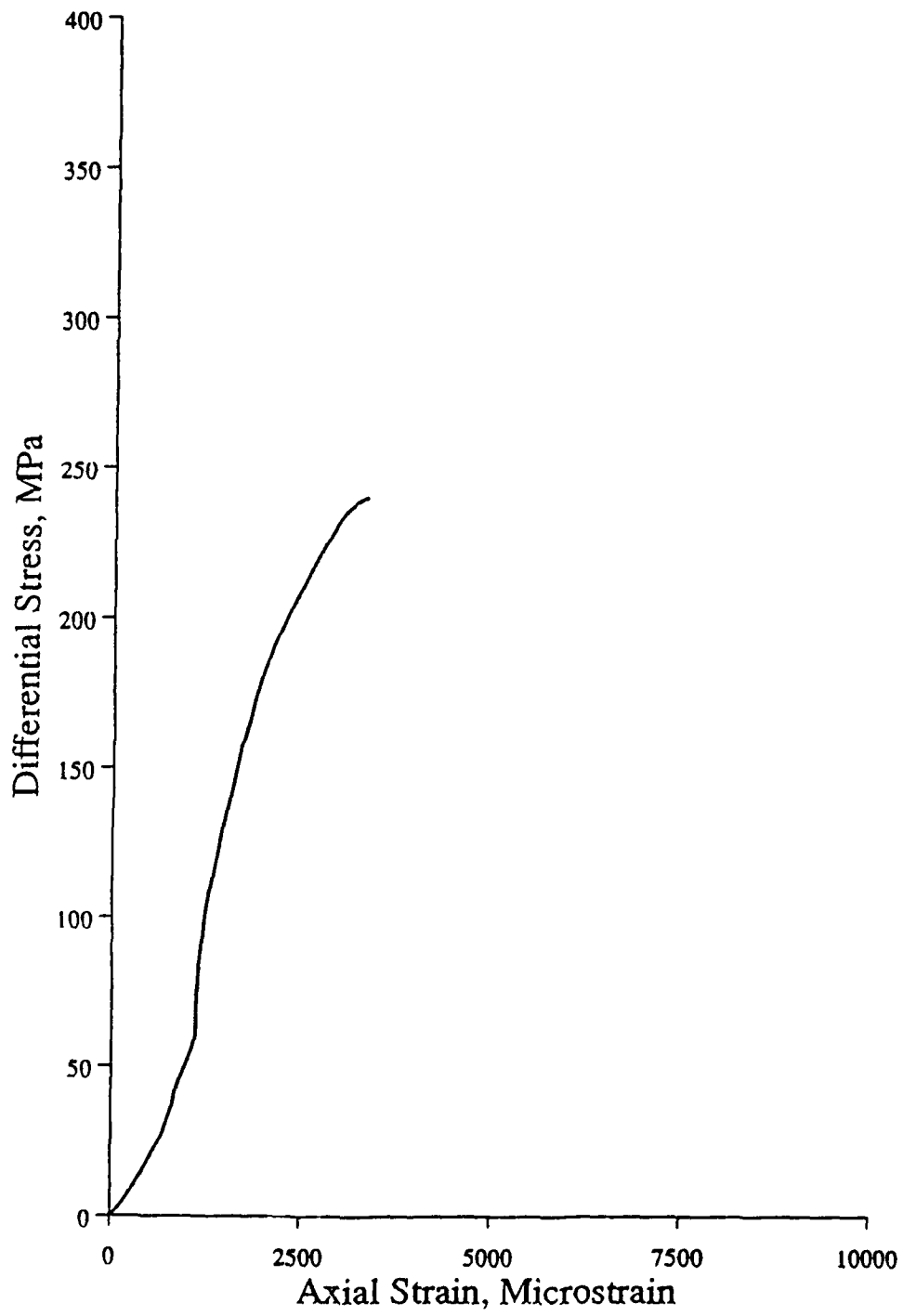
SW 4



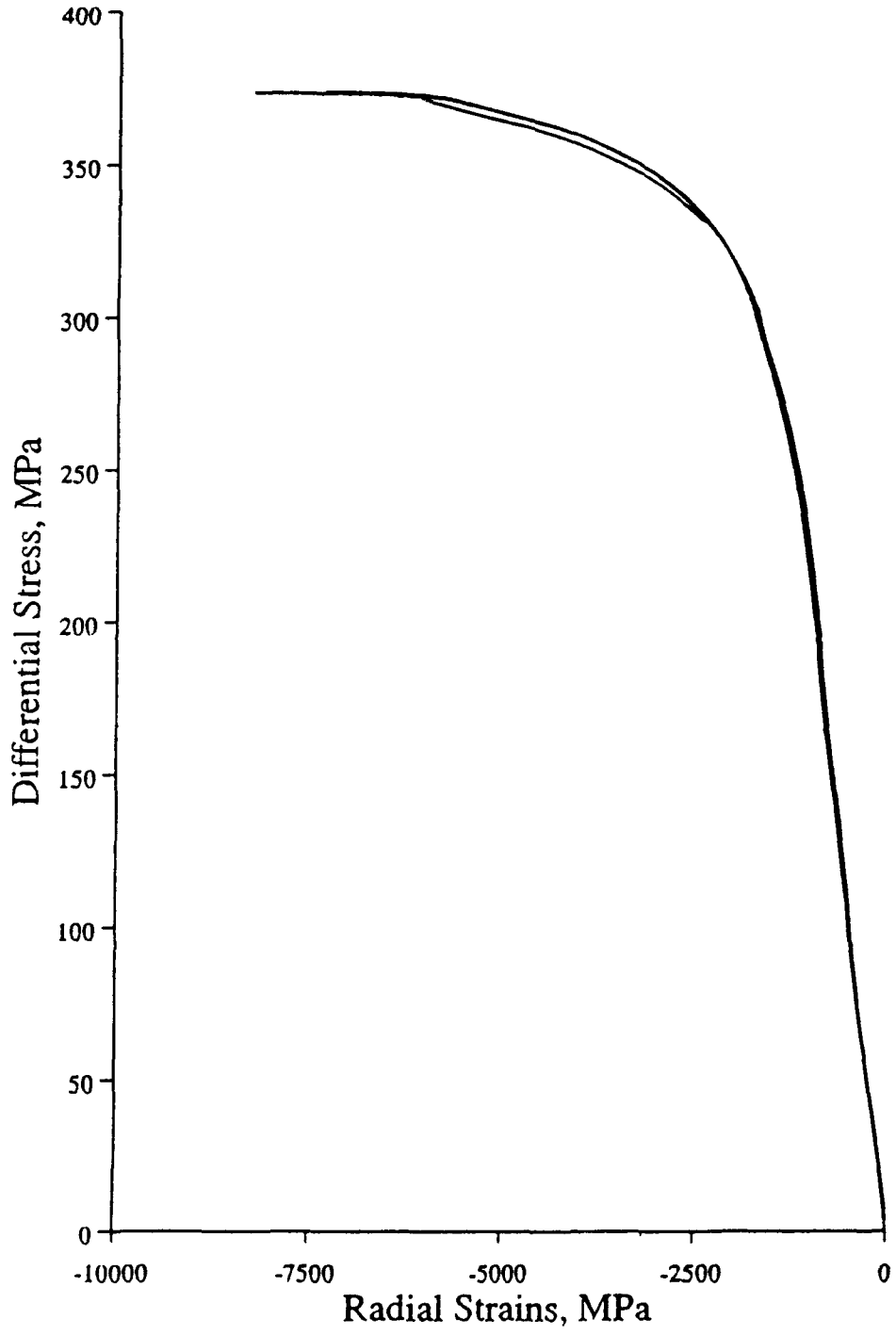
NL 1



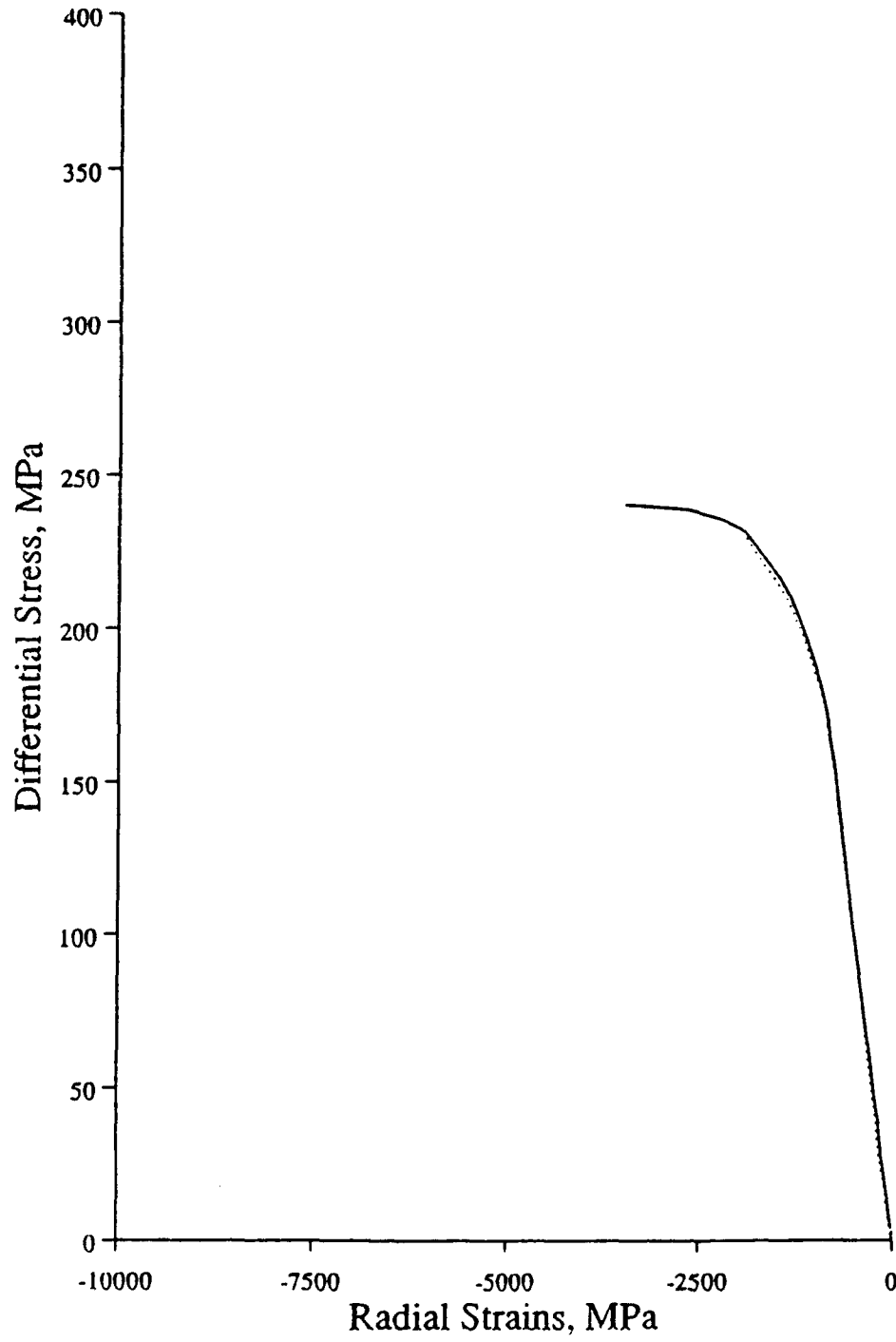
NL 2



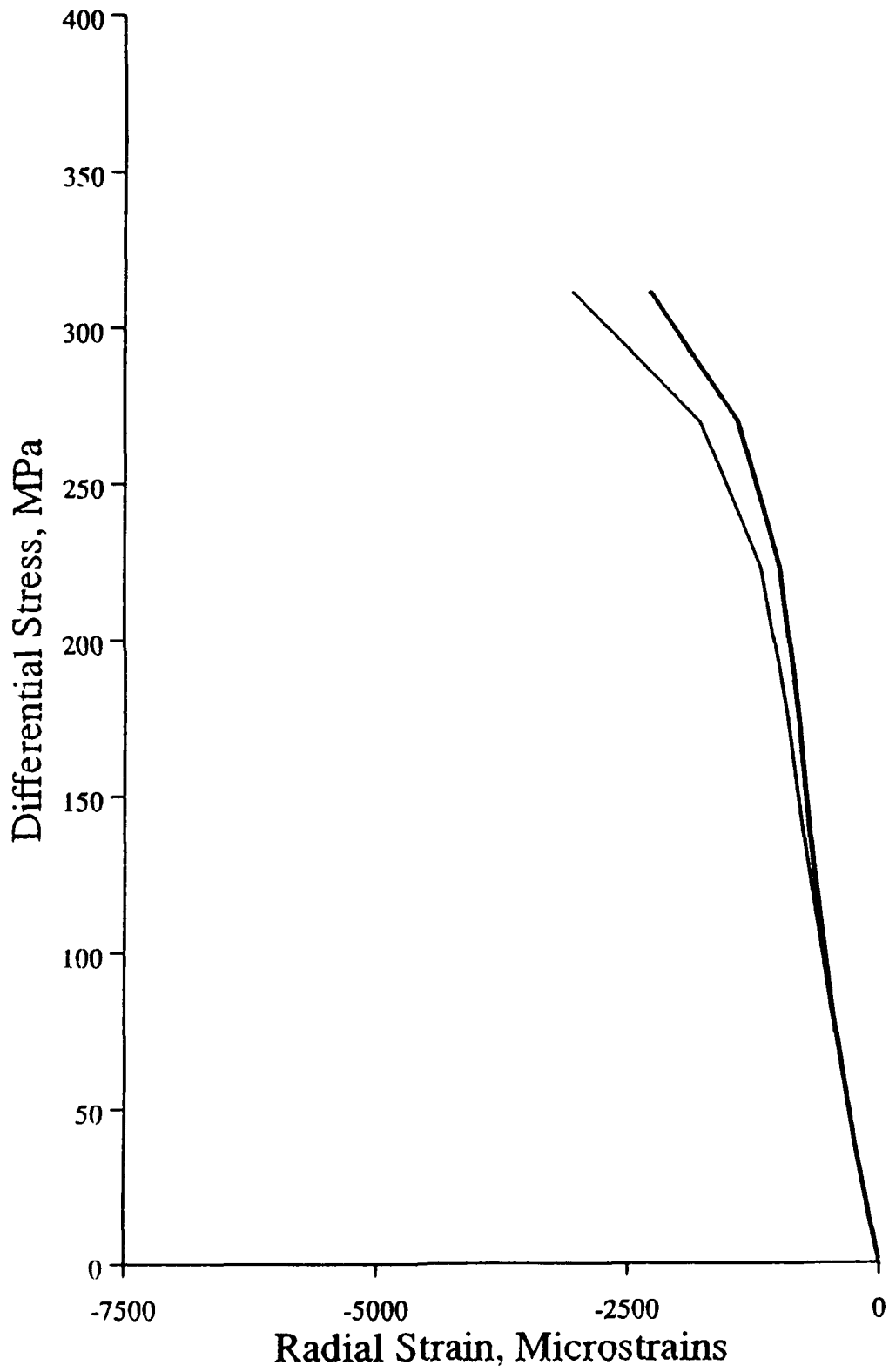
NL 1



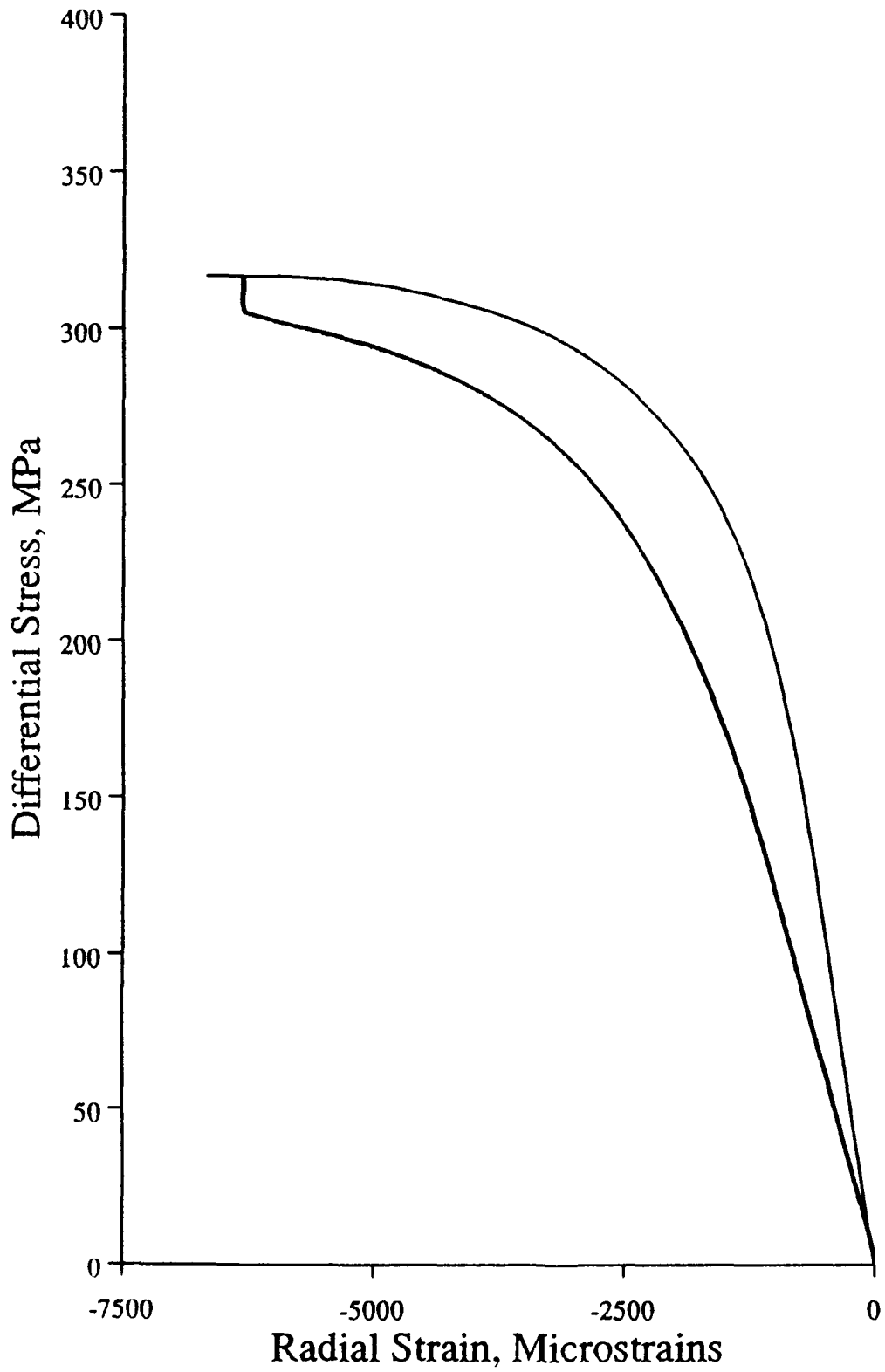
NL 2



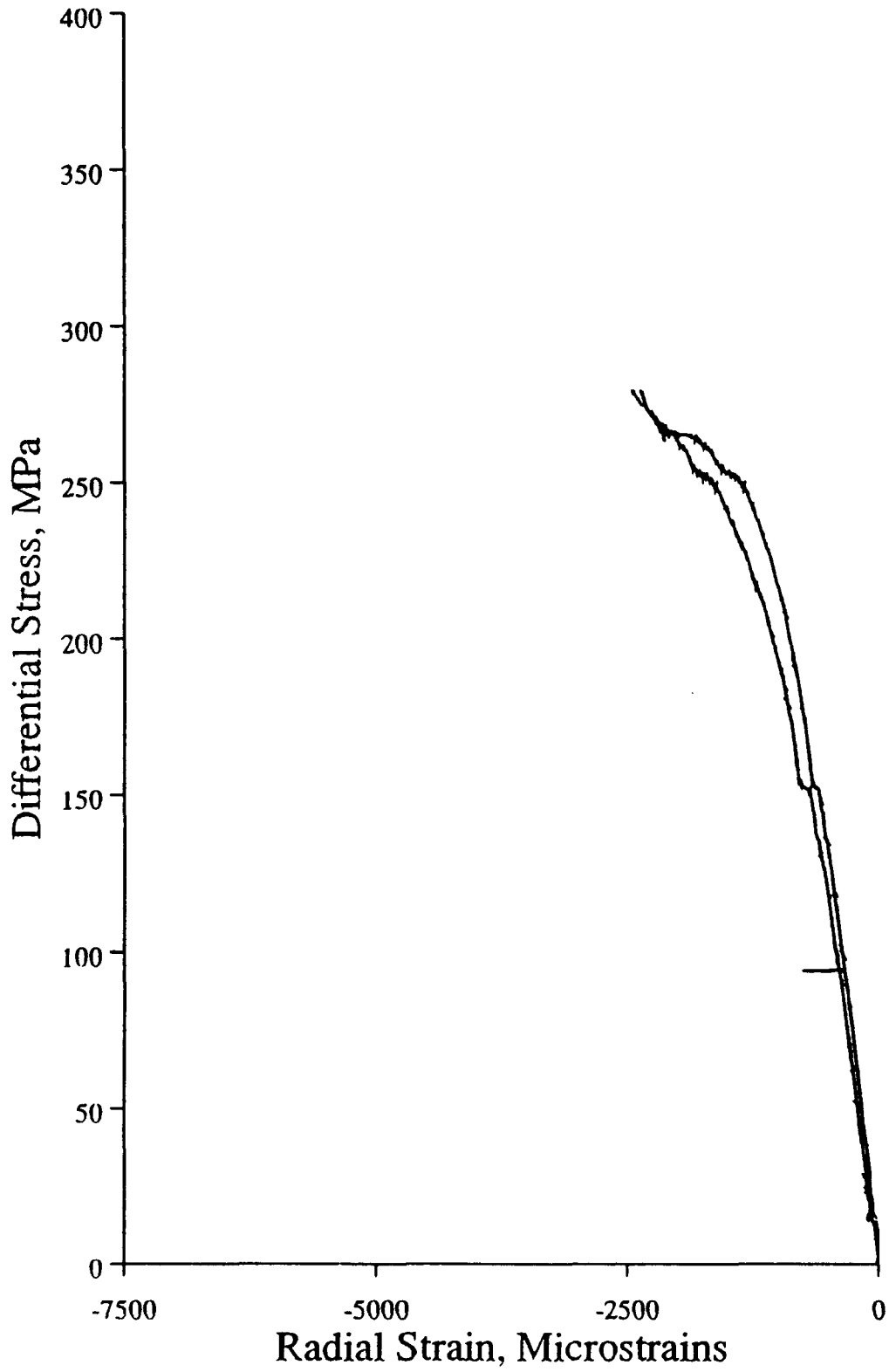
KG 5



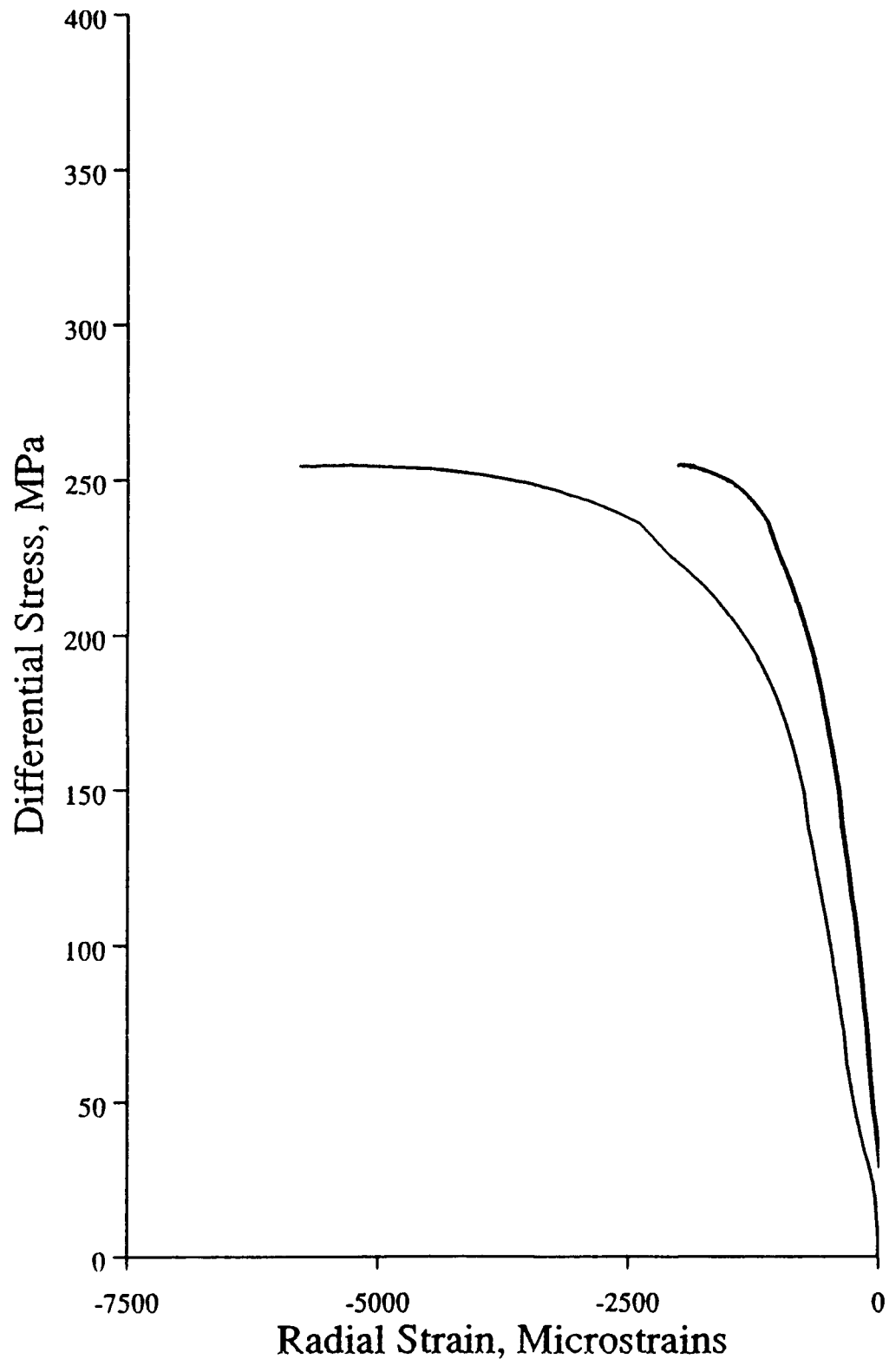
KG 15



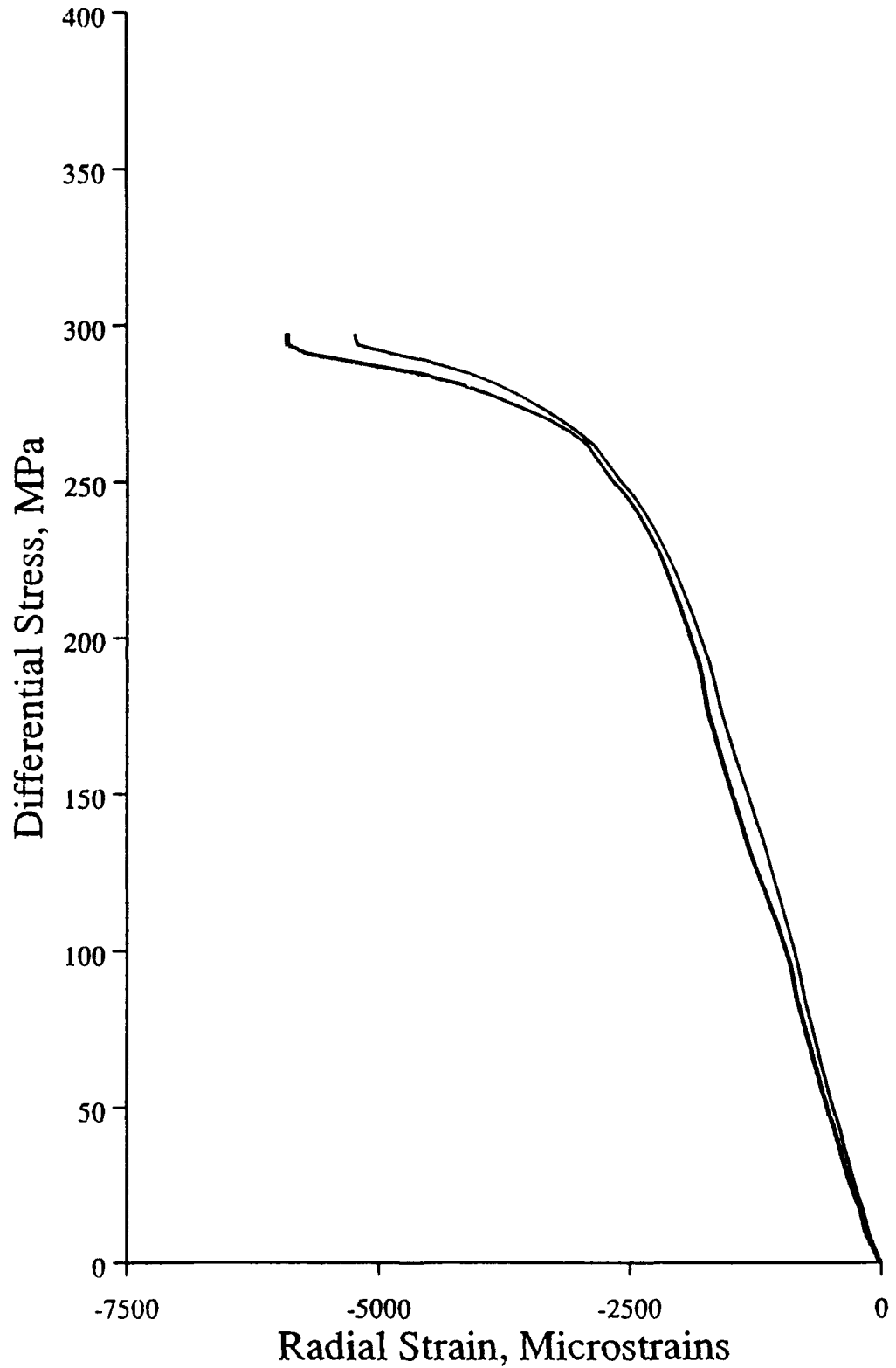
KG 6



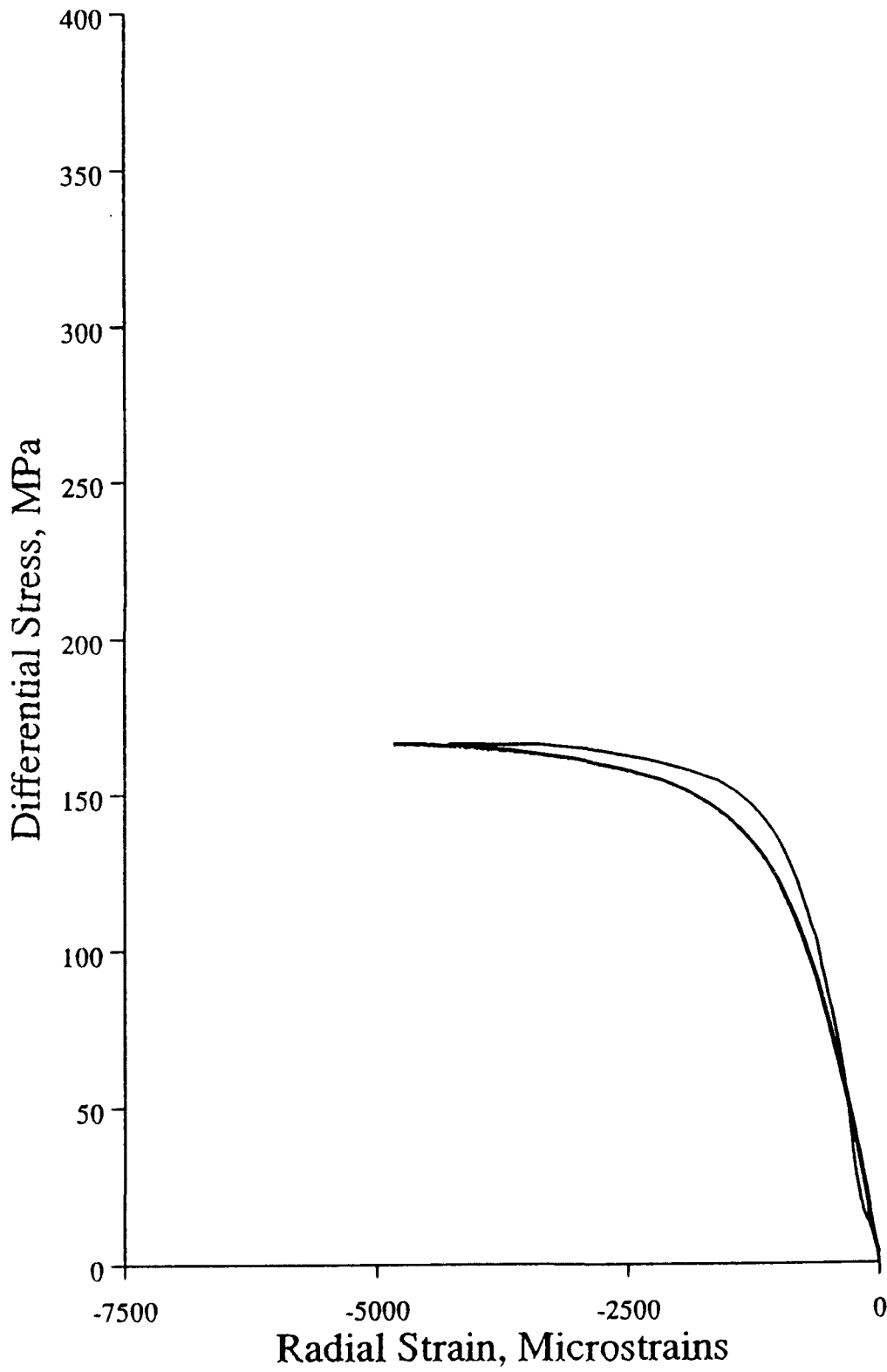
KG 17



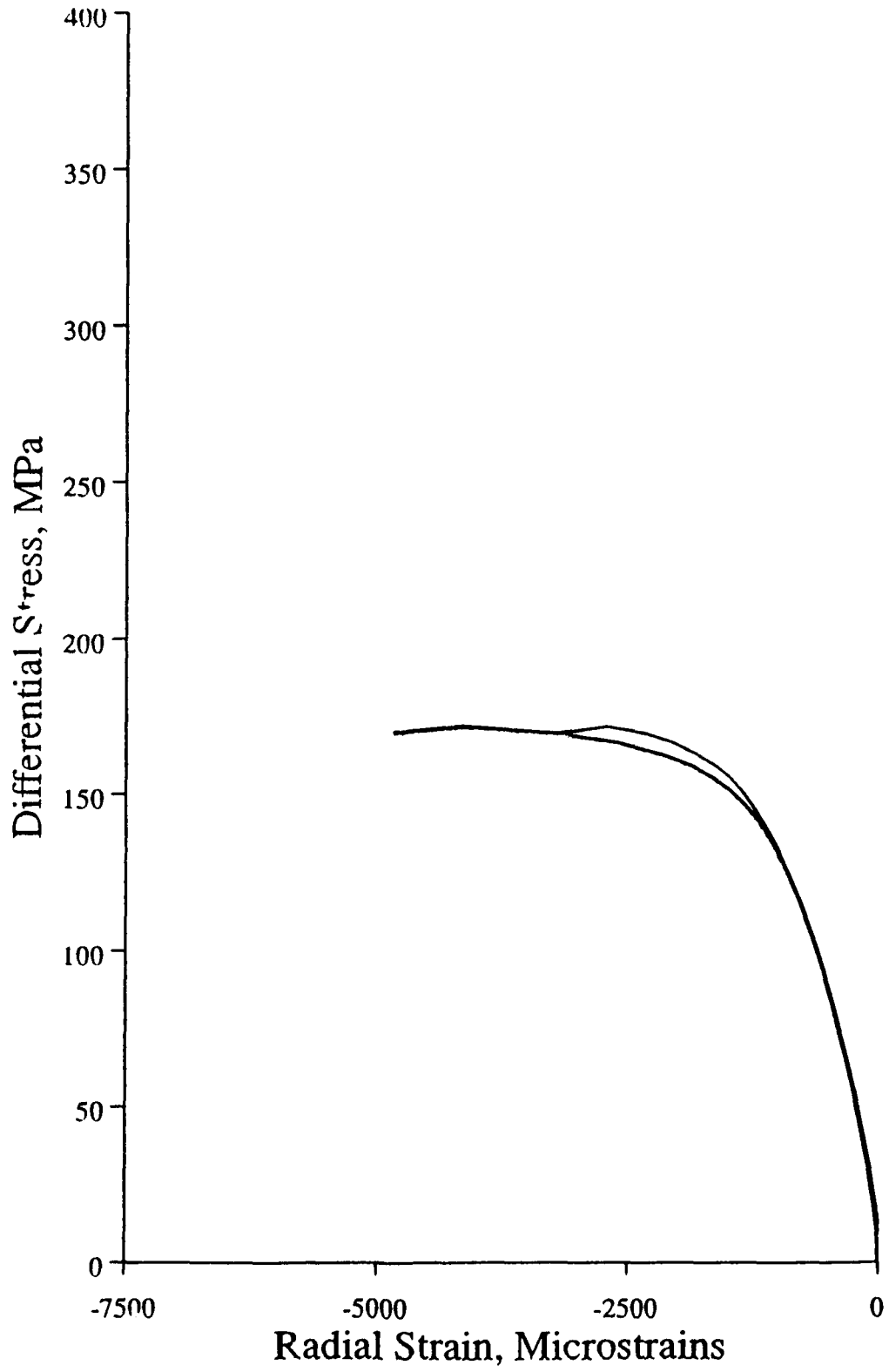
KG 18



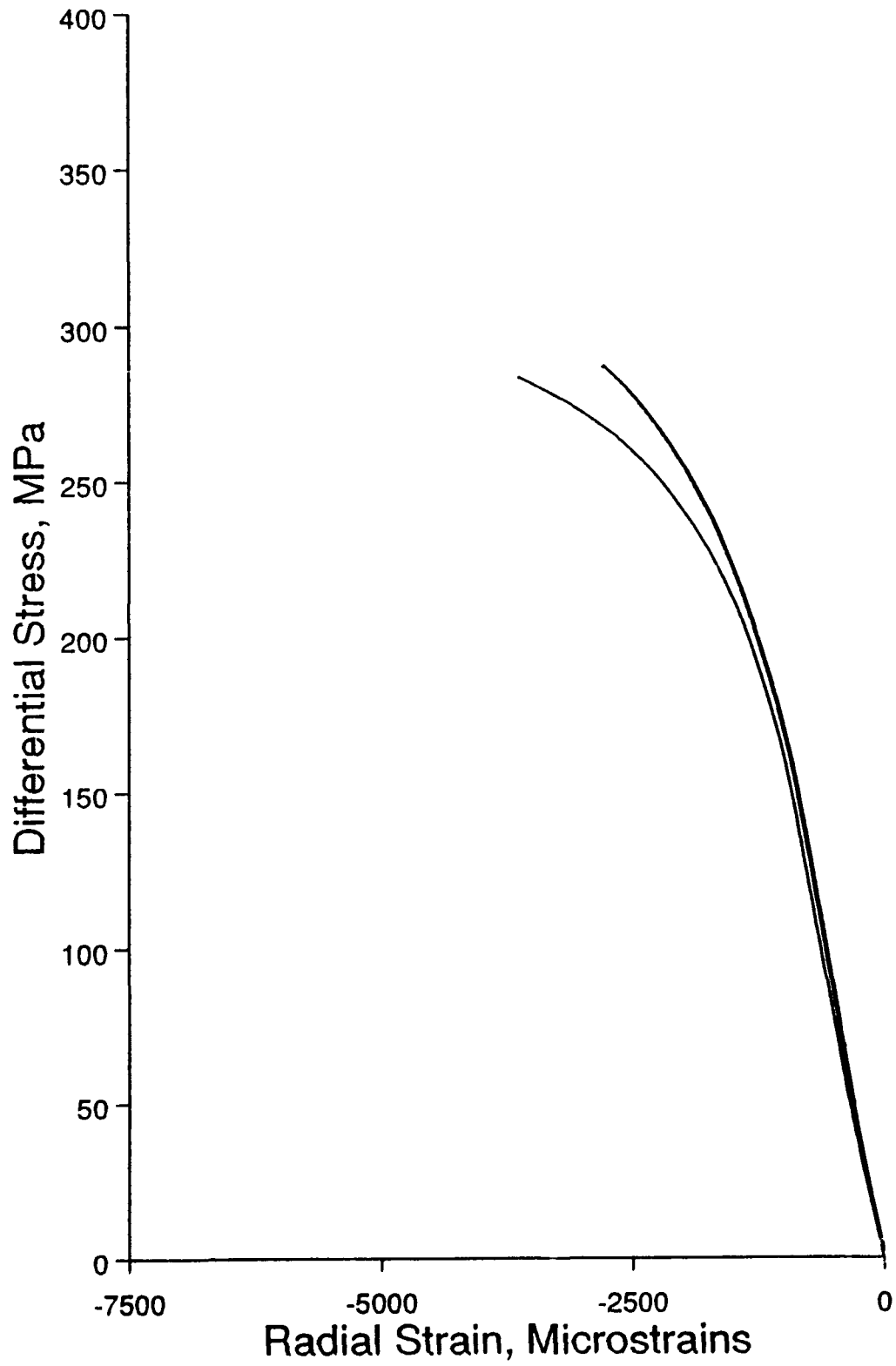
KG 19

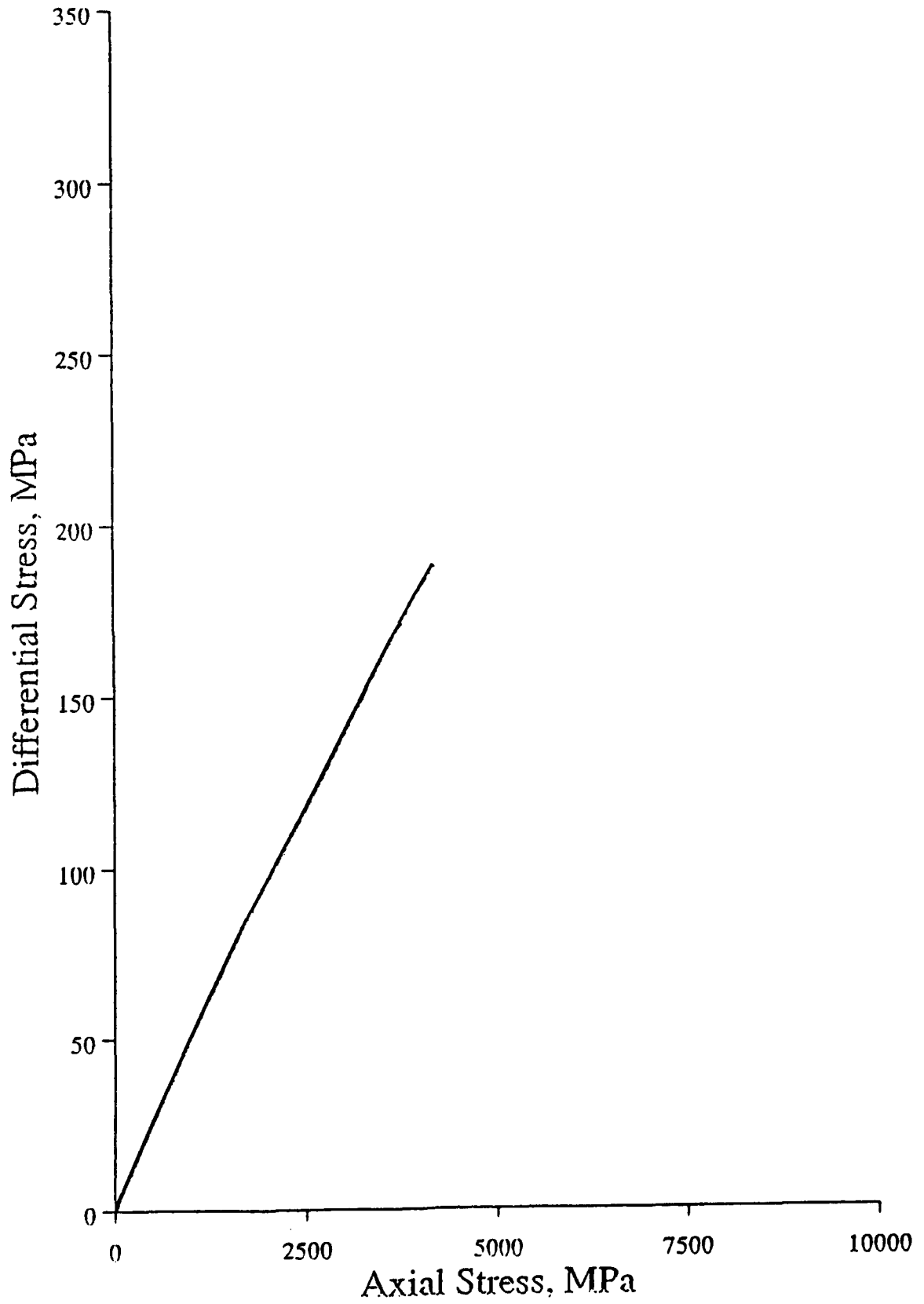


KG 20

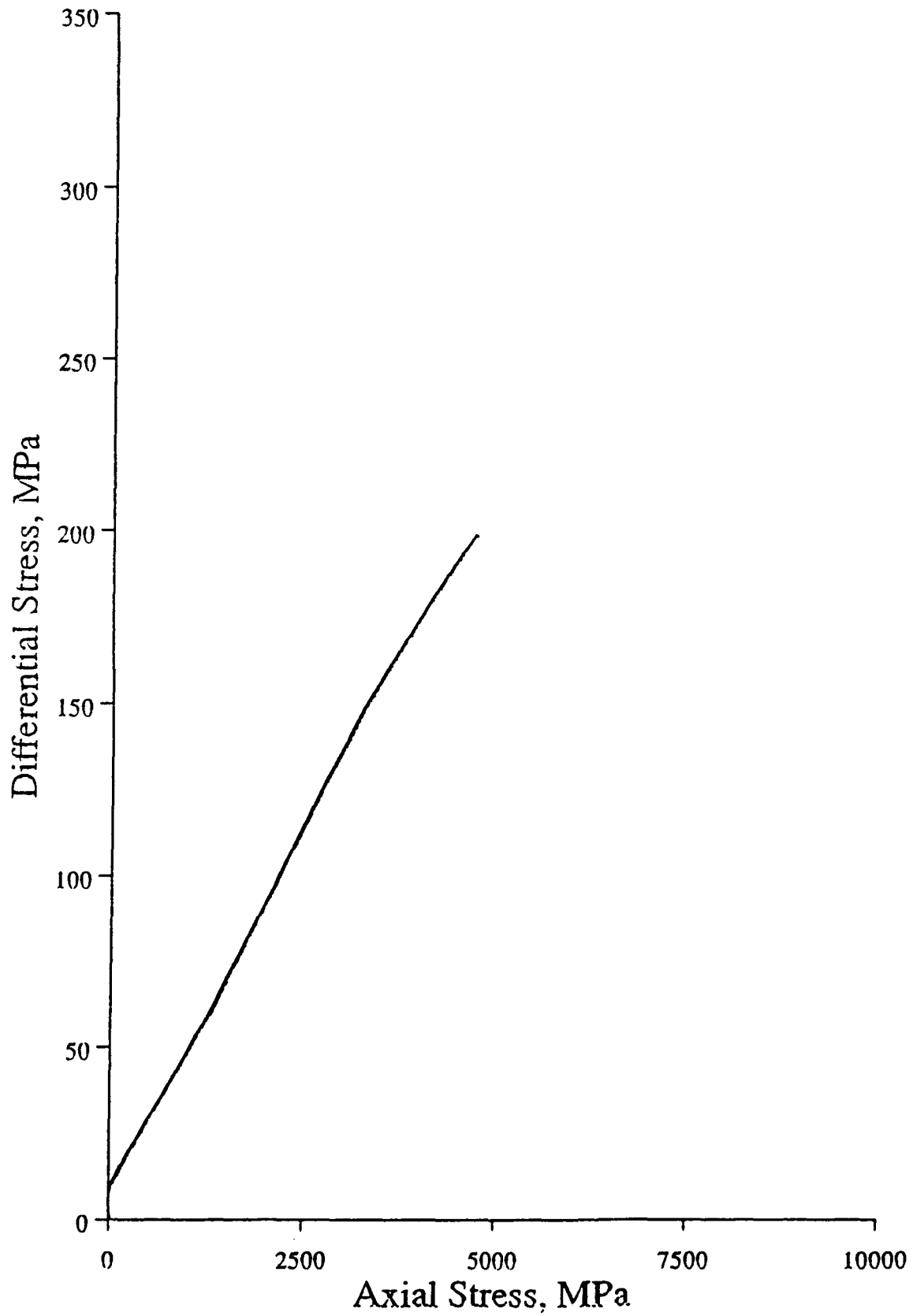


KG 4

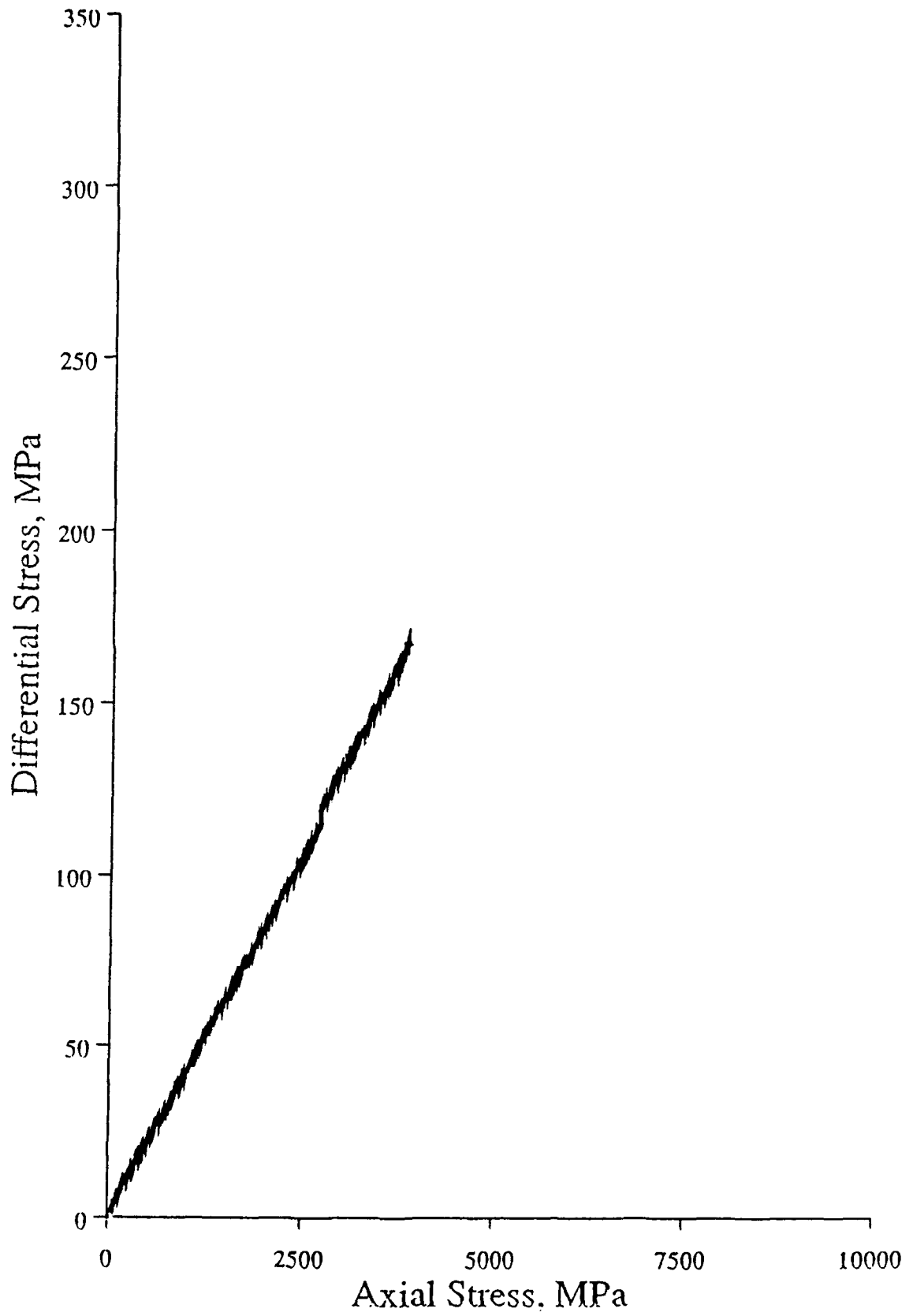




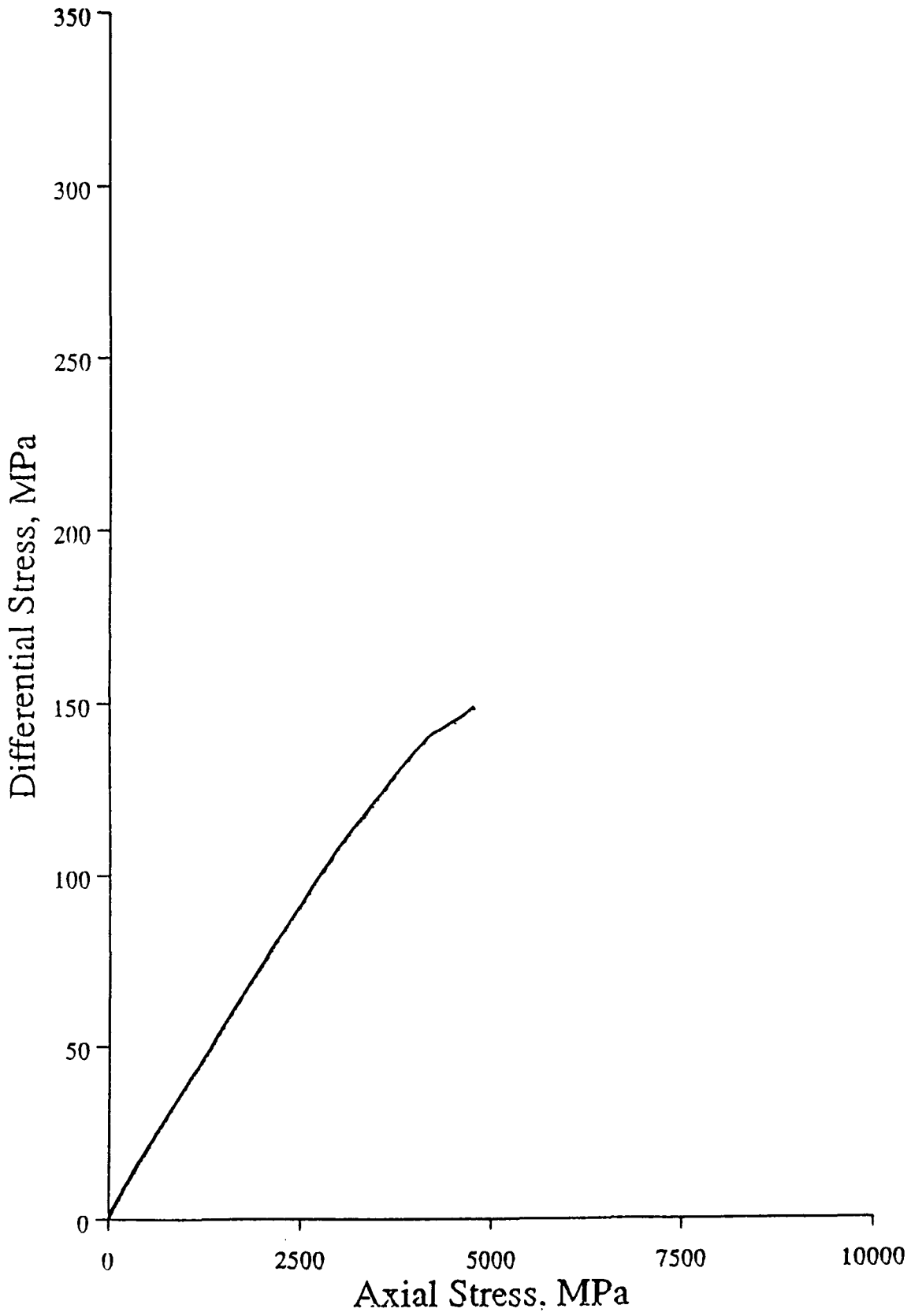
TS 1B



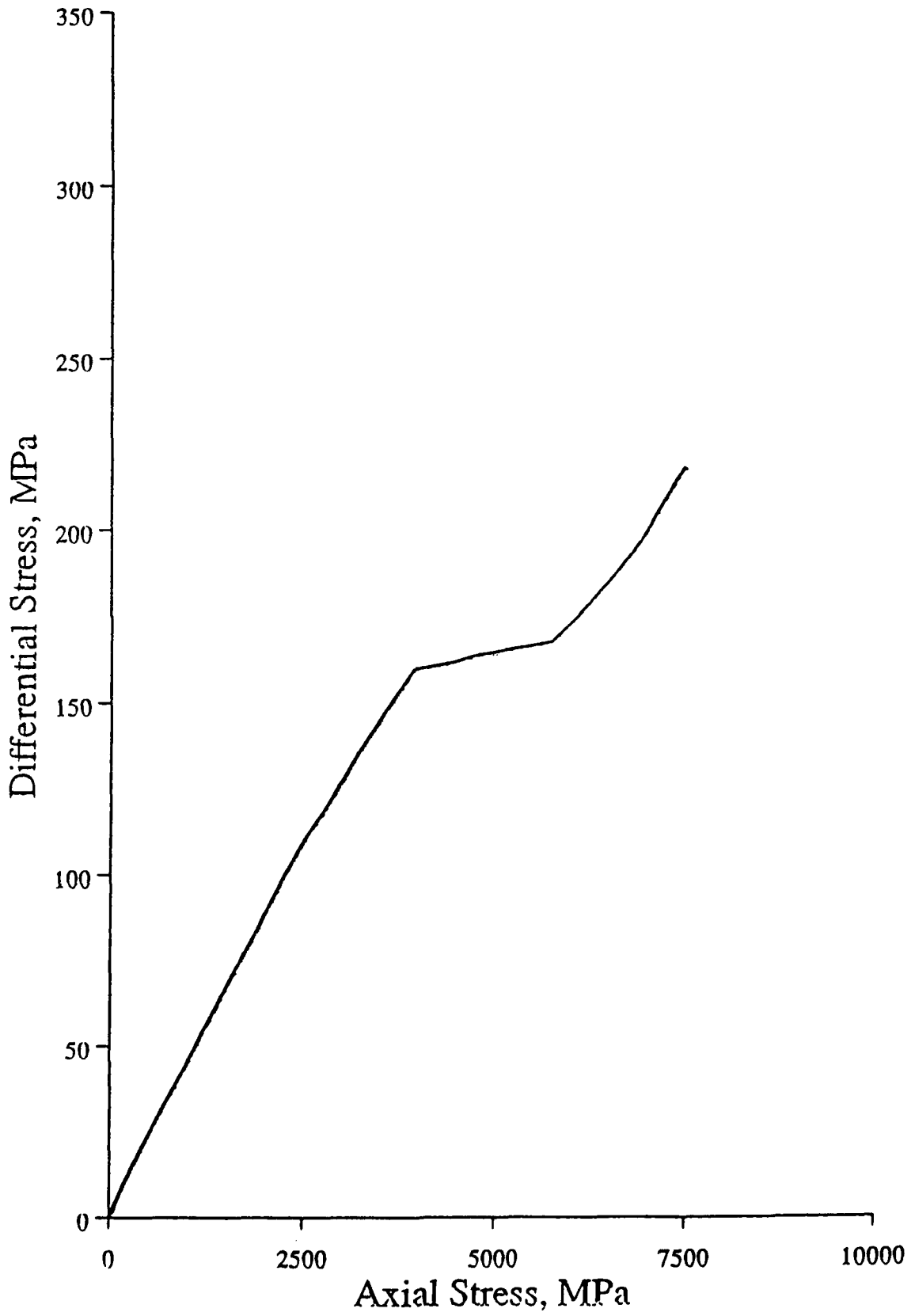
TS 9



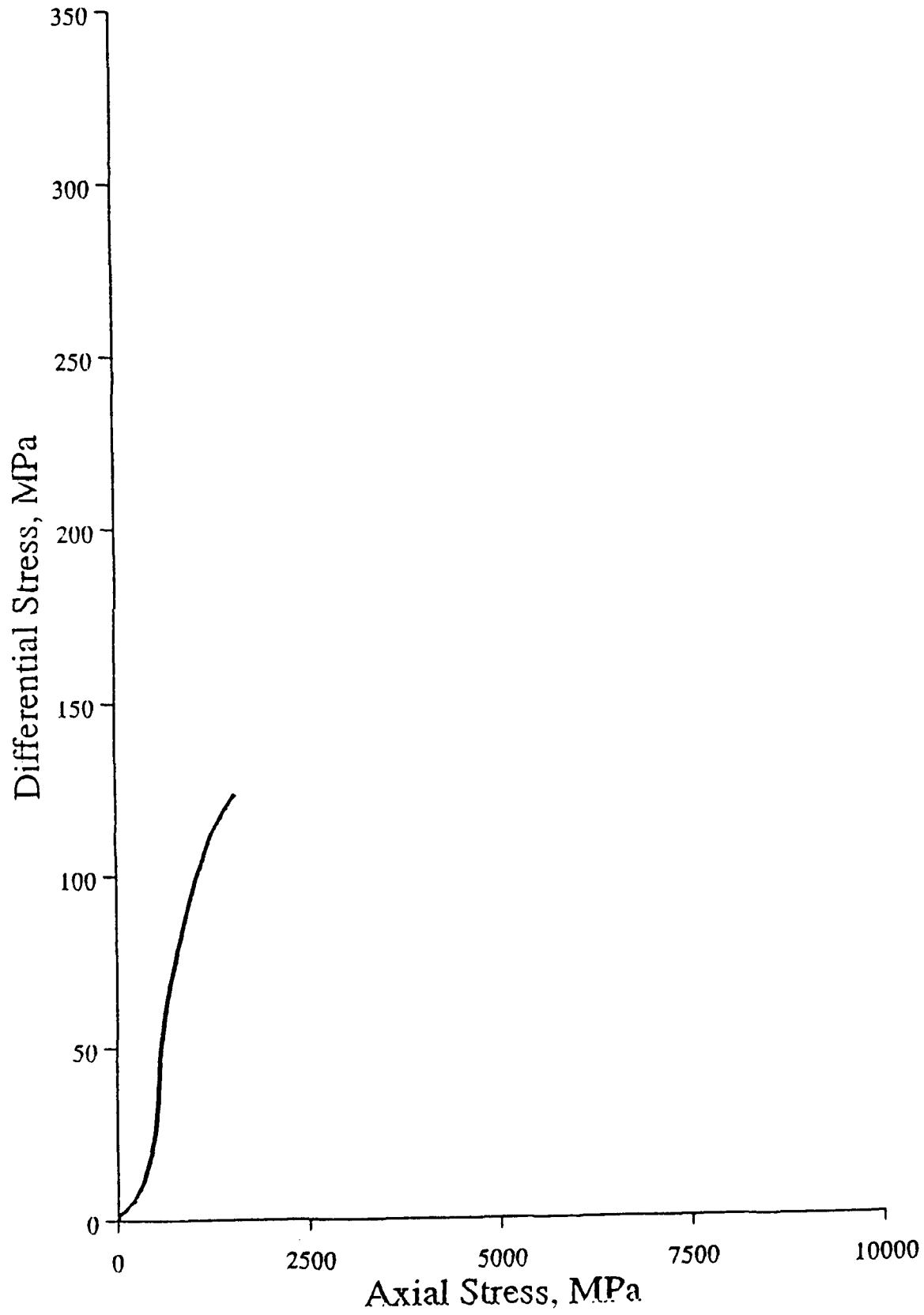
TS 8



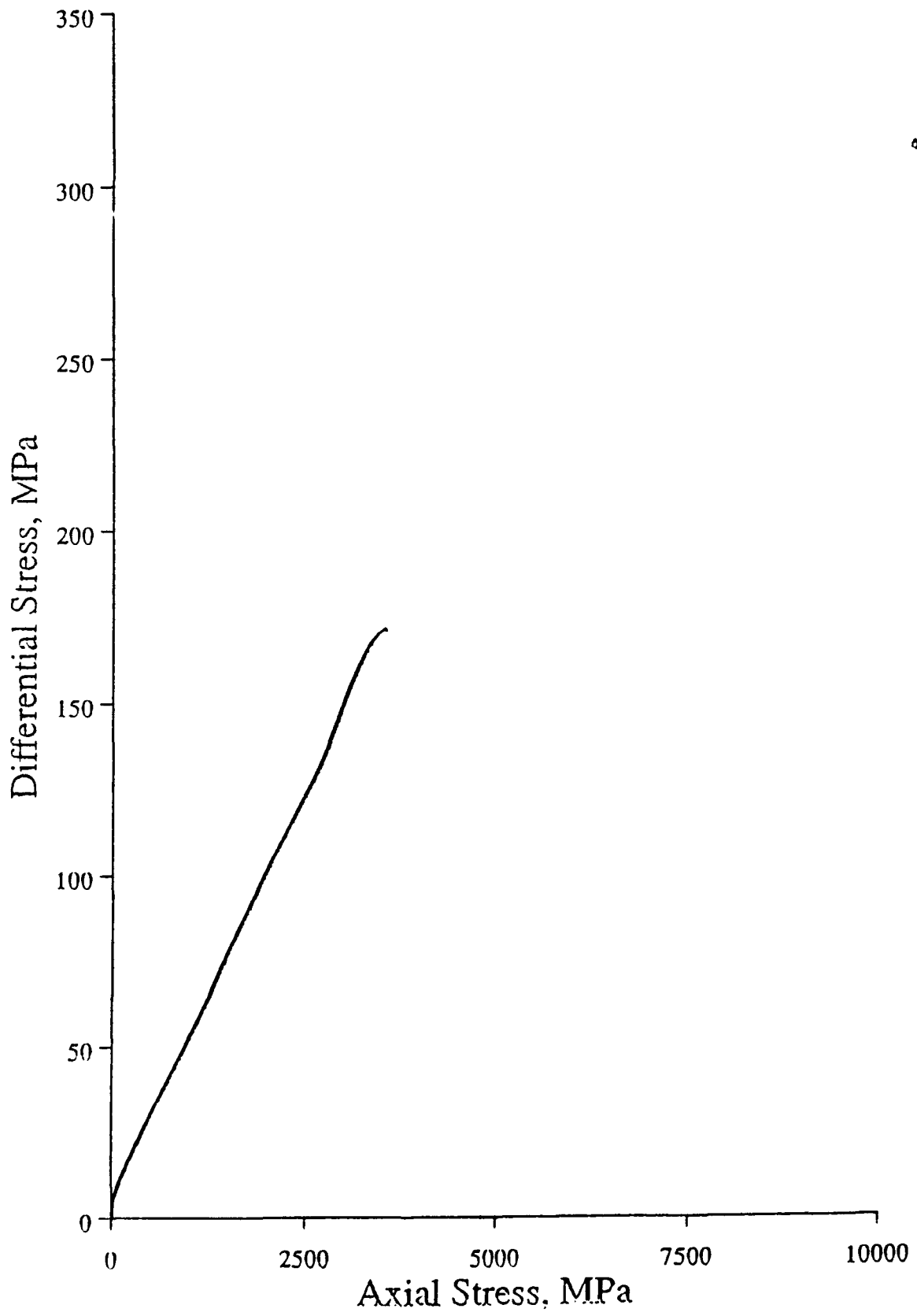
TS 10



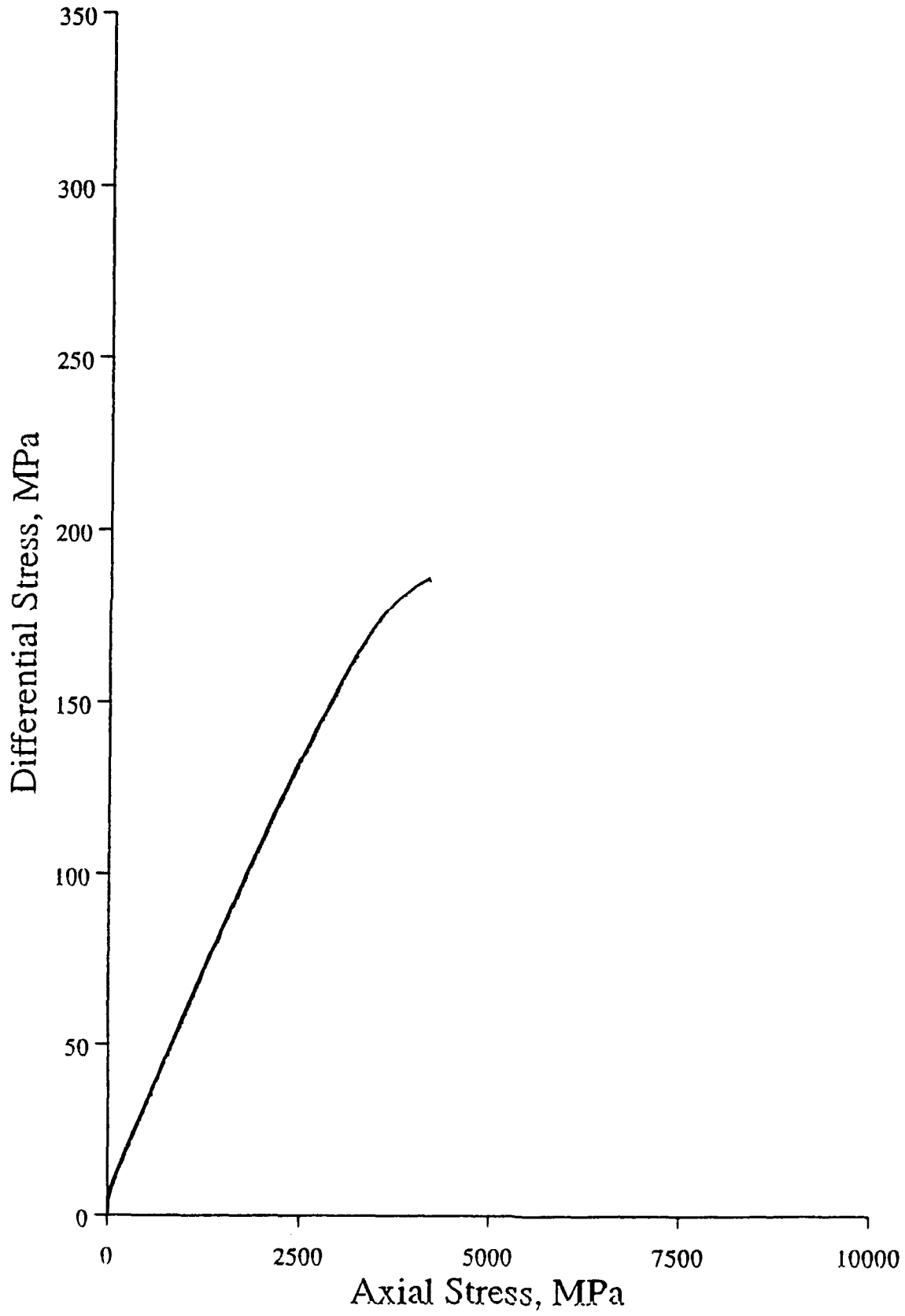
TS 2



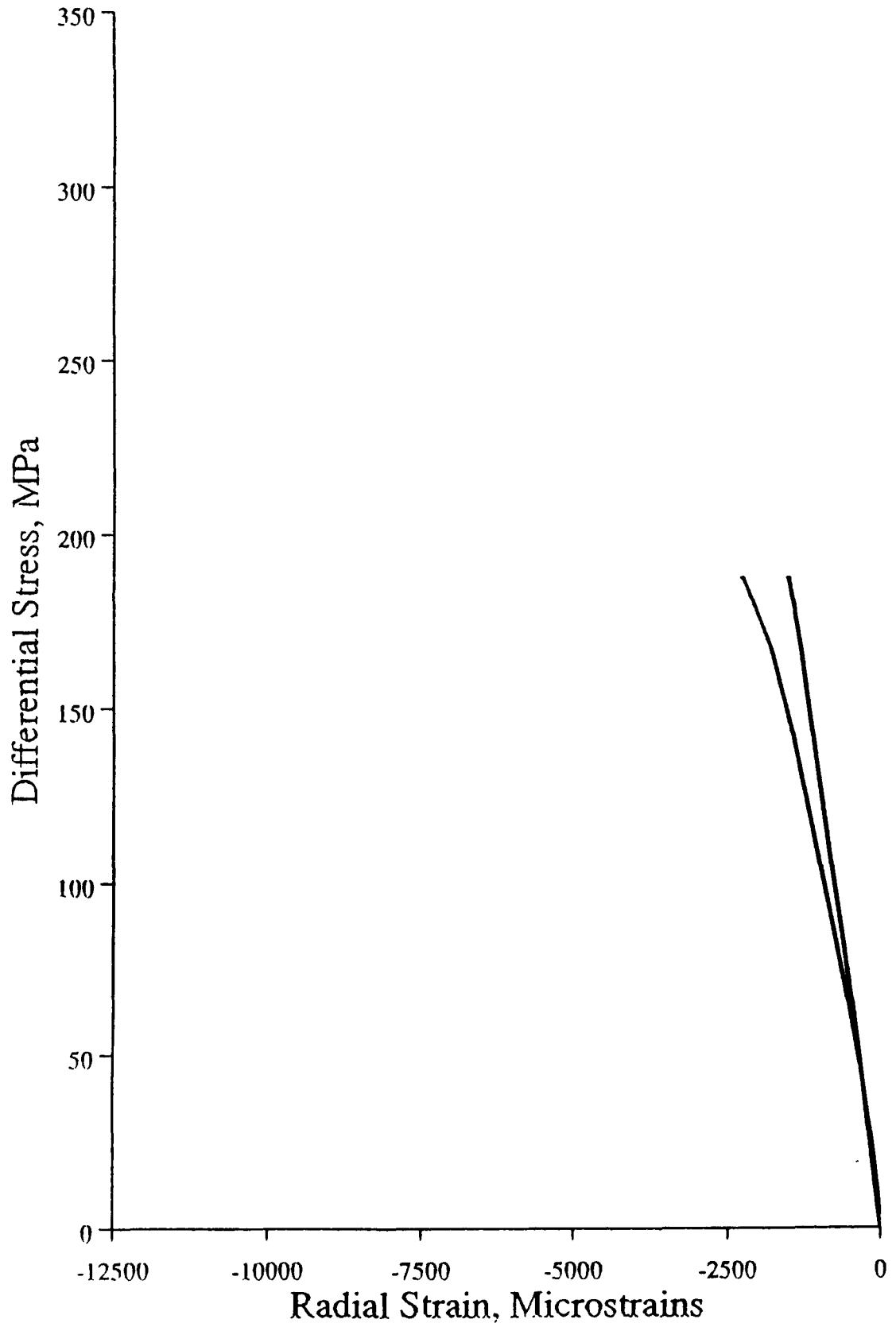
TS 4



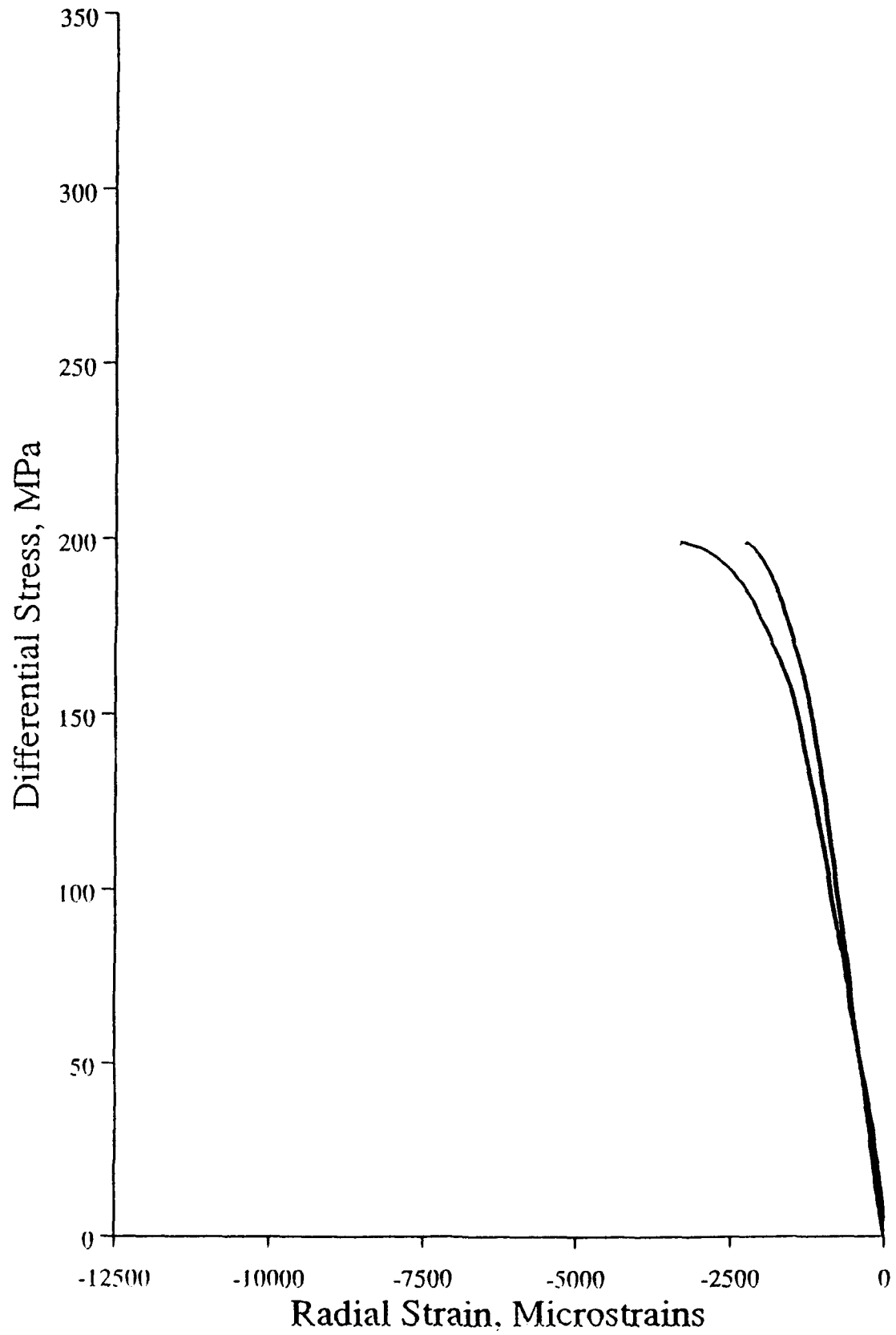
TS 6C

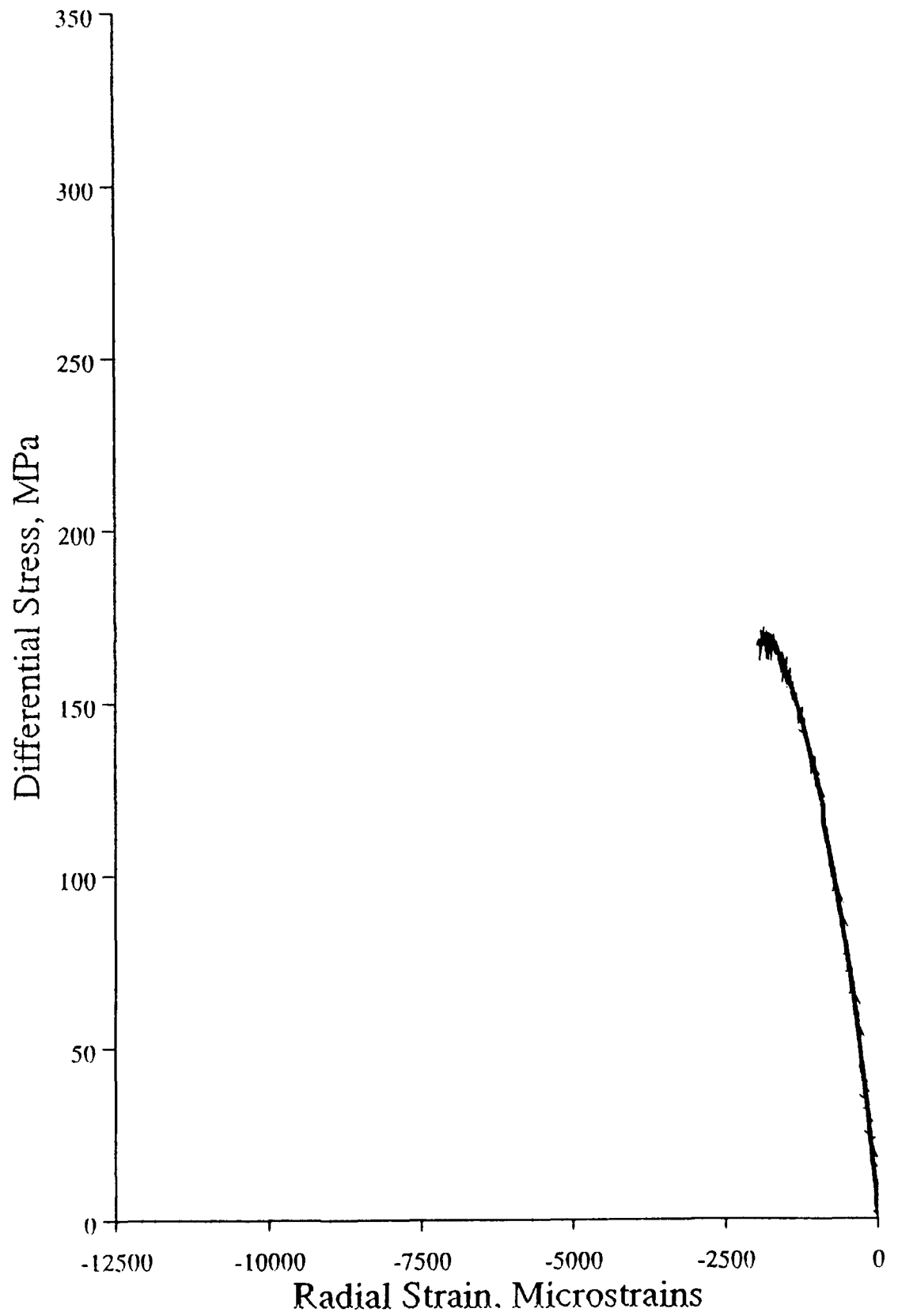


TS 7

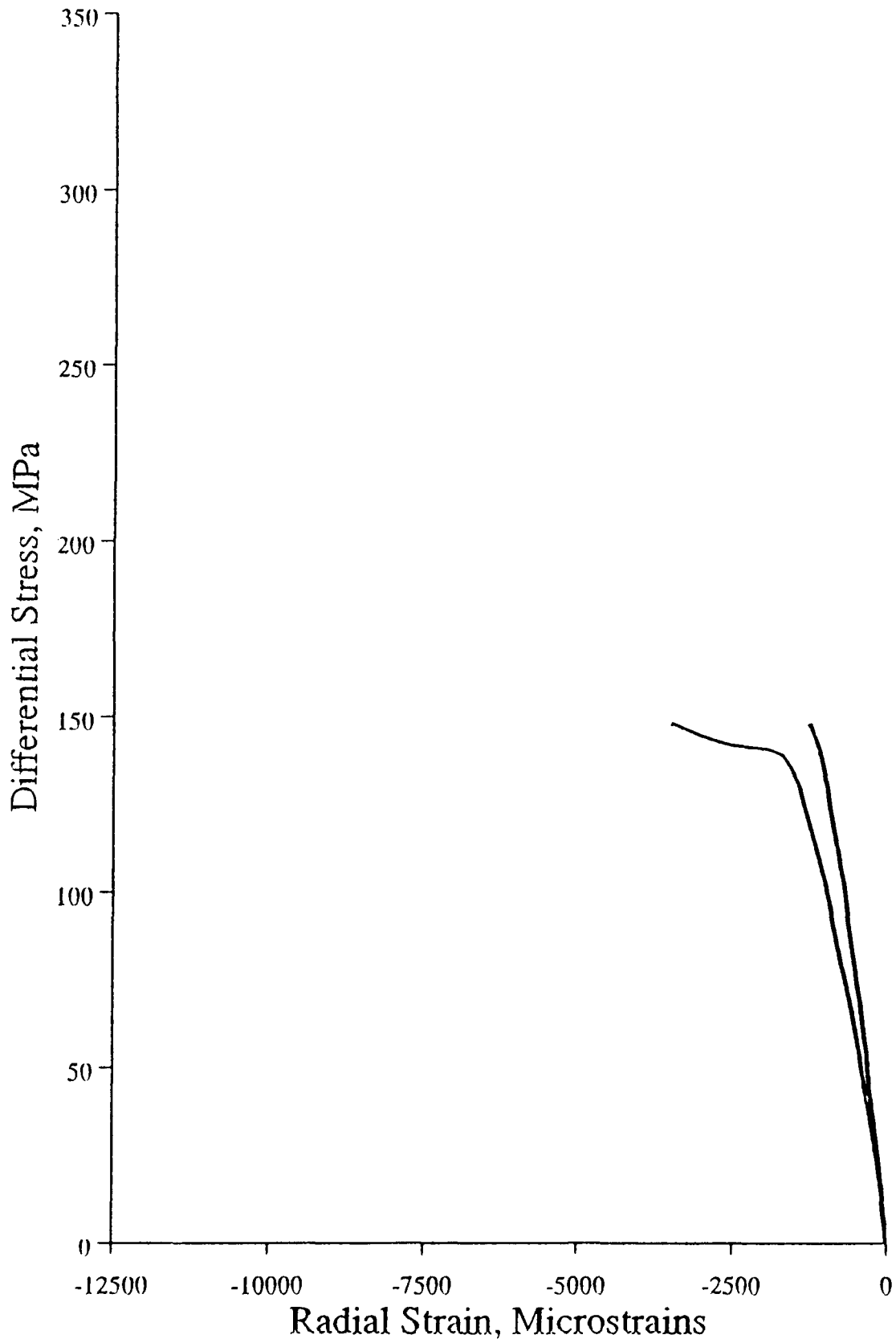


TS 1B

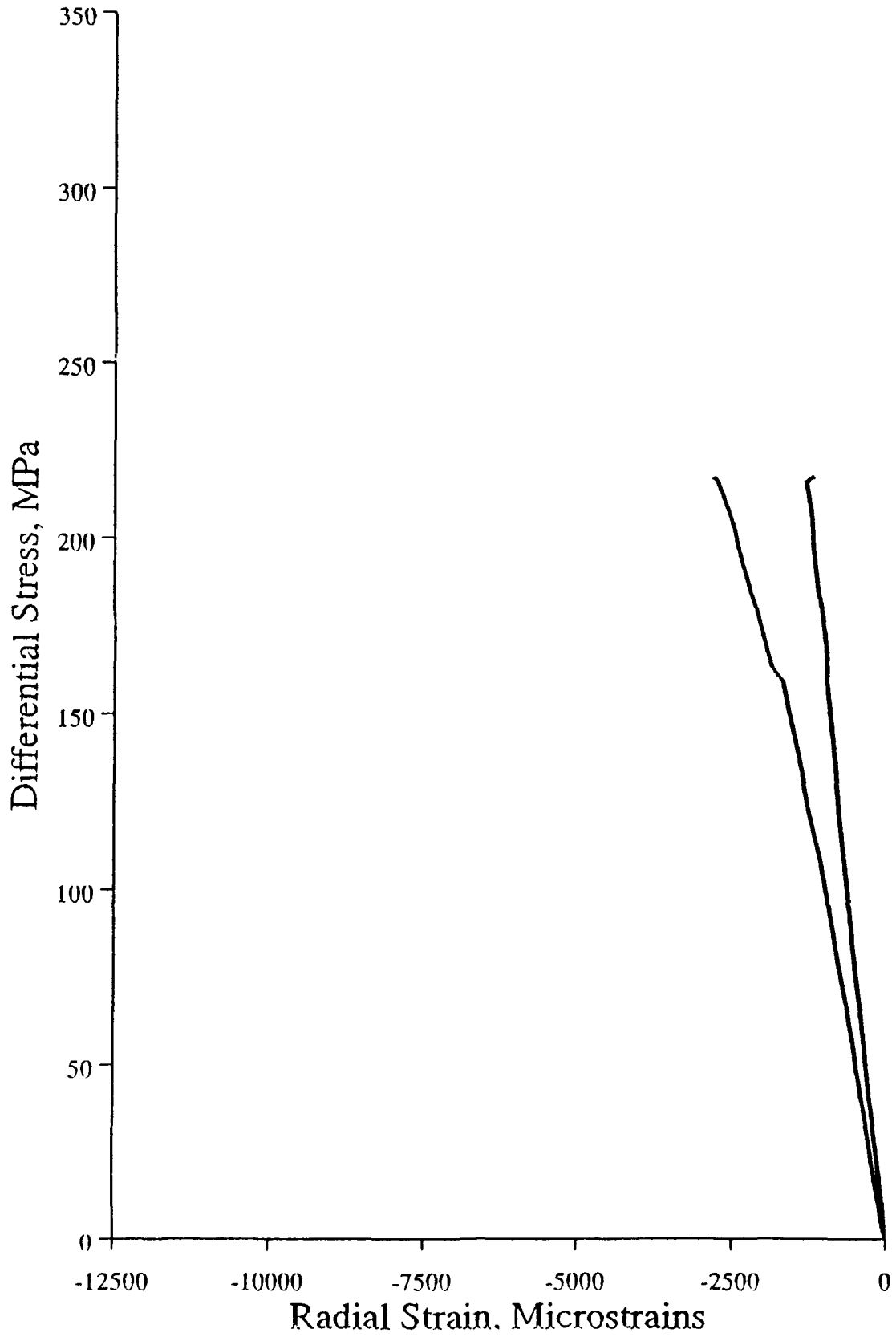




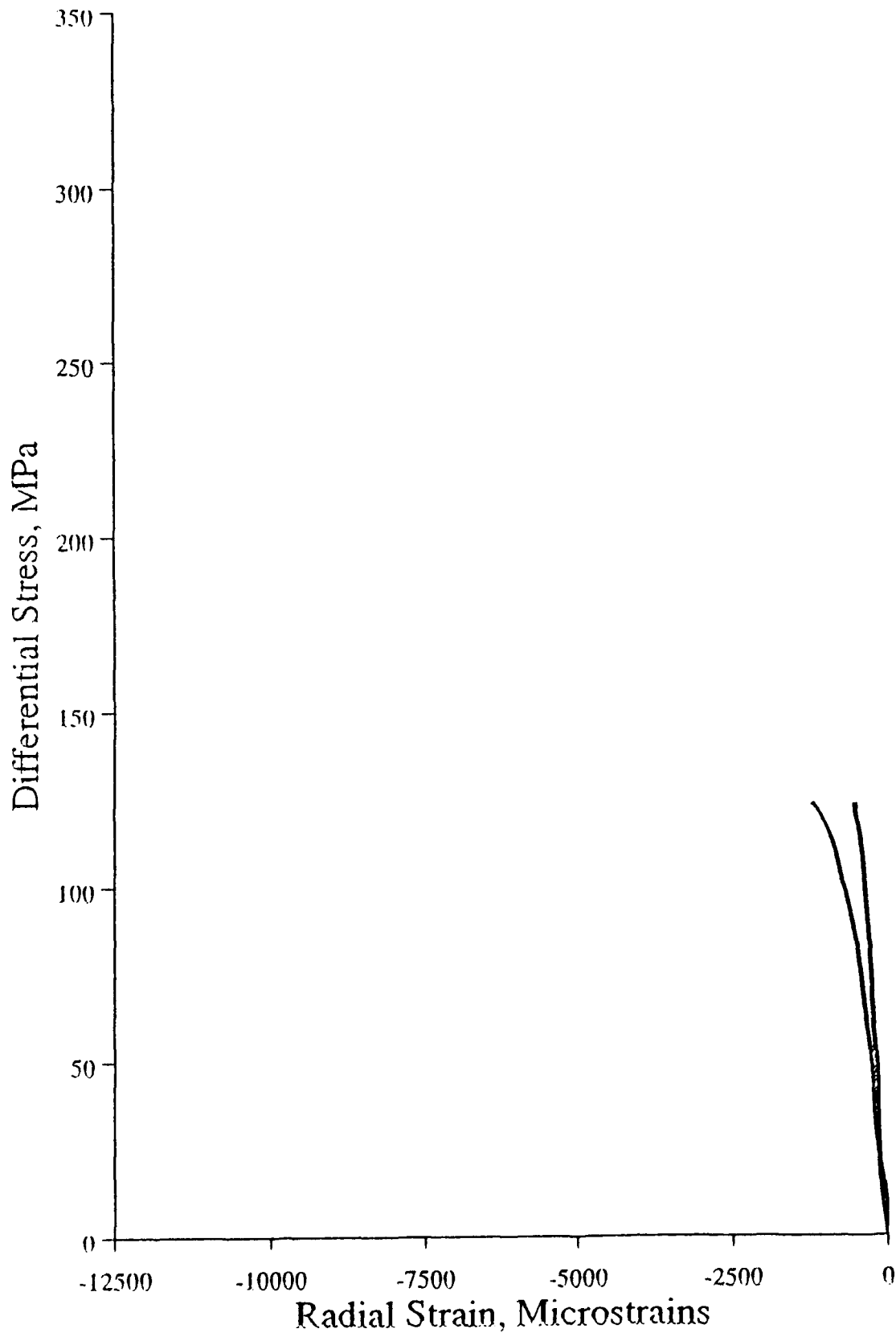
TS 8

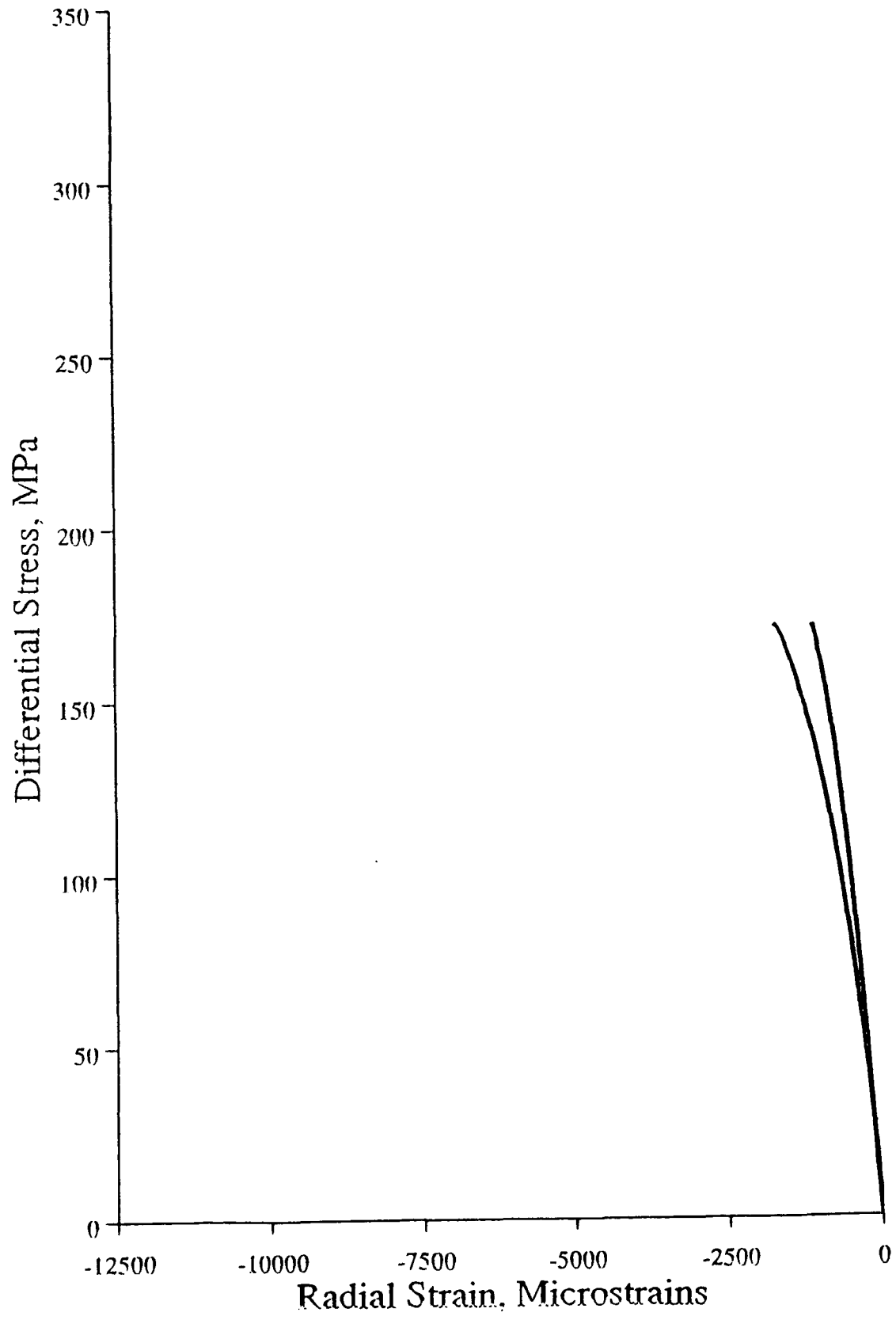


TS 10

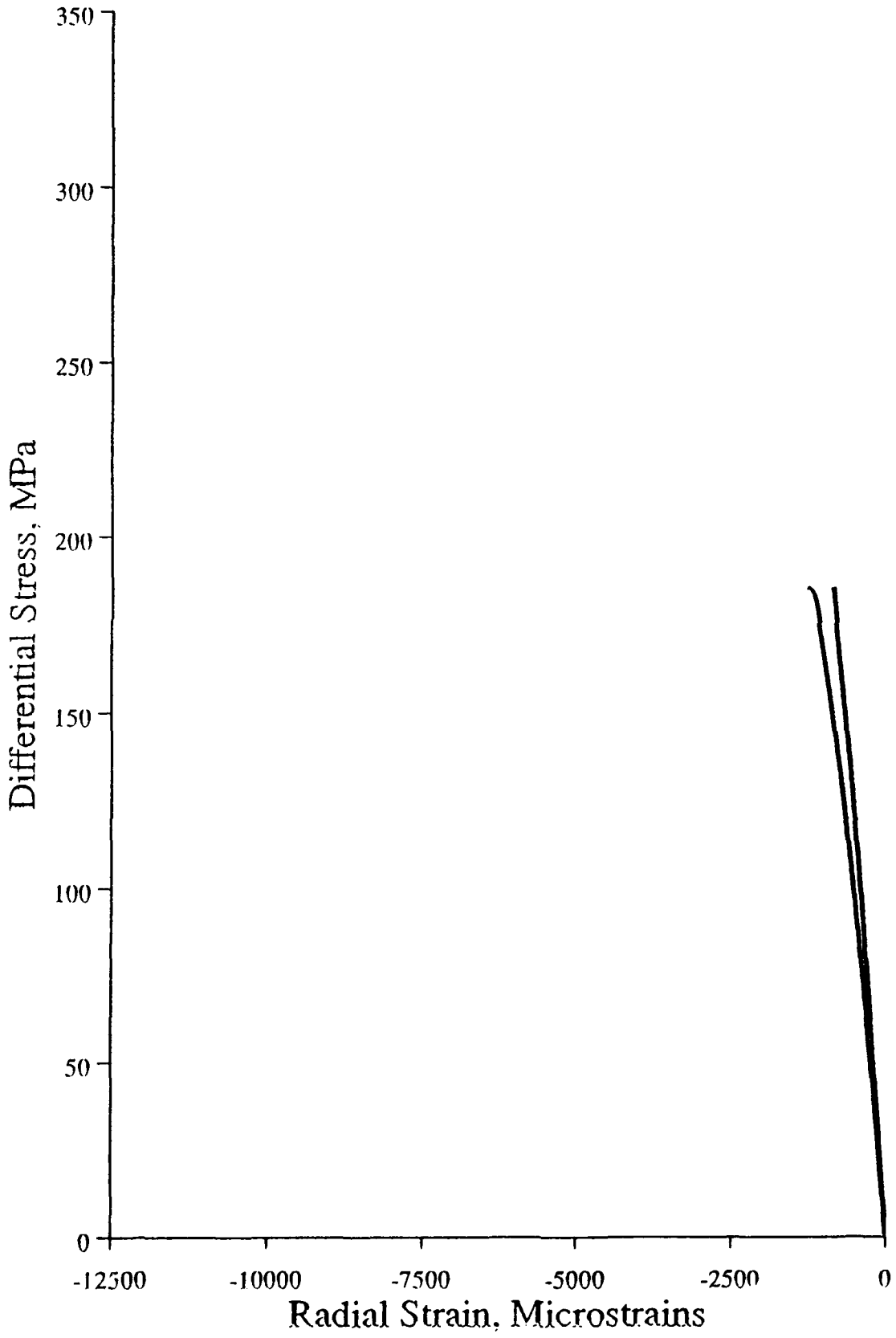


TS 2





TS 6C



Prof. Thomas Ahrens
Seismological Lab, 252-21
Division of Geological & Planetary Sciences
California Institute of Technology
Pasadena, CA 91125

Prof. Charles B. Archambeau
CIRES
University of Colorado
Boulder, CO 80309

Dr. Thomas C. Bache, Jr.
Science Applications Int'l Corp.
10260 Campus Point Drive
San Diego, CA 92121 (2 copies)

Prof. Muawia Barazangi
Institute for the Study of the Continent
Cornell University
Ithaca, NY 14853

Dr. Douglas R. Baumgardt
ENSCO, Inc
5400 Port Royal Road
Springfield, VA 22151-2388

Prof. Jonathan Berger
IGPP, A-025
Scripps Institution of Oceanography
University of California, San Diego
La Jolla, CA 92093

Dr. Lawrence J. Burdick
Woodward-Clyde Consultants
566 El Dorado Street
Pasadena, CA 91109-3245

Dr. Jerry Carter
Center for Seismic Studies
1300 North 17th St., Suite 1450
Arlington, VA 22209-2308

Dr. Karl Coyner
New England Research, Inc.
76 Olcott Drive
White River Junction, VT 05001

Prof. Vernon F. Cormier
Department of Geology & Geophysics
U-45, Room 207
The University of Connecticut
Storrs, CT 06268

Professor Anton W. Dainty
Earth Resources Laboratory
Massachusetts Institute of Technology
42 Carleton Street
Cambridge, MA 02142

Prof. Steven Day
Department of Geological Sciences
San Diego State University
San Diego, CA 92182

Dr. Zoltan A. Der
ENSCO, Inc.
5400 Port Royal Road
Springfield, VA 22151-2388

Prof. John Ferguson
Center for Lithospheric Studies
The University of Texas at Dallas
P.O. Box 830688
Richardson, TX 75083-0688

Dr. Mark D. Fisk
Mission Research Corporation
735 State Street
P. O. Drawer 719
Santa Barbara, CA 93102

Prof. Stanley Flatte
Applied Sciences Building
University of California
Santa Cruz, CA 95064

Dr. Alexander Florence
SRI International
333 Ravenswood Avenue
Menlo Park, CA 94025-3493

Prof. Henry L. Gray
Vice Provost and Dean
Department of Statistical Sciences
Southern Methodist University
Dallas, TX 75275

Dr. Indra Gupta
Teledyne Geotech
314 Montgomery Street
Alexandria, VA 22314

Prof. David G. Harkrider
Seismological Laboratory
Division of Geological & Planetary Sciences
California Institute of Technology
Pasadena, CA 91125

Prof. Donald V. Helmberger
Seismological Laboratory
Division of Geological & Planetary Sciences
California Institute of Technology
Pasadena, CA 91125

Prof. Eugene Herrin
Institute for the Study of Earth and Man
Geophysical Laboratory
Southern Methodist University
Dallas, TX 75275

Prof. Bryan Isacks
Cornell University
Department of Geological Sciences
SNEE Hall
Ithaca, NY 14850

Dr. Rong-Song Jih
Teledyne Geotech
314 Montgomery Street
Alexandria, VA 22314

Prof. Lane R. Johnson
Seismographic Station
University of California
Berkeley, CA 94720

Dr. Richard LaCoss
MIT-Lincoln Laboratory
M-200B
P. O. Box 73
Lexington, MA 02173-0073 (3 copies)

Prof Fred K. Lamb
University of Illinois at Urbana-Champaign
Department of Physics
1110 West Green Street
Urbana, IL 61801

Prof. Charles A. Langston
Geosciences Department
403 Deike Building
The Pennsylvania State University
University Park, PA 16802

Prof. Thorne Lay
Institute of Tectonics
Earth Science Board
University of California, Santa Cruz
Santa Cruz, CA 95064

Prof. Arthur Lerner-Lam
Lamont-Doherty Geological Observatory
of Columbia University
Palisades, NY 10964

Dr. Christopher Lynnes
Teledyne Geotech
314 Montgomery Street
Alexandria, VA 22314

Professor Peter E. Malin
Department of Geology
Old Chemistry Building
Duke University
Durham, NC 27706

Dr. Randolph Martin, III
New England Research, Inc.
76 Olcott Drive
White River Junction, VT 05001

Prof. Thomas V. McEvelly
Seismographic Station
University of California
Berkeley, CA 94720

Dr. Keith L. McLaughlin
S-CUBED
A Division of Maxwell Laboratory
P.O. Box 1620
La Jolla, CA 92038-1620

Prof. William Menke
Lamont-Doherty Geological Observatory
of Columbia University
Palisades, NY 10964

Stephen Miller
SRI International
333 Ravenswood Avenue
Box AF 116
Menlo Park, CA 94025-3493

Prof. Bernard Minster
IGPP, A-025
Scripps Institute of Oceanography
University of California, San Diego
La Jolla, CA 92093

Prof. Brian J. Mitchell
Department of Earth & Atmospheric Sciences
St. Louis University
St. Louis, MO 63156

Mr. Jack Murphy
S-CUBED, A Division of Maxwell Laboratory
11800 Sunrise Valley Drive
Suite 1212
Reston, VA 22091 (2 copies)

Prof. John A. Orcutt
IGPP, A-025
Scripps Institute of Oceanography
University of California, San Diego
La Jolla, CA 92093

Prof. Keith Priestley
University of Cambridge
Bullard Labs, Dept. of Earth Sciences
Madingley Rise, Madingley Rd.
Cambridge CB3 0EZ, ENGLAND

Dr. Jay J. Pulli
Radix Systems, Inc.
2 Taft Court, Suite 203
Rockville, MD 20850

Prof. Paul G. Richards
Lamont Doherty Geological Observatory
of Columbia University
Palisades, NY 10964

Dr. Wilmer Rivers
Teledyne Geotech
314 Montgomery Street
Alexandria, VA 22314

Prof. Charles G. Sammis
Center for Earth Sciences
University of Southern California
University Park
Los Angeles, CA 90089-0741

Prof. Christopher H. Scholz
Lamont-Doherty Geological Observatory
of Columbia University
Palisades, NY 10964

Thomas J. Sereno, Jr.
Science Application Int'l Corp.
10260 Campus Point Drive
San Diego, CA 92121

Prof. David G. Simpson
Lamont-Doherty Geological Observatory
of Columbia University
Palisades, NY 10964

Dr. Jeffrey Stevens
S-CUBED
A Division of Maxwell Laboratory
P.O. Box 1620
La Jolla, CA 92038-1620

Prof. Brian Stump
Institute for the Study of Earth & Man
Geophysical Laboratory
Southern Methodist University
Dallas, TX 75275

Prof. Jeremiah Sullivan
University of Illinois at Urbana-Champaign
Department of Physics
1110 West Green Street
Urbana, IL 61801

Prof. Clifford Thurber
University of Wisconsin-Madison
Department of Geology & Geophysics
1215 West Dayton Street
Madison, WI 53706

Prof. M. Nafi Toksoz
Earth Resources Lab
Massachusetts Institute of Technology
42 Carleton Street
Cambridge, MA 02142

Prof. John E. Vidale
University of California at Santa Cruz
Seismological Laboratory
Santa Cruz, CA 95064

Prof. Terry C. Wallace
Department of Geosciences
Building #77
University of Arizona
Tucson, AZ 85721

Dr. William Wortman
Mission Research Corporation
735 State Street
P. O. Drawer 719
Santa Barbara, CA 93102

OTHERS (UNITED STATES)

Dr. Monem Abdel-Gawad
Rockwell International Science Center
1049 Camino Dos Rios
Thousand Oaks, CA 91360

Prof. Keiiti Aki
Center for Earth Sciences
University of Southern California
University Park
Los Angeles, CA 90089-0741

Prof. Shelton S. Alexander
Geosciences Department
403 Deike Building
The Pennsylvania State University
University Park, PA 16802

Dr. Kenneth Anderson
BBNSTC
Mail Stop 14/1B
Cambridge, MA 02238

Dr. Ralph Archuleta
Department of Geological Sciences
University of California at Santa Barbara
Santa Barbara, CA 93102

Dr. Jeff Barker
Department of Geological Sciences
State University of New York
at Binghamton
Vestal, NY 13901

Dr. Susan Beck
Department of Geosciences
Bldg. # 77
University of Arizona
Tucson, AZ 85721

Dr. T.J. Bennett
S-CUBED
A Division of Maxwell Laboratory
11800 Sunrise Valley Drive, Suite 1212
Reston, VA 22091

Mr. William J. Best
907 Westwood Drive
Vienna, VA 22180

Dr. N. Biswas
Geophysical Institute
University of Alaska
Fairbanks, AK 99701

Dr. G.A. Bollinger
Department of Geological Sciences
Virginia Polytechnical Institute
21044 Derring Hall
Blacksburg, VA 24061

Dr. Stephen Bratt
Center for Seismic Studies
1300 North 17th Street
Suite 1450
Arlington, VA 22209

Michael Browne
Teledyne Geotech
3401 Shiloh Road
Garland, TX 75041

Mr. Roy Burger
1221 Serry Road
Schenectady, NY 12309

Dr. Robert Burrige
Schlumberger-Doll Research Center
Old Quarry Road
Ridgefield, CT 06877

Dr. W. Winston Chan
Teledyne Geotech
314 Montgomery Street
Alexandria, VA 22314-1581

Dr. Theodore Cherry
Science Horizons, Inc.
710 Encinitas Blvd., Suite 200
Encinitas, CA 92024 (2 copies)

Prof. Jon F. Claerbout
Department of Geophysics
Stanford University
Stanford, CA 94305

Prof. Robert W. Clayton
Seismological Laboratory
Division of Geological & Planetary Sciences
California Institute of Technology
Pasadena, CA 91125

Prof. F. A. Dahlen
Geological and Geophysical Sciences
Princeton University
Princeton, NJ 08544-0636

Mr. Charles Doll
Earth Resources Laboratory
Massachusetts Institute of Technology
42 Carleton St.
Cambridge, MA 02142

Prof. Adam Dziewonski
Hoffman Laboratory
Harvard University
20 Oxford St
Cambridge, MA 02138

Prof. John Ebel
Department of Geology & Geophysics
Boston College
Chestnut Hill, MA 02167

Eric Fielding
SNEE Hall
INSTOC
Cornell University
Ithaca, NY 14853

Dr. John Foley
GL/LWH
Hanscom AFB, MA 01731-5000

Prof. Donald Forsyth
Department of Geological Sciences
Brown University
Providence, RI 02912

Dr. Cliff Frolich
Institute of Geophysics
8701 North Mopac
Austin, TX 78759

Dr. Anthony Gangi
Texas A&M University
Department of Geophysics
College Station, TX 77843

Dr. Freeman Gilbert
IGPP, A-025
Scripps Institute of Oceanography
University of California
La Jolla, CA 92093

Mr. Edward Giller
Pacific Sierra Research Corp.
1401 Wilson Boulevard
Arlington, VA 22209

Dr. Jeffrey W. Given
SAIC
10260 Campus Point Drive
San Diego, CA 92121

Prof. Stephen Grand
University of Texas at Austin
Department of Geological Sciences
Austin, TX 78713-7909

Prof. Roy Greenfield
Geosciences Department
403 Deike Building
The Pennsylvania State University
University Park, PA 16802

Dan N. Hagedorn
Battelle
Pacific Northwest Laboratories
Battelle Boulevard
Richland, WA 99352

Dr. James Hannon
Lawrence Livermore National Laboratory
P. O. Box 808
Livermore, CA 94550

Prof. Robert B. Herrmann
Dept. of Earth & Atmospheric Sciences
St. Louis University
St. Louis, MO 63156

Ms. Heidi Houston
Seismological Laboratory
University of California
Santa Cruz, CA 95064

Kevin Hutchenson
Department of Earth Sciences
St. Louis University
3507 Laclede
St. Louis, MO 63103

Dr. Hans Israelsson
Center for Seismic Studies
1300 N. 17th Street, Suite 1450
Arlington, VA 22209-2308

Prof. Thomas H. Jordan
Department of Earth, Atmospheric
and Planetary Sciences
Massachusetts Institute of Technology
Cambridge, MA 02139

Prof. Alan Kafka
Department of Geology & Geophysics
Boston College
Chestnut Hill, MA 02167

Robert C. Kemerait
ENSCO, Inc.
445 Pineda Court
Melbourne, FL 32940

William Kikendall
Teledyne Geotech
3401 Shiloh Road
Garland, TX 75041

Prof. Leon Knopoff
University of California
Institute of Geophysics & Planetary Physics
Los Angeles, CA 90024

Prof. L. Timothy Long
School of Geophysical Sciences
Georgia Institute of Technology
Atlanta, GA 30332

Dr. Gary McCartor
Department of Physics
Southern Methodist University
Dallas, TX 75275

Prof. Art McGarr
Mail Stop 977
Geological Survey
345 Middlefield Rd.
Menlo Park, CA 94025

Dr. George Mellman
Sierra Geophysics
11255 Kirkland Way
Kirkland, WA 98033

Prof. John Nabelek
College of Oceanography
Oregon State University
Corvallis, OR 97331

Prof. Geza Nagy
University of California, San Diego
Department of Ames, M.S. B-010
La Jolla, CA 92093

Dr. Keith K. Nakanishi
Lawrence Livermore National Laboratory
L-205
P. O. Box 808
Livermore, CA 94550

Dr. Bao Nguyen
GL/LWH
Hanscom AFB, MA 01731-5000

Prof. Amos Nur
Department of Geophysics
Stanford University
Stanford, CA 94305

Prof. Jack Oliver
Department of Geology
Cornell University
Ithaca, NY 14850

Dr. Kenneth Olsen
P. O. Box 1273
Linwood, WA 98046-1273

Howard J. Patton
Lawrence Livermore National Laboratory
L-205
P. O. Box 808
Livermore, CA 94550

Prof. Robert Phinney
Geological & Geophysical Sciences
Princeton University
Princeton, NJ 08544-0636

Dr. Paul Pomeroy
Rondout Associates
P.O. Box 224
Stone Ridge, NY 12484

Dr. Jay Pulli
RADIX System, Inc.
2 Taft Court, Suite 203
Rockville, MD 20850

Dr. Norton Rimer
S-CUBED
A Division of Maxwell Laboratory
P.O. Box 1620
La Jolla, CA 92038-1620

Prof. Larry J. Ruff
Department of Geological Sciences
1006 C.C. Little Building
University of Michigan
Ann Arbor, MI 48109-1063

Dr. Richard Sailor
TASC Inc.
55 Walkers Brook Drive
Reading, MA 01867

Dr. Susan Schwartz
Institute of Tectonics
1156 High St.
Santa Cruz, CA 95064

John Sherwin
Teledyne Geotech
3401 Shiloh Road
Garland, TX 75041

Dr. Matthew Sibol
Virginia Tech
Seismological Observatory
4044 Derring Hall
Blacksburg, VA 24061-0420

Dr. Albert Smith
Lawrence Livermore National Laboratory
L-205
P. O. Box 808
Livermore, CA 94550

Prof. Robert Smith
Department of Geophysics
University of Utah
1400 East 2nd South
Salt Lake City, UT 84112

Dr. Stewart W. Smith
Geophysics AK-50
University of Washington
Seattle, WA 98195

Donald L. Springer
Lawrence Livermore National Laboratory
L-205
P. O. Box 808
Livermore, CA 94550

Dr. George Sutton
Rondout Associates
P.O. Box 224
Stone Ridge, NY 12484

Prof. L. Sykes
Lamont-Doherty Geological Observatory
of Columbia University
Palisades, NY 10964

Prof. Pradeep Talwani
Department of Geological Sciences
University of South Carolina
Columbia, SC 29208

Dr. David Taylor
ENSCO, Inc.
445 Pineda Court
Melbourne, FL 32940

Dr. Steven R. Taylor
Lawrence Livermore National Laboratory
L-205
P. O. Box 808
Livermore, CA 94550

Professor Ta-Liang Teng
Center for Earth Sciences
University of Southern California
University Park
Los Angeles, CA 90089-0741

Dr. R.B. Tittmann
Rockwell International Science Center
1049 Camino Dos Rios
P.O. Box 1085
Thousand Oaks, CA 91360

Dr. Gregory van der Vink
IRIS, Inc.
1616 North Fort Myer Drive
Suite 1440
Arlington, VA 22209

Professor Daniel Walker
University of Hawaii
Institute of Geophysics
Honolulu, HI 96822

William R. Walter
Seismological Laboratory
University of Nevada
Reno, NV 89557

Dr. Raymond Willeman
GL/LWH
Hanscom AFB, MA 01731-5000

Dr. Gregory Wojcik
Weidlinger Associates
4410 El Camino Real
Suite 110
Los Altos, CA 94022

Dr. Lorraine Wolf
GL/LWH
Hanscom AFB, MA 01731-5000

Prof. Francis T. Wu
Department of Geological Sciences
State University of New York
at Binghamton
Vestal, NY 13901

Dr. Gregory B. Young
ENSCO, Inc.
5400 Port Royal Road
Springfield, VA 22151-2388

Dr. Eileen Vergino
Lawrence Livermore National Laboratory
L-205
P. O. Box 808
Livermore, CA 94550

J. J. Zucca
Lawrence Livermore National Laboratory
P. O. Box 808
Livermore, CA 94550

GOVERNMENT

Dr. Ralph Alewine III
DARPA/NMRO
1400 Wilson Boulevard
Arlington, VA 22209-2308

Mr. James C. Battis
GL/LWH
Hanscom AFB, MA 01731-5000

Dr. Robert Blandford
AFTAC/TT
Center for Seismic Studies
1300 North 17th St., Suite 1450
Arlington, VA 22209-2308

Eric Chael
Division 9241
Sandia Laboratory
Albuquerque, NM 87185

Dr. John J. Cipar
GL/LWH
Hanscom AFB, MA 01731-5000

Cecil Davis
Group P-15, Mail Stop D406
P.O. Box 1663
Los Alamos National Laboratory
Los Alamos, NM 87544

Mr. Jeff Duncan
Office of Congressman Markey
2133 Rayburn House Bldg.
Washington, DC 20515

Dr. Jack Evernden
USGS - Earthquake Studies
345 Middlefield Road
Menlo Park, CA 94025

Art Frankel
USGS
922 National Center
Reston, VA 22092

Dr. Dale Glover
DIA/DT-1B
Washington, DC 20301

Dr. T. Hanks
USGS
Nat'l Earthquake Research Center
345 Middlefield Road
Menlo Park, CA 94025

Paul Johnson
ESS-4, Mail Stop J979
Los Alamos National Laboratory
Los Alamos, NM 87545

Janet Johnston
GL/LWH
Hanscom AFB, MA 01731-5000

Dr. Katharine Kadinsky-Cade
GL/LWH
Hanscom AFB, MA 01731-5000

Ms. Ann Kerr
IGPP, A-025
Scripps Institute of Oceanography
University of California, San Diego
La Jolla, CA 92093

Dr. Max Koontz
US Dept of Energy/DP 5
Forrestal Building
1000 Independence Avenue
Washington, DC 20585

Dr. W.H.K. Lee
Office of Earthquakes, Volcanoes,
& Engineering
345 Middlefield Road
Menlo Park, CA 94025

Dr. William Leith
U.S. Geological Survey
Mail Stop 928
Reston, VA 22092

Dr. Richard Lewis
Director, Earthquake Engineering & Geophysics
U.S. Army Corps of Engineers
Box 631
Vicksburg, MS 39180

James F. Lewkowicz
GL/LWH
Hanscom AFB, MA 01731-5000

Mr. Alfred Lieberman
ACDA/VI-OA' State Department Bldg
Room 5726
320 - 21st Street, NW
Washington, DC 20451

Stephen Mangino
GL/LWH
Hanscom AFB, MA 01731-5000

Dr. Robert Masse
Box 25046, Mail Stop 967
Denver Federal Center
Denver, CO 80225

Art McGarr
U.S. Geological Survey, MS-977
345 Middlefield Road
Menlo Park, CA 94025

Richard Morrow
ACDA/VI, Room 5741
320 21st Street N.W
Washington, DC 20451

Dr. Carl Newton
Los Alamos National Laboratory
P.O. Box 1663
Mail Stop C335, Group ESS-3
Los Alamos, NM 87545

Dr. Kenneth H. Olsen
Los Alamos Scientific Laboratory
P. O. Box 1663
Mail Stop D-406
Los Alamos, NM 87545

Mr. Chris Paine
Office of Senator Kennedy
SR 315
United States Senate
Washington, DC 20510

Colonel Jerry J. Perrizo
AFOSR/NP, Building 410
Bolling AFB
Washington, DC 20332-6448

Dr. Frank F. Pilotte
HQ AFTAC/IT
Patrick AFB, FL 32925-6001

Katie Poley
CIA-ACIS/TMC
Room 4X16NHB
Washington, DC 20505

Mr. Jack Rachlin
U.S. Geological Survey
Geology, Rm 3 C136
Mail Stop 928 National Center
Reston, VA 22092

Dr. Robert Reinke
WL/NTESG
Kirtland AFB, NM 87117-6008

Dr. Byron Ristvet
HQ DNA, Nevada Operations Office
Attn: NVCG
P.O. Box 98539
Las Vegas, NV 89193

Dr. George Rothe
HQ AFTAC/TTR
Patrick AFB, FL 32925-6001

Dr. Alan S. Ryall, Jr.
DARPA/NMRO
1400 Wilson Boulevard
Arlington, VA 22209-2308

Dr. Michael Shore
Defense Nuclear Agency/SPSS
6801 Telegraph Road
Alexandria, VA 22310

Mr. Charles L. Taylor
GL/LWG
Hanscom AFB, MA 01731-5000

Dr. Larry Turnbull
CIA-OSWR/NED
Washington, DC 20505

Dr. Thomas Weaver
Los Alamos National Laboratory
P.O. Box 1663, Mail Stop C335
Los Alamos, NM 87545

GL/SULL
Research Library
Hanscom AFB , MA 01731-5000 (2 copies)

Defense Intelligence Agency
Directorate for Scientific & Technical Intelligence
Attn: DT1B
Washington, DC 20340-6158

Secretary of the Air Force
(SAFRD)
Washington, DC 20330

AFTAC/CA
(STINFO)
Patrick AFB, FL 32925-6001

Office of the Secretary Defense
DDR & E
Washington, DC 20330

TACTEC
Battelle Memorial Institute
505 King Avenue
Columbus, OH 43201 (Final Report Only)

HQ DNA
Attn: Technical Library
Washington, DC 20305

DARPA/RMO/RETRIEVAL
1400 Wilson Boulevard
Arlington, VA 22209

DARPA/RMO/Security Office
1400 Wilson Boulevard
Arlington, VA 22209

Geophysics Laboratory
Attn: XO
Hanscom AFB, MA 01731-5000

Geophysics Laboratory
Attn: LW
Hanscom AFB, MA 01731-5000

DARPA/PM
1400 Wilson Boulevard
Arlington, VA 22209

Defense Technical Information Center
Cameron Station
Alexandria, VA 22314 (5 copies)

CONTRACTORS (FOREIGN)

Dr. Ramon Cabre, S.J.
Observatorio San Calixto
Casilla 5939
La Paz, Bolivia

Prof. Hans-Peter Harjes
Institute for Geophysik
Ruhr University/Bochum
P.O. Box 102148
4630 Bochum 1, FRG

Prof. Eystein Husebye
NTNF/NORSAR
P.O. Box 51
N-2007 Kjeller, NORWAY

Prof. Brian L.N. Kennett
Research School of Earth Sciences
Institute of Advanced Studies
G.P.O. Box 4
Canberra 2601, AUSTRALIA

Dr. Bernard Massinon
Societe Radiomana
27 rue Claude Bernard
75005 Paris, FRANCE (2 Copies)

Dr. Pierre Mecheler
Societe Radiomana
27 rue Claude Bernard
75005 Paris, FRANCE

Dr. Svein Mykkeltveit
NTNF/NORSAR
P.O. Box 51
N-2007 Kjeller, NORWAY (3 copies)

FOREIGN (OTHERS)

Dr. Peter Basham
Earth Physics Branch
Geological Survey of Canada
1 Observatory Crescent
Ottawa, Ontario, CANADA K1A 0Y3

Dr. Eduard Berg
Institute of Geophysics
University of Hawaii
Honolulu, HI 96822

Dr. Michel Bouchon
I.R.I.G.M.-B.P. 68
38402 St. Martin D'Herès
Cedex, FRANCE

Dr. Hilmar Bungum
NTNF/NORSAR
P.O. Box 51
N-2007 Kjeller, NORWAY

Dr. Michel Campillo
Observatoire de Grenoble
I.R.I.G.M.-B.P. 53
38041 Grenoble, FRANCE

Dr. Kin Yip Chun
Geophysics Division
Physics Department
University of Toronto
Ontario, CANADA M5S 1A7

Dr. Alan Douglas
Ministry of Defense
Blacknest, Brimpton
Reading RG7-4RS, UNITED KINGDOM

Dr. Roger Hansen
NTNF/NORSAR
P.O. Box 51
N-2007 Kjeller, NORWAY

Dr. Manfred Henger
Federal Institute for Geosciences & Nat'l Res.
Postfach 510153
D-3000 Hanover 51, FRG

Ms. Eva Johannisson
Senior Research Officer
National Defense Research Inst.
P.O. Box 27322
S-102 54 Stockholm, SWEDEN

Dr. Fekadu Kebede
Geophysical Observatory, Science Faculty
Addis Ababa University
P. O. Box 1176
Addis Ababa, ETHIOPIA

Dr. Tormod Kvaerna
NTNF/NORSAR
P.O. Box 51
N-2007 Kjeller, NORWAY

Dr. Peter Marshall
Procurement Executive
Ministry of Defense
Blacknest, Brimpton
Reading FG7-4RS, UNITED KINGDOM

Prof. Ari Ben-Menahem
Department of Applied Mathematics
Weizman Institute of Science
Rehovot, ISRAEL 951729

Dr. Robert North
Geophysics Division
Geological Survey of Canada
1 Observatory Crescent
Ottawa, Ontario, CANADA K1A 0Y3

Dr. Frode Ringdal
NTNF/NORSAR
P.O. Box 51
N-2007 Kjeller, NORWAY

Dr. Jorg Schlittenhardt
Federal Institute for Geosciences & Nat'l Res.
Postfach 510153
D-3000 Hannover 51, FEDERAL REPUBLIC OF
GERMANY

Universita Degli Studi Di Trieste
Facolta Di Ingegneria
Istituto Di Miniere E. Geofisica Applicata, Trieste,
ITALY